TECHNICAL REPORT 1402

Survey of Millimetre Wave Channel Measurements and Models

prepared by

Dennis Jong-Rong Liang

Baradan Johshi Chhetri

Youtai Xue

James Li

Nazanin Hamzei

Linli Cui

Supervisor: Prof. David G. Michelson

for

Huawei Technologies Canada

In fulfillment of

UBC PG 11R20813

Contract: Air Interface Design and Channel Measurement for High Frequency – Phase I

31 October 2014

UBC Radio Science Lab

http://rsl.ece.ubc.ca/

Table of Contents

1 INTRODUCTION

1.1 Overview

The objective of channel modeling is to capture our knowledge and understanding of the manner in which the propagation environment impairs and distorts wireless signals in a form useful in the design, test and simulation of wireless communications systems. Designers and developers use such channel models to predict and compare the performance of wireless communications systems under realistic conditions and to devise and evaluate methods for mitigating the impairments and distortions that degrade wireless signals. The importance of channel models in wireless system design has long been recognized. Indeed, J. D. Parsons, writing in *The Mobile Propagation Channel*, proclaimed that:

> *Of all the research activities related to mobile radio that have taken place over the years, those involving characterisation and modeling of the radio propagation channel are among the most important and fundamental.*

Channel models are the basis for the software simulators, channel emulators and RF planning tools that are used during the design, implementation, testing and deployment of wireless communications systems, as summarized in Fig. I-1. They can also be used to precisely define the degree of impairment that a wireless system must be able to tolerate in order to: (1) meet the requirements for certification by standards groups and/or (2) comply with contractual obligations.

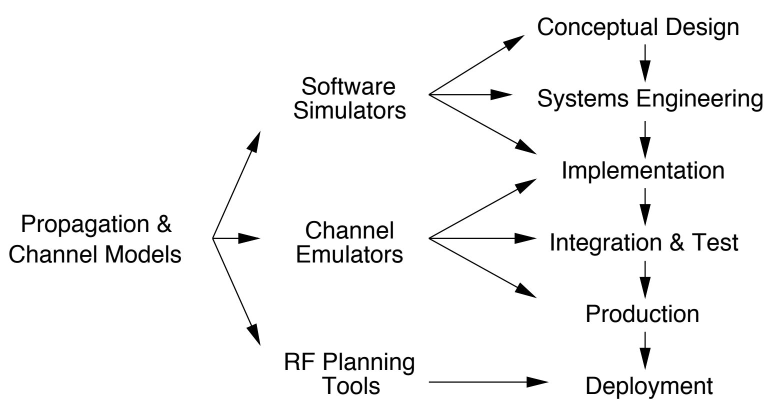

Fig. I-1 – Role of Propagation and Channel Models in Wireless System Design

Like any other mathematical model, a channel model is an abstract, simplified, mathematical construct that describes a portion of reality. In order to limit its complexity, a channel model must necessarily focus on those aspects of the channel that affect the performance of a system of interest and ignore the rest. As researchers develop more sophisticated signalling schemes in order to deliver faster, more reliable communications, it will be necessary to develop new channel models that capture the nature of the relevant impairments and their dependence on the environment. As systems are deployed in ever more demanding environments and, in some cases, in higher frequency bands, it will be necessary to extend existing models.

Channel models capture the distortions and impairments that result as wireless signals traverse the path from a transmitter to a receiver and are diffracted, scattered and absorbed by the terrain, trees, buildings, vehicles and people that comprise the propagation environment. The presence of obstructions along the path may cause the signal to experience greater attenuation than it would under free space conditions. If the signal is scattered by obstacles located throughout the coverage area, replicas of the signal may take multiple paths from the transmitter to the receiver. Because the replicas will arrive at the receiver after different delays, the signal will experience time dispersion. Because the replicas will also arrive from different directions, the signal will experience angular dispersion. If either the scatterers or one of the terminals is in motion, rapid changes in the phase relationship between multipath components will cause the signal to fade randomly, perhaps deeply. Such variation in received signal strength over time is equivalent to frequency dispersion. The correlation between fading observed at the output of adjacent receiving antennas will depend upon the type and configuration of the antennas and the range of angles over which the incident signals arrive.

1.2 Development of New Channel Models

It is commonly but erroneously believed that channel modelling involves time consuming collection of large amounts of measurement data followed by exploratory data analysis that seeks to identify relationships and correlations between the physical parameters and channel model parameters. However, such an approach is both inefficient and ineffective.

A better approach to develop a new channel model is to begin with discussion between the channel modeller and the wireless system designer/developer. First, they must agree upon which aspects of channel behaviour are important and must be captured, and which can be ignored. If important aspects are neglected, the model will not be useful. If, however, too many aspects are considered, the resulting model could be overly complex and would likely require considerable additional effort to develop.

The channel modeller and the designer/developer must also agree upon the nature of the physical environment(s) to be considered and the manner in which the transmitting and receiving antennas will be deployed. This will be often be captured in the form of usage scenarios that will describe, in broad terms, how devices that employ the technology will be used. They must also decide whether the model is to be broadly representative of the scenarios in which wireless devices based upon the technology are likely to be used, i.e., site-general, and the extent to which it must capture the manner in which the channel parameters depend upon the design parameters that describe the configuration of the link.

The nature and degree of the propagation impairments observed on a wireless channel will be affected by the gains, beamwidths, polarizations and orientations of the transmitting and receiving antennas. If the width of the angle of arrival distribution of incident signals is narrower than or at least comparable to the beamwidth of the receiving antenna, then one can usually separate the distortions introduced by the wireless channel (which are captured by the channel model) from the distortions introduced by the antennas (which are captured by the antenna model). If the two sets of distortions cannot be easily separated, one often has little choice but to model them together. The combination of the wireless channel and the transmitting and receiving antennas is often referred to as the radio channel.

The nature and degree of the propagation impairments also depend upon many design parameters and environmental factors including the carrier frequency, the distance between the transmitting and receiving antennas, the relative heights of the antennas above ground level, the nature, height and density of the scatterers in the environment and the nature of any obstructions that lie between the antennas. The decision to fix a design parameter or environmental factor, treat it as an independent variable or simply ignore it will depend upon: (1) the extent to which the channel parameters are affected by that design parameter or environmental factor and (2) the likely range of values which the design parameter or environmental factor might take on in the usage scenario.

The channel modeller and the designer/developer must decide whether to develop the model by simulation, by measurement, or some combination. Although simulation-based methods such as ray tracing are potentially less expensive and time-consuming than measurement-based approaches, they are limited by the assumptions upon which they are based and the possibly tremendous amounts of de- tail regarding the type and location of the scatterers in a typical environment that one may need to supply to them. Measurement-based methods are widely used to characterize wireless channels because they can provide results that are: (1) of immediate use to designers and developers and (2) useful in the validation of results obtained from simulation-based methods. The limitations of measurement-based approaches are described in the next section. Measurement- and simulation-based approaches to channel modeling are increasingly seen as complementary; many channel modeling studies employ both approaches.

Once the decision to collect channel measurement data has been made, whether as the primary basis for the channel model or to validate simulation results, the channel modeller must configure a suitable channel sounder. Alternative approaches are described in the next section. Important considerations include: (1) whether the channel is static or time-varying, (2) the nature of the antennas, including the manner in which the antenna pattern varies with frequency and, if applicable, the degree of mutual coupling between co-located antennas, (3) non-linearities in the transfer functions of active devices used in the instrument, especially if multi-carrier or other complex signals are used as stimulus signals, (4) the amount of phase noise in signals generated by oscillators in the system, (5) the size, weight, and transportability of the equipment, (6) the sensitivity of the equipment to the environment, especially temperature and (7) cost.

The next step is to collect the required measurement data and reduce them, i.e., extract the channel parameters of interest. Often, measurement campaigns are con- ducted in two stages, as depicted in Fig. I-2. Development runs are used to assess the performance of the channel sounder, identify potential models against which the measurement data can be reduced, and to provide an opportunity to fine-tune the instrument and the data collection protocol as required. Upon completion of the development runs, production runs are conducted in order to collect the vast amount of measurement data required to yield statistically reliable results. In order to ensure the consistency of the data set collected during production runs, changes to the equipment and/or the data collection protocol are strongly discouraged. The next step is to estimate the channel parameters and their marginal distributions, mutual correlation, relationship to environmental and design parameters and so forth. The final step is to cast the results in the form of a model useful in the analysis, design and simulation of wireless communications systems and verify that the model is consistent with the measurement data upon which it is based.

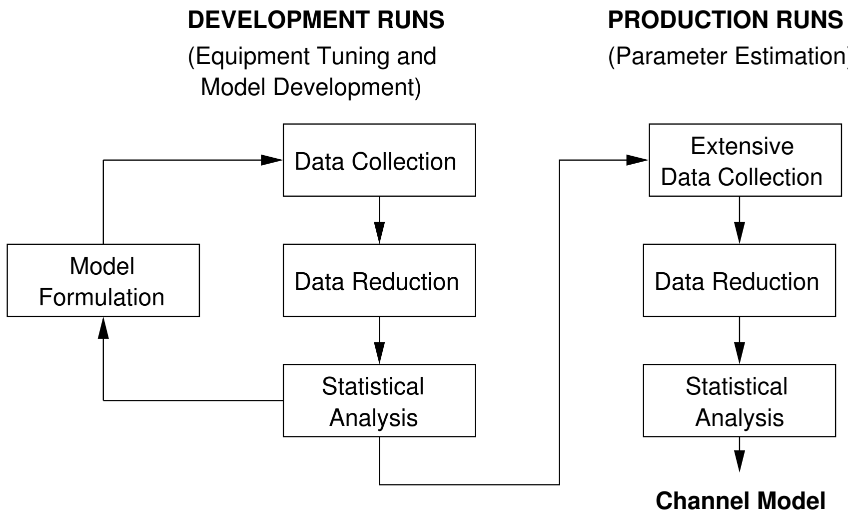

Fig. I-2 – Measurement-based Channel Modeling

2 5G WIRELESS

As the present LTE cellular frequency bands between 700 MHz and 2.6 GHz are becoming increasingly congested by a larger and more diverse set of user equipment that use increasing amounts of data, the possibility of develop 5G wireless systems that can access the GHz of bandwidth that is available in frequency bands above 6 GHz is becoming increasing attractive [1]. Many different usage scenarios, each with different challenges, have been proposed. In response, the European METIS (Mobile and wireless communication Enablers for Twenty-twenty Information Society) initiative has laid out performance upgrade targets for future 5G mobile wireless communications system by 2020. These are summarized in Table 1 [2].

Huawei and Samsung are among the leading telecommunications equipment manufacturers who have shared competing visions for 5G wireless. Huawei's vision for 5G is summarized by the "5G HyperService Cube" presented in Figure 1 [86]. Samsung's vision for 5G is summarized by the Rainbow of Requirements presented in Figure 2 [87]. Huawei's figure emphasizes the diversity of application requirements. While Samsung's 5G rainbow mentions only the "limit values" (or "high water marks") for some important KPI, the Huawei view motivates us to pursue flexibility in our 5G solutions – we want to network to adapt to the job it has to do for a given application category.

The proposed time schedule under discussion in the International Telecommunication Union (ITU) is presented in Figure 3 [88]. ITU's proposed timeline has 5G performance requirements under development in 2H2015/FY2016/1Q2017. The circular letter is the "request for proposals" that the industry (including 3GPP) will try to respond to with new RAN standard(s). High frequency channel models will be very valuable to move along the performance requirements activity. Yet, the allocation of bands to 5G may happen only in WRC 2018/2019. So various contingency scenarios have to be worked.

Table 1: METIS overall goals mapped with scenarios and its challenges [2].

Scenario		Amazingly fast	Great service in a crowd	Ubiquitous things communi-cating	Best experience follows you	Super real-time and reliable connections
Challenge		Very high data rate	Very dense crowds of users	Very low energy, cost, and a massive number of devices	Mobility	Very low latency
METIS overall goals	1000x data volume	X	X			
	10-100x data-rate	X	X		X	
	10-100x number of devices		X	X		
	10x longer battery life			X		
	5x reduced E2E latency					X

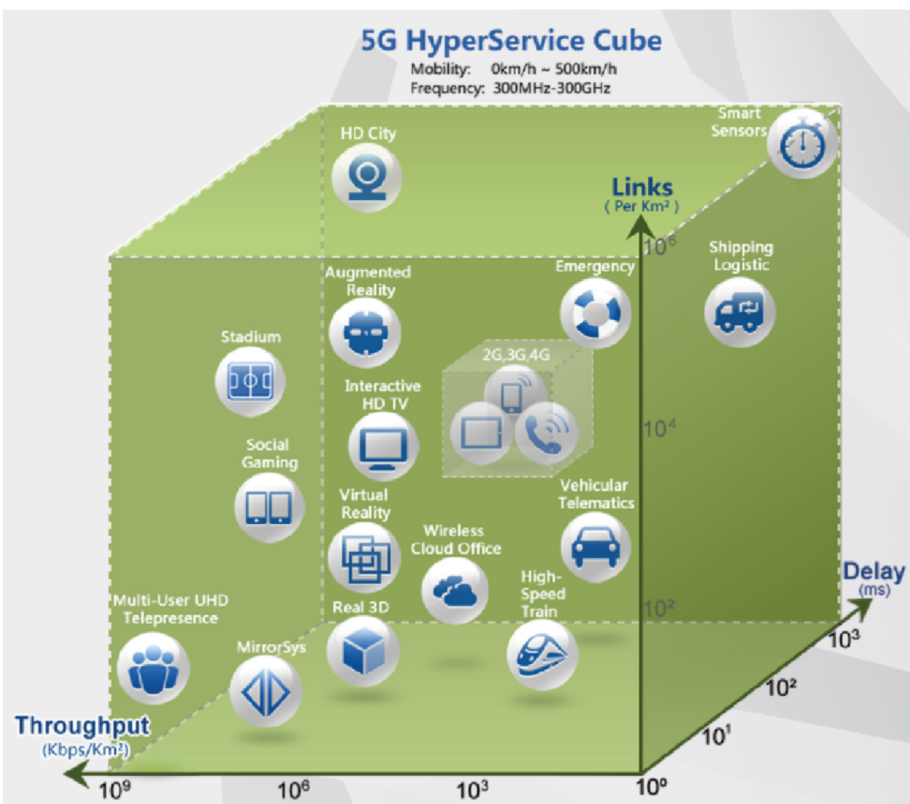

Figure 1: Huawei's 5G vision – The 5G Hypercube [86].

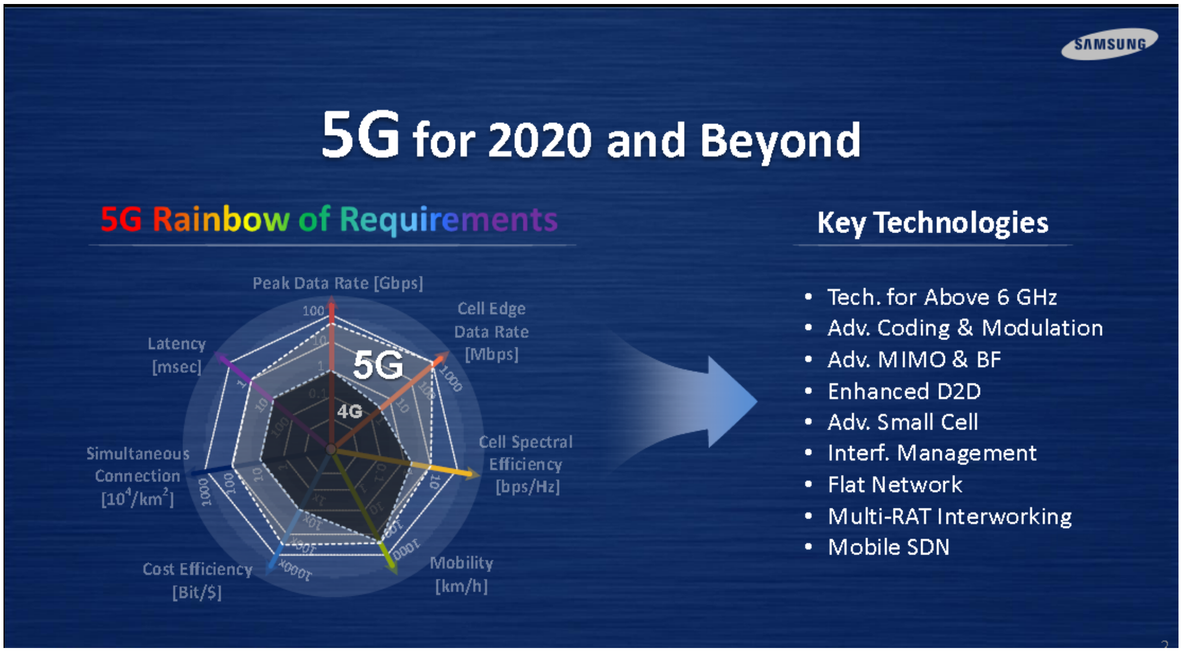

Figure 2: Samsung's 5G vision – The 5G Rainbow of Requirements [87].

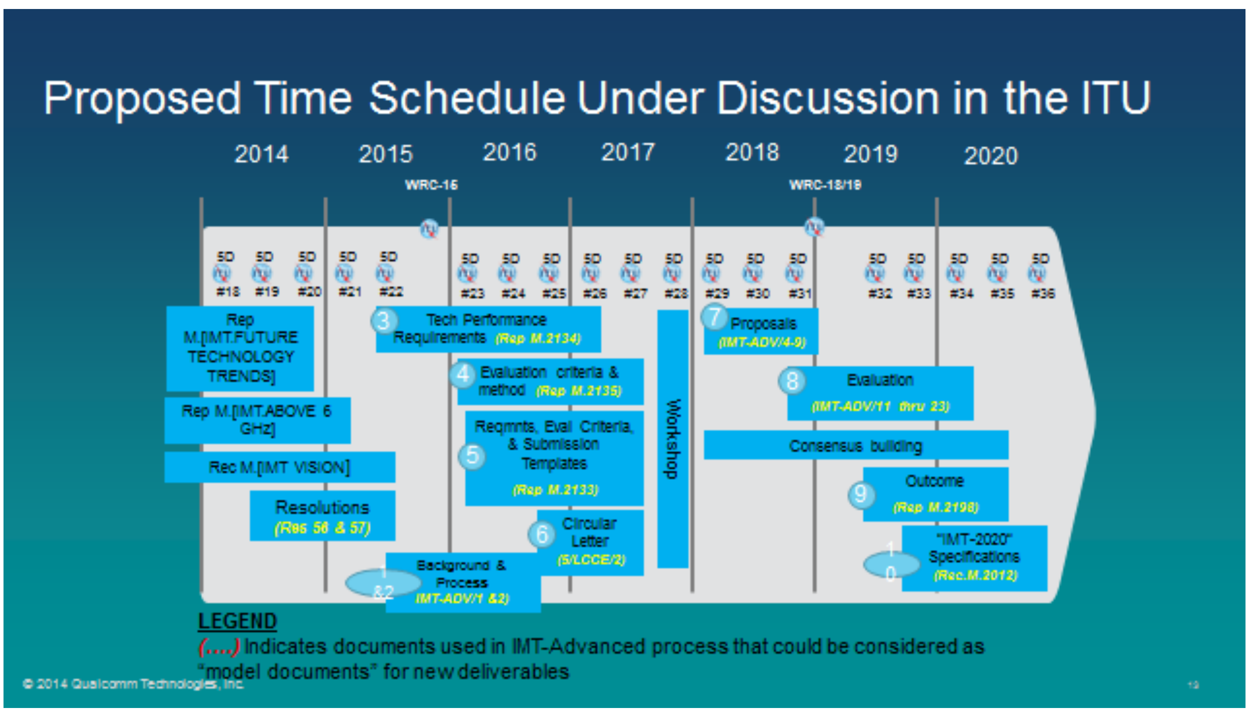

Figure 3: The proposed time schedule for 5G under development in the ITU [88].

Currently, many telecom operators are exploring the underutilized millimetre-wave (mm-wave) frequency bands such as 15 GHz, 28 GHz, 38 GHz, 60 GHz, 73 GHz, etc, for the next generation mobile network 5G [1]. These bands are less occupied by other applications and wider bandwidths are available to be allocated to each carrier. However, radio wave propagation at such higher frequencies (thus smaller wavelengths) has different physical mechanism (diffraction, reflection, scattering, refraction, absorption, penetration, etc), higher free-space path loss and building penetration loss compared to the present 4G/LTE system [3]. A series of our Wireless Insite ray-tracing simulation results in downtown Ottawa scenario throughout 2 GHz to 38 GHz (referring to Figure 4 to Figure 7 below) illustrated that, as frequency increased, diffraction over sharp edges contributed to a smaller portion of overall multipath propagation, while reflection off grounds, rooftop, and vertical walls played a major role, especially when no LOS links could be established. In addition, smaller apertures of mm-wave antennas require higher power to send and receive data [4].

2GHz With diffraction- received power

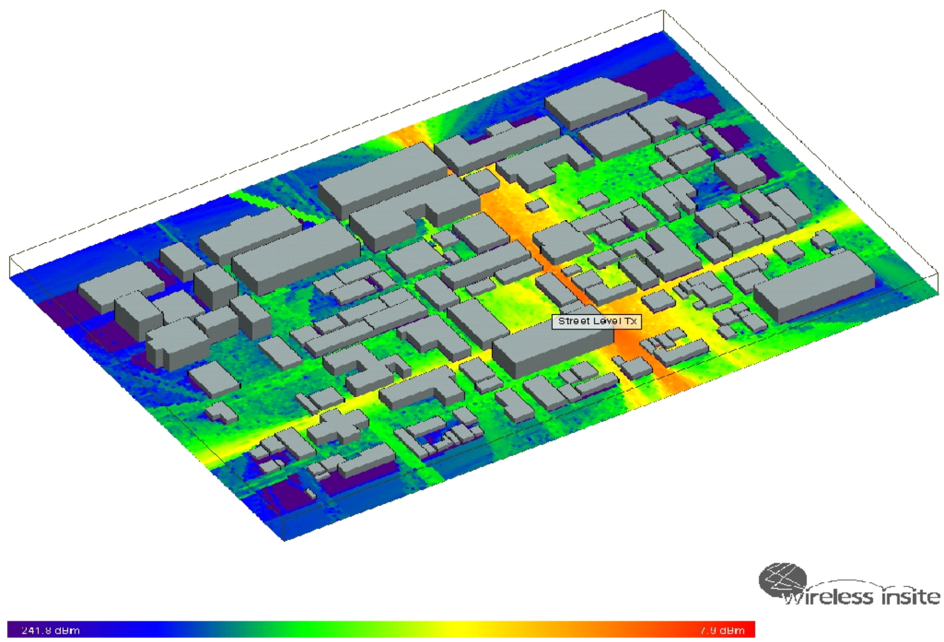

Figure 4: Received power coverage map of 2GHz with diffraction

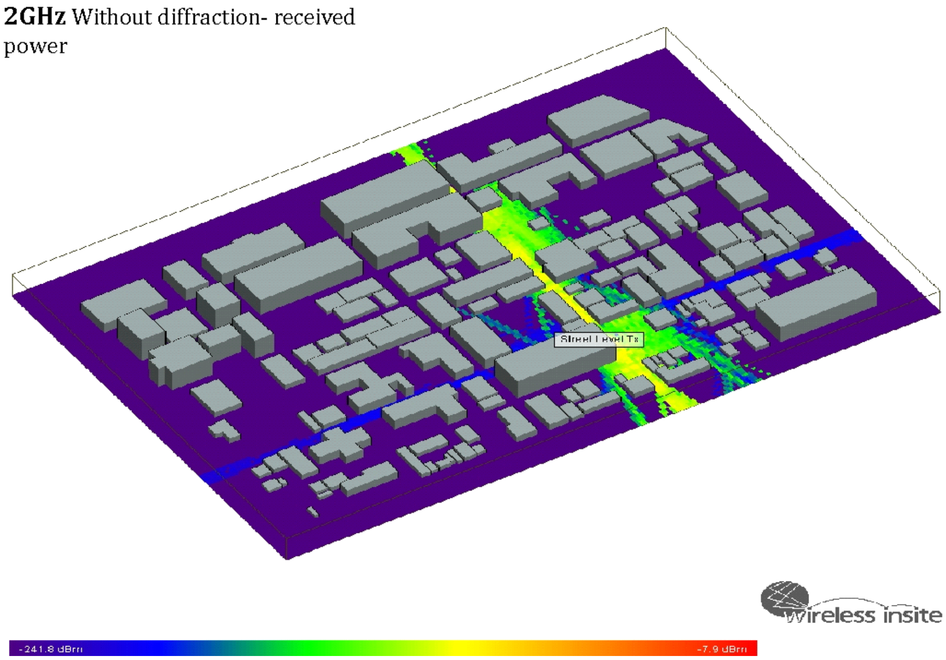

Figure 5: Received power coverage map of 2GHz without diffraction

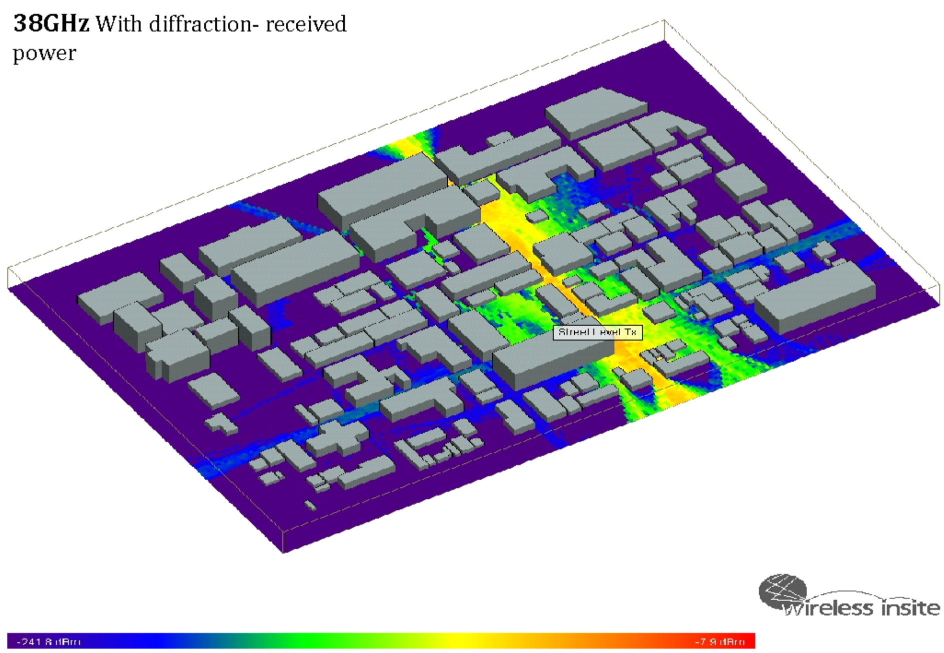

Figure 6:Received power coverage map of 28GHz with diffraction

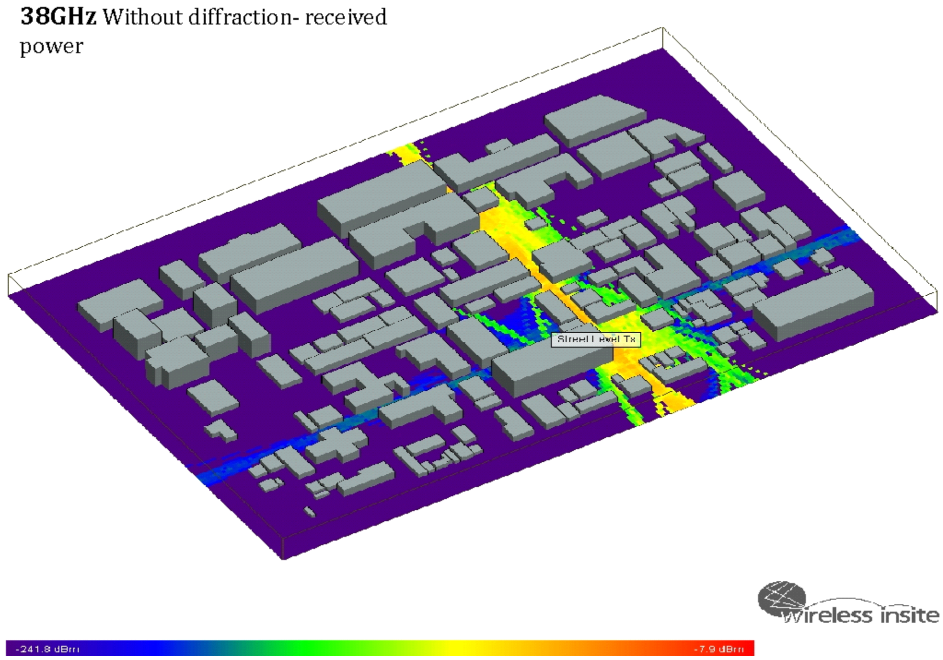

Figure 7: Received power coverage map of 28GHz without diffraction

Hence, we need to analyze and characterize the wireless propagation behaviour at these mm-wave frequencies for carriers' future base station deployment plan for optimal coverage and capacity. Antenna types, antenna heights, antenna configurations, cell ranges, line of sight (LOS) or non-line-of-sight (NLOS) transmission, geographic nature surrounding the base stations are some of the parameters that will be changing for the next major phase of mobile telecommunications standards. This change will pose a major challenge of the base station design since it will have to serve different frequency bands with different cell sites to accomplish downward/backward compatibility with 3G, 4G, LTE-A, etc. [5]

This report explores applicable papers that have investigated past works of wireless cellular communications at mm-wave frequencies under different environments such as indoor/outdoor, urban/sub-urban/rural, university campus and residential areas. Relevant past activities started as early as in the 1990s for the local multipoint distribution service (LMDS) application to release licensees for mobile cellular and backhaul [6]. LMDS focused on fixed receivers, macrocell configuration, suburban neighbourhoods, and LOS paths. Since the 2000s, there were more 5G related activities to investigate the characteristics of mobile users, microcell configuration of more compact radii, urban neighbourhoods and NLOS paths. The majority of research activities took place firstly with higher 60GHz band and later shifted down to 38 GHz, 28 GHz and 10GHz bands.

This report is structured in the following sequence. Sections 2 and 3 cover outdoor propagation measurements for macrocell and microcell network configuration, respectively. Section 4 describes indoor and outdoor-to-indoor building penetration measurement. Section 5 illustrates how presence of human activities in the path of a radio channel affects the channel. Each section first starts off with an overview of the channel characteristics for that particular environment followed by three subsections of different frequency bands in the ascending order.

The use cases, measurements parameters (such as path loss (PL), power delay profile (PDP), delay spread, etc), results and patterns will be presented in detail for the various frequency bands. Lastly, the conclusion in section 6 summarizes the milestones in the mmWave frequencies measurement for 5G and identifies the uncovered gaps and questions which need to be filled.

3 MACROCELL MEASUREMENT AND MODELS (LMDS)

3.1 Overview

This and the next section describe outdoor propagation (both transmitter and receiver antennas are placed outdoor) and past measurement researches in macrocell and microcell configuration, respectively. Mobile phone networks classify cells into macrocells and microcells based on size. Table 2 compares macrocell and microcell parameters [10].

Table 2: Typical macrocells and microcell parameters comparison [10].

Parameter	Macrocell	Microcell
Cell radius	1~20 km	0.1~1 km
Transmitter height	Above rooftop level	Below rooftop level
Transmitter power	1~10 W	0.1~1 W
Receiver height	1-2 m; below rooftop level	1-2 m; below rooftop level
Propagation mechanism	Non-line-of-sight; diffraction and scattering by rooftops	Line-of-sight and reflection from buildings
Fading	Rayleigh	Nakagami-Rice
RMS delay spread	0.1~10 us	10~100 ns
Max. bit rate	0.3 Mb/s	1 Mb/s

Macrocell configuration usually applies high radiation centerlines with antennas mounted at high points above surroundings such as ground-based masts or rooftops, covering large cell range up to tens of kilometres with high transmitter powers of tens of Watts. There are usually no LOS paths in such conditions, and signal propagates mainly by diffraction, reflection and refraction (for large cells.) Therefore, predicting average field strengths and multipath signals are difficult [11]. Many models have been proposed based on knowledge of topography, land usage and building height information. COST 231 final report summarizes modelling in urban areas, influence of vegetation, large-scale terrain effects, multipath prediction and more general models—Hata model, Ikegami model, Walfisch-Ikegami mode, etc [3].

As mentioned in section 1, early mm-wave activities started with LMDS, a broadband wireless access (BWA) networking solution in the 1990s, to offer broadband wireless access to fixed networks providing services including one-way video distribution and telephony and fully-interactive switched broadband multimedia applications [6]. LMDS operated mainly in 28, 38, and 40 GHz frequency bands with much available bandwidth. Traditional LMDS network architecture was one-layered relying on LOS transmission, thus suitable for high-rise buildings or rural areas, and repeaters and mirrors were deployed in difficult propagation measurements. Later, more flexible two-layered network (TLN) architecture was developed and it complied better with Internet traffic and capacity requirements [7]. A typical TLN architecture is shown in Figure 8 below. Layer 1 composed of wide-area macrocells supporting Layer 2 which consisted of local-area microcells [8]. A fundamental LMDS network has an omnidirectional or sectorized base station, user antennas with network interface units and/or set-top boxes, and required equipment for wide area network (WAN) interconnection including links. [9]

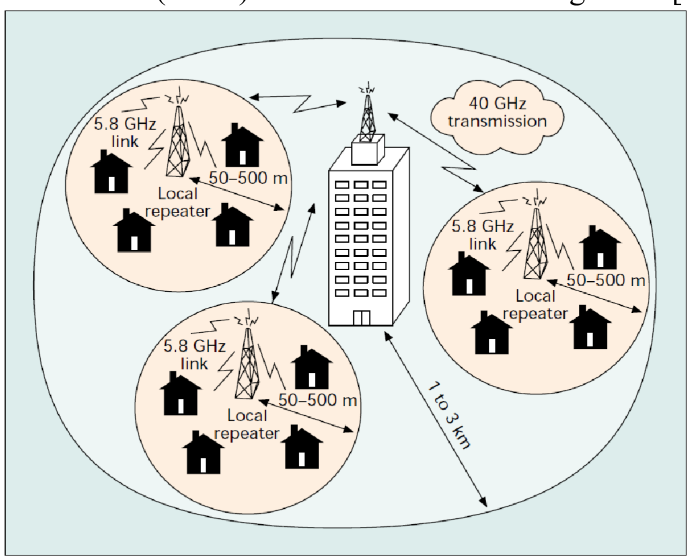

Figure 8: TLN LMDS architecture of LOS macrocells and lower-frequency microcells [7].

3.2 28~38GHz Frequency Bands

Use cases:

All macrocell mmWave activities surveyed were in the 28~38 GHz frequency range, more specifically at 28GHz [6][34-40] and two at 38GHz bands [41][42]. The LMDS application dated back in the late 1990s until early 2000s. Measurement campaign occurred at various propagation environments including urban (Singapore, Eugene, OR, and Brighton Beach, NY) [35][38][6], suburban (Singapore, San Jose and Fremont, CA, and Northglenn, CO) [35][40], and rural (Singapore)[35] outdoor use cases. With LOS, partially obstructed LOS, and NLOS paths, one can understand and characterize channel behaviours in teRMS of received power level, path loss, channel impulse response, power delay profile, delay spread, excess loss, time of arrival (TOA), angle of arrival (AOA), etc. Typical channel coverage can be ranged from the order of hundreds of meters to several kilometres. Transmitter antennas were typically mounted on a higher position than the receivers. Major impairments for LMDS system was excess path loss caused by different obstructions and attenuations. The study of propagation conditions at 28GHz band included rough surface scattering (Blacksburg, VA) [34], foliage/vegetation (Japan, Spain) [37][39], and rain/weather conditions (Turkey) [36]. Impairment studied at 38GHz band was rain/weather condition (Blacksburg, VA) [41][42]. Figure 9 shows a typical ray-tracing analysis of multipath signal trajectories in an urban scenario and its simulated PDP outcome [38].

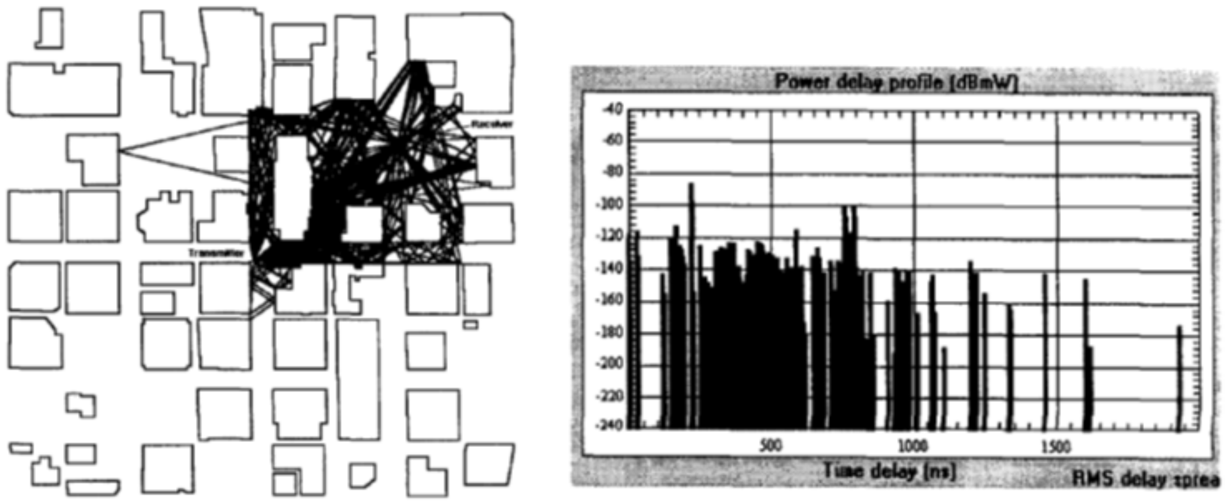

Figure 9: Multipath ray-tracing study in an urban environment and its PDP for analysis point [38].

<u>Measurement results:</u>

In [34], Dillard et al investigated rough surface scattering properties of limestone and brick walls to characterize radio paths at 28GHz involving one more bounces from these walls. They found evident diffuse scattering presence in the 28GHz LMDS band. The rougher limestone walls caused reflections which were more spread out in time than those from the smoother brick walls. Large incident angle paths could provide reasonable signal levels in shadowed area. Soma et al conducted propagation measurements in urban, suburban, and rural Singapore to develop the static & time-variant dynamic LMDS measurement-based channel impulse response (IR) models. Measurement sites include residential blocks, business centres, foliage, sport grounds, and hilly terrain to analyze attenuation by vegetation and density of buildings. Excess path loss was found the most serious propagation impairment to an operational LMDS system. Excess loss highly depended on the nature of blockage, and LOS or near LOS paths were required to achieve satisfactory coverage. Figure 10 illustrates the complimentary cumulative distribution function (CCDF) curves of the RMS delay spread for various channel types. 95% of the time delay spread lied below 10, 20ns, 40ns, and greater than 120ns for rural, suburban, typical urban areas, and high dense urban areas, respectively [35]. From the propagation measurement at residential urban environment in Brighton Beach, Brooklyn where transmitter antenna was mounted on top of a 95m apartment, receiver antenna height varied from 3 to 11.3m AGL, and multi-story apartments and 3-story or lower houses were present in the link, Seidel et al found building blockage a major impairment. Strong received signals were detected when there were direct LOS links. Sufficient signal coverage depended on the ability to provide LOS paths [6]. Anderson used a ray-tracing propagation model to investigate the dispersive nature of the transmission channel in a typical urban environment in downtown Eugene, Oregon. He characterized the channel dispersion by RMS delay spread and coherence bandwidth. Higher antenna directionality could reduce receiver's channel dispersion effectively. Moreover, proper use of stable reflection paths could help to achieve coverage to NLOS locations [38]. Elrefaie and Shakouri conducted propagation measurements at suburban Northglenn, CO, San Jose and Fremont, CA to characterize coverage with various cell size, hub antenna position and height, and nature of the measurement sites. In suburban most transmission was "near" LOS with possible obstructions such as tall trees. The largest cell-size of the three locations is located 2km away from suburban San Jose. Using 80ft antenna height, there could accomplish 80% of the coverage [40].

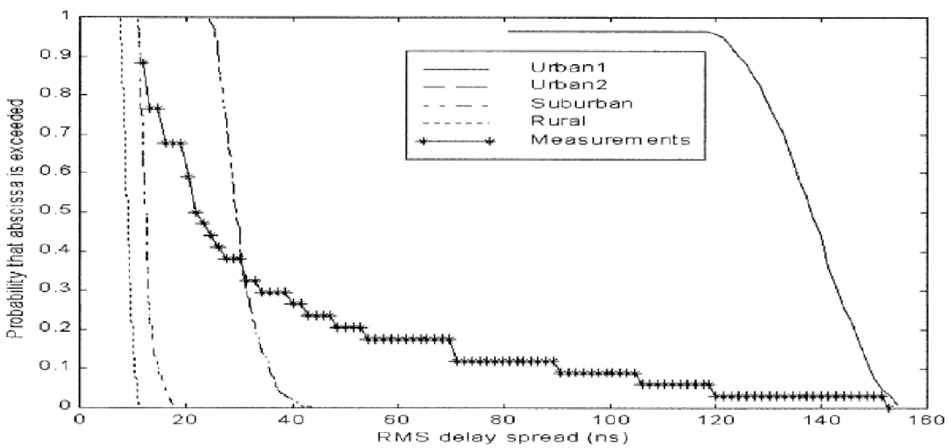

Figure 10: CCDF curves of RMS delay spread for various channel types [35].

Foliage/vegetation presence in the LMDS radio channel could attenuate the signal strength. Kajiwara investigated wet foliage attenuation as a function of azimuthal direction using summer plane and ginkgo characteristics at 29.5GHz. Results showed significant attenuation by foliage obstructing LOS paths and the logarithmic attenuation level likely fit Rician distribution where K-factor probably depended on leaf size, the total area of leaves, and humid climate. Wind blowing caused foliage swaying and resulted in significant channel fading. The fading depth depended on wind direction and velocity, tree species, foliage density, humid climate and complicated leaf structure [37]. Polo and Marti studied scattering impact of vegetation in Spain. The channel was statistically modeled using Smirnov-Kolmogorov test. Results showed a single tree canopy-induced scattering causing 19 to 26dB attenuation depending on the transmitted signal polarization as well as received antenna beamwidth. Although the LOS link was obstructed by a single tree, a high signal variability less than 10dB was still observed [39].

Propagation attenuation due to rain and various weather events were also investigated in Turkey at 26GHz [36] and in Virginia at 38GHz [41][42]. Uslu and Tekin modelled rainfall attenuation prediction recommended in ITU-R PN.838 and investigated the variation of channel obscured by rain attenuation in 7 cities representing typical climate of Turkey. They concluded rainfall was the main component of the path loss for wireless communication systems which operating above 10 GHz. It was rain drops which caused attenuation effects in signal like absorption and scattering. Some regions calculated as high as 3 dB rain attenuation. Rain attenuation depended on shape & size distribution of rain drops as well as on temperature, angle and velocity of rainfall, and rain rate [36]. Xu et al studied 38GHz wideband (200MHz RF bandwidth), short-hop mmWave point-to-multipoint radio links under various weather events to determine multipath and time varying channel behaviour. Measurement took place on 3 links across Virginia Polytech campus: a 605 m unobstructed LOS path, a 262 m obstructed path due to dense canopy of a large oak tree and a 262 m partially obstructed path due to nearby oak tree that would obstruct the LOS path during windy conditions. Results showed following trends and conclusions referring to the summary as Table 3. Multipath could occur due to the foliage and reflection from wet surfaces during rain. Multipath was observed in unobstructed LOS links during rain but not during clear weather. Measured rain attenuation exceeded Crane model prediction by several dB. Specular reflection could increase by as much as 6.8dB when the surface was wet. Attenuation measurement showed 17dB attenuation through dense canopy of an oak tree, and 25.5dB thru a double-pane, tempered, and tinted window glass. A novel prediction technique was presented that applied canonical antenna patterns and site specific info to estimate worst case multipath channel characteristics including relative power, TOA, AOA of each multipath component. New metrics, excess delay zone and relative power zone were defined and contour plots are developed to determine potential reflectors from an area site map [41][42].

Table 3: Summary of multipath occurrence and maximum observed multipath level at 38GHz wideband point-to-multipoint channels under different weather events [41].

Link	Date	R(mm/h)	# PDPs	% of PDPs with multipath > ΔP					Max MP
Threshold: $\Delta P = P_{MP} - P_{LOS}$(dB)				-10	-12	-14	-16	-18	(dB)
L1	4/23	clear	190	0	0	0	0	0	<-18
		0–15.2	100	0	0	0	0	0	<-18
	5/1	0–39.6	60	1.7	53	67	67	67	-9.1
		hail	58	1.7	1.7	1.7	1.7	6.9	-5.2
	5/3	clear	10	0	0	0	0	0	<-18
		0–45.7	620	0	0	0	3.7	27	-14.2
L2	5/27	clear	4400	0.068	0.14	0.20	1	27	-9.0
		0–15.2	3000	0.83	2.4	8.6	21	28	-9.3
L3	5/30	clear	800	0.25	0.25	0.25	0.25	21.8	-4.5
		0–15.2	8350	0.08	0.12	0.74	7.7	21	-4.75
	6/2	clear	7550	0.066	0.066	0.066	0.12	0.49	-3.1
		0–213.4	16850	0.17	0.22	0.81	4.7	17.6	-2.6
	6/3	clear	2000	0.05	0.05	0.55	11	52	-6.9
		0–45.72	4300	0.047	0.047	0.12	1.8	11	-1.4

4 MICROCELL MEASUREMENT AND MODELS

4.1 Overview

Macrocells covering ranges of several kilometres inevitably leave coverage gaps/holes and can be overloaded by data traffic especially during peak hours. Microcell system with smaller cell sizes is an attractive solution to improve the coverage and capacity for future 5G cellular communication system. It accommodates more subscribers in a service area with frequency reuse over short distances. It also allows access by low-power portables and cheaper infrastructure. Today microcells are extensively used in IS-95, OCS, DCS, GSM, DECT, etc. These microcells are mainly tested in urban area with dense concentration of cellular mobile users, where strong multipath propagation is present [10][11]. Future 5G mm-wave cellular communication systems will also likely apply microcell configuration with a measured achievable 200m cell radius from the outage study in Austin, Texas and New York [1][12][13].

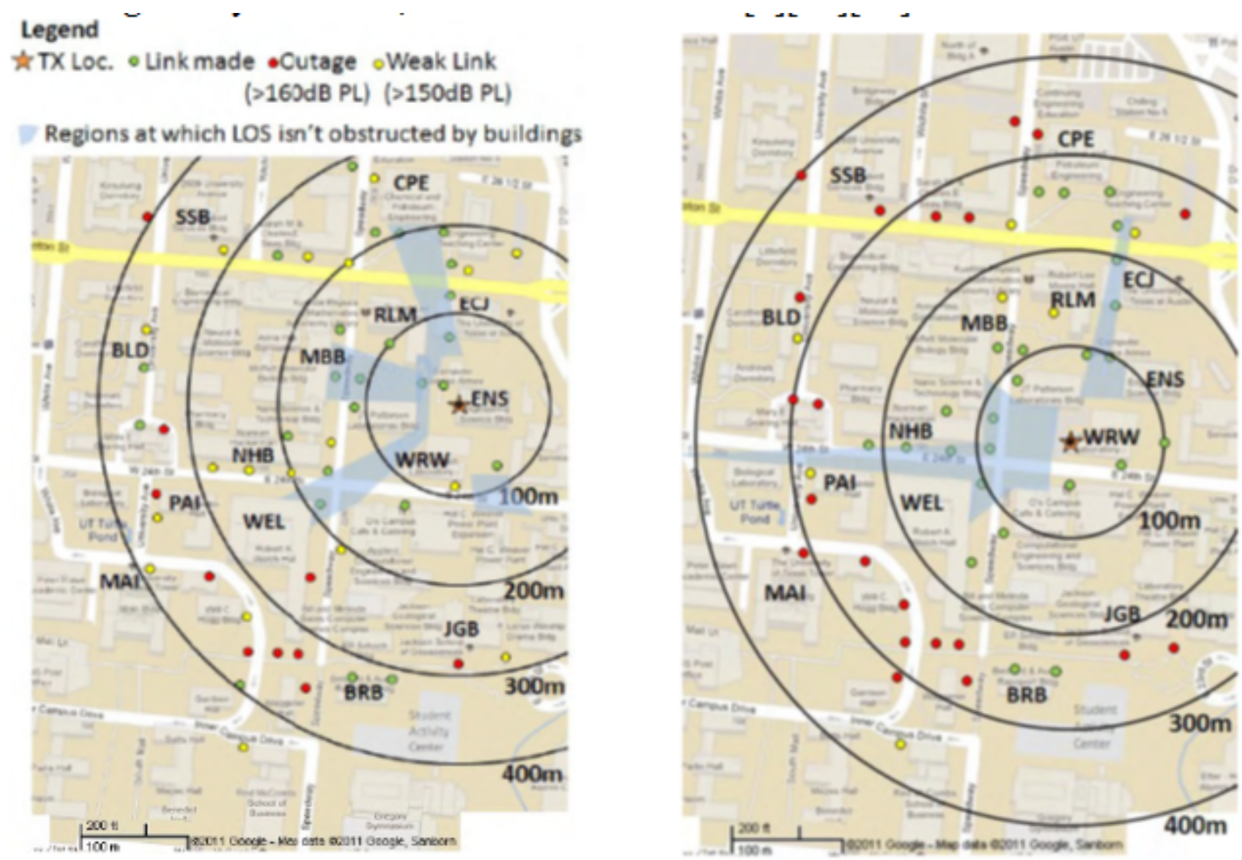

Figure 11: Outage study at University of Texas at Austin, transmitter at a) ENS, b) WRW[12]

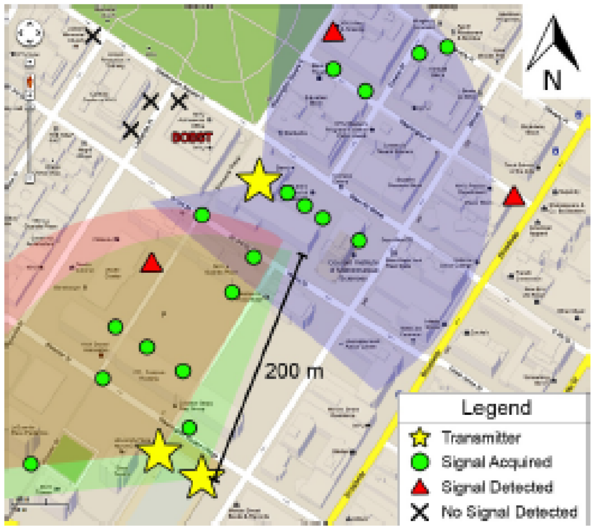

Figure 12: Outage study at Manhattan New York [13].

Microcell propagation differed from macrocell significantly with milder propagation characteristics due to shorter cell coverage plus lower transmitted power and lower antenna height [10]. A microcell base station antenna is typically between 3 to 6m above ground level (AGL) which is about the same height as a street lamppost. In some cases, antennas are mounted at a similar height on the side of a building but usually below the rooftops of surrounding buildings as shown in Figure 13. Coverage range and shape depend mostly on specific locations and electrical characteristics of surrounding buildings [3][10][11][14]. Microcell propagation mechanisms are mainly free space propagation, multiple reflection and scattering within the cell's desired coverage area. At lower frequencies, diffraction over rooftops and around building edges are crucial when determining interference between co-channel cells [14]. The multipath delay spread and shallow fading are smaller compared to macrocell, indicating a feasible broadband signal transmission without excessive counter-measure techniques required for multipath fading [10]. COST 231 developed microcell propagation models based on theoretical and empirical approaches, proposing ray optical methods with simplified analytical solutions or pure ray tracing simulation. Two- and three-dimensional prediction models are classified according to base station antenna heights. Table 4 provides a summary of these prediction models [3].

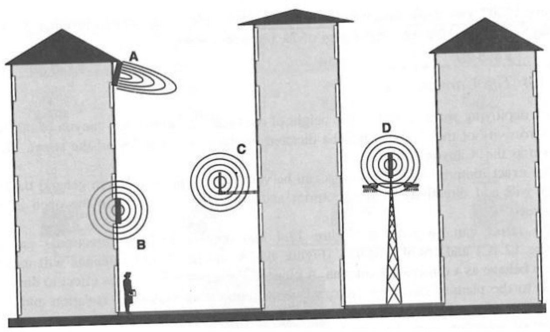

Figure 13: Examples of applicable antenna locations for microcell deployment [15].

Table 4: An overview of small- and microcell prediction models [3].

prediction model	method	features/restrictions	terrain data	results
Uni-Lund (S)	empirical	BS below roof-top	2D building layout	path loss
CNET micro cell model (F)	analyt. LOS + NLOS model	2D (horizontal plane) + 2D (over-roof-top)	2D building layout	path loss
RT - Swiss Telecom PTT (CH)	ray tracing	2D (horizontal plane)	2D building layout	path loss and CIR
Uni. Geneva / Swiss Telecom PTT(CH)	TLM like	2D (plane)	2D building layout	path loss
2D-URBAN-PICO Uni. Karlsruhe (D)	ray launching	2D (horizontal plane)	2D building layout	path loss and CIR
Telekom (D)	analyt. LOS +NLOS model	2D (horizontal plane) + 2D (over-roof-top)	2D building layout	path loss
Ericsson (S)	ray tracing + COST-WI	2D (horizontal plane) +2D (over-roof-top)	2D building layout	path loss
COST-231 small-cell	Walfisch-Ikegami mod.	2D (over-roof-top)	building classes	path loss
Uni. Valencia (ES)	Walfisch-Bertoni mod.	2D (vertical plane) + 3D reflections at Rx	2D building layout + building height	path loss, FS distribution
MCOR - Swiss Telecom PTT (CH)	modified Deygout	2D (over-roof-top)	2D building layout + building height	path loss
CSELT (I)	Deygout	2D (over-roof-top) BS above roof-top	3D raster data	path loss
CNET ray launching model (F)	ray launching	3D (no diffraction at vertical wedges)	3D building layout	path loss and CIR
ASCOM-ETH (CH)	Ray-tracing by image source	3D, only reflections	2D building layout + building height	path loss and CIR
Villa Griffone Lab, Bologna (I)	ray tracing; Saunders-Bonar	transverse plane + ground reflection; 2D (over-roof-top)	2D building layout + building height	path loss and CIR
Uni. Stuttgart (D)	ray launching + W/I model for 2D case =>	3D (2 diffr. + 6 reflec. processes); 2D (vertical plane)	2D building layout + building height	path loss and CIR
3D-URBAN-MICRO Uni. Karlsruhe (D)	ray tracing	2D (transverse plane) 3D surface scatter	2D building layout + building height or raster data	path loss and CIR

In [89] [90], Heath et al studied full system (multi-cell, multi base stations) coverage and capacity of mmWave cellular channels focusing on its limited scattering nature and narrow beamforming of linearly steerable antenna arrays, i.e., highly directional MIMO transmission. The transmitter and receiver of the mmWave systems employed large arrays to ensure enough array gain to provide high data rate communication. The cellular network model applied stochastic geometry (capable of obtaining closed form solutions for available coverage probability) for mmWave cellular analysis, in which base stations were distributed as an independent two-dimensional homogenous Poisson point process (PPP) and buildings were modelled by the random shape theory as rectangle Boolean scheme. Number of points was a Poisson random variable with mean λS, and each point was assigned an independent and identically distributed (i.i.d) random variable forming a marked PPP. The advantage of PPP is that it is the simplest point process, and useful results such as Campbell's Theorem and Displacement Theorem can apply.

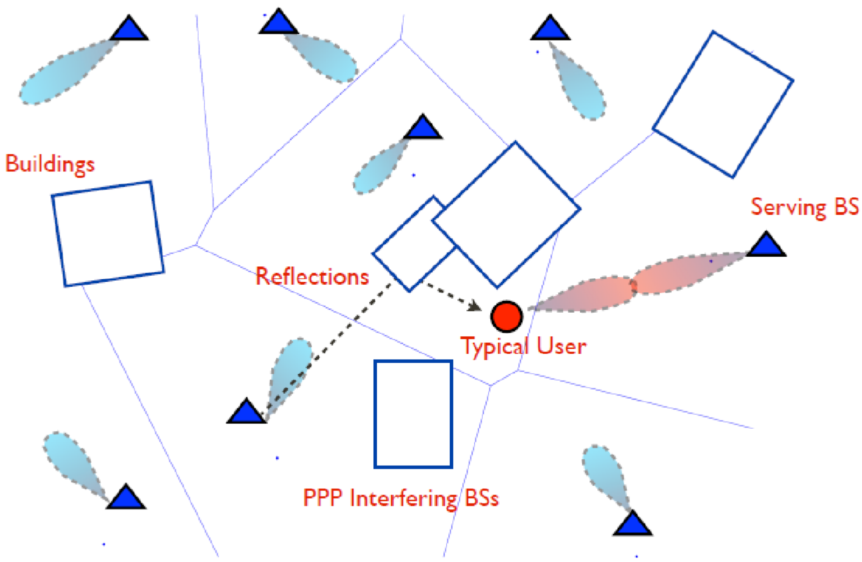

Figure 14: mmWave model proposed by Heath et al [89].

Figure 14 portrays Heath et al's proposed full system channel simulation model [89]. This model considered both LOS and NLOS links where penetration and reflections, respectively, were prime propagation behaviours. Diffraction and generally small scale fading were neglected since these parameters were usually minor at mmWave frequencies. The LOS link probability was calculated according to the building model where number of blockages on the path was also a Poisson random variable. This resulted in the probability of a clear LOS without any blockage to be. The system parameters consisted of different path loss models in dB for LOS and NLOS links, respectively, PL1=C+20logR(m) and PL2=C+K+40logR(m), where C=50dB and K=10dB for 28GHz system. The link budget specified transmitter antenna input power of 30dBm, a signal bandwidth of 500MHz and a noise figure of 5dB.

The coverage probability was analyzed by base stations through examining the complementary cumulative distribution function (CCDF) of SINR, P[SINR>T]; the probability that a randomly chosen user in the cell had an instantaneous threshold SINR greater than some target T. For single user systems in which each base station served only one user per cell, the only source of interference came from inter-cell interference. In multi-user systems, intra-cell interference was present as well as inter-cell interference. From simulation results, performance of mmWave systems was compared to microwave systems and the following trends were observed: 1) Large arrays resulted in better coverage probability (referring to Figure 15). 2)

Higher density increased coverage probability (referring to Figure 16). 3) Coverage probability differed in LOS and NLOS (referring to Figure 17). 4) Reflections improved coverage probability especially in shadowed areas (referring to Figure 18). 5) Coverage probability of mmWave system was comparable to microwave system. In other words, both systems could accomplish comparable spectral efficiency. However, mmWave has much broader available bandwidth of 1GHz compared to present cellular systems transmissions bandwidth of 20MHz, resulting in a much higher average per-user rate in mmWave systems, as shown in the cell throughput comparison in Figure 19 [89].

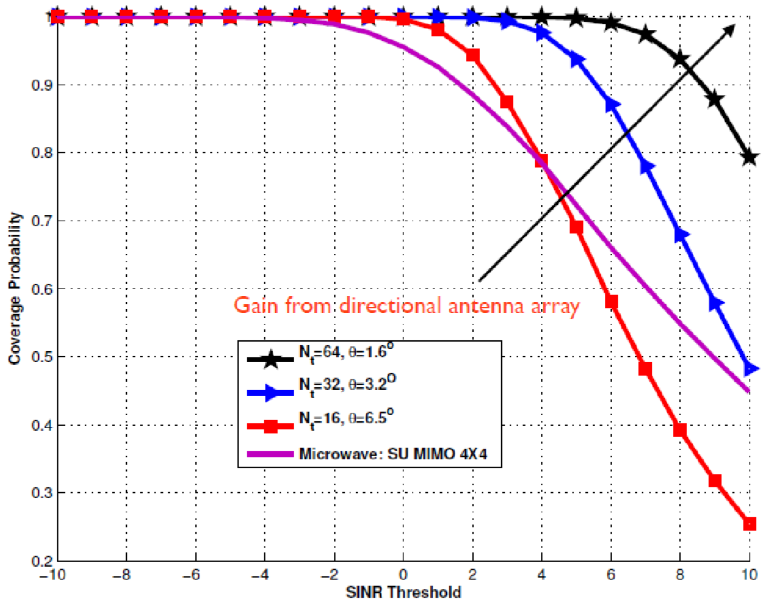

Figure 15: Coverage gain from large antenna arrays; mobile user 16 antennas, BS density 200m, buildings cover 5% of land area, and average building size was 15m by 15m [89].

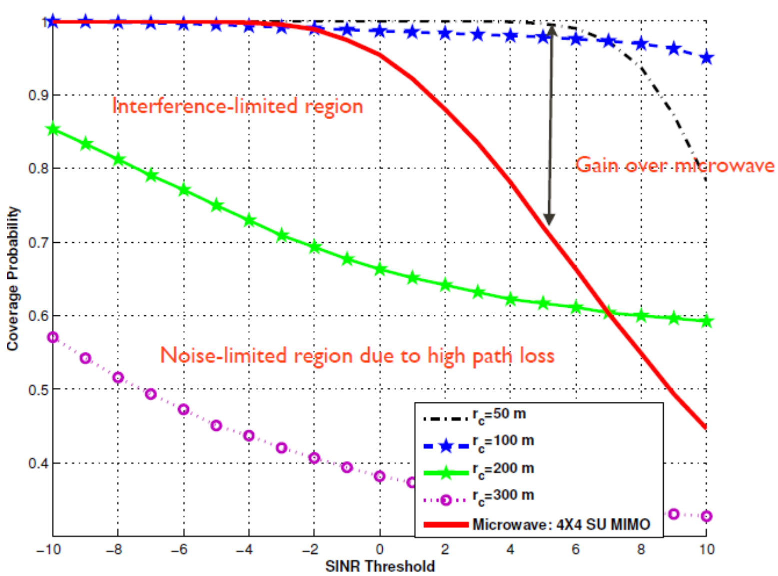

Figure 16: Coverage gain from higher density; 32 BS antennas, and propagation blockages cover 10% of land area [89].

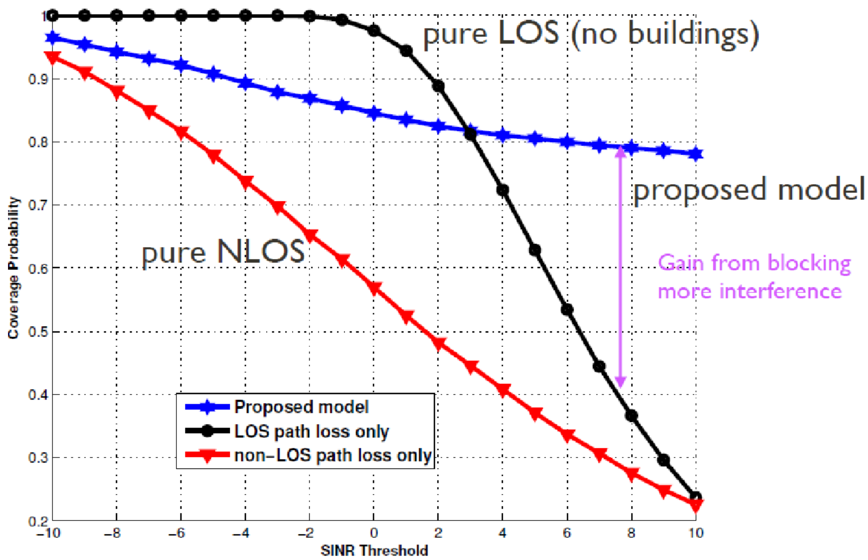

Figure 17: LOS & NLOS Path Loss; 32 BS antennas, propagation blockages covers 10% of land area, and BS density was 100m [89].

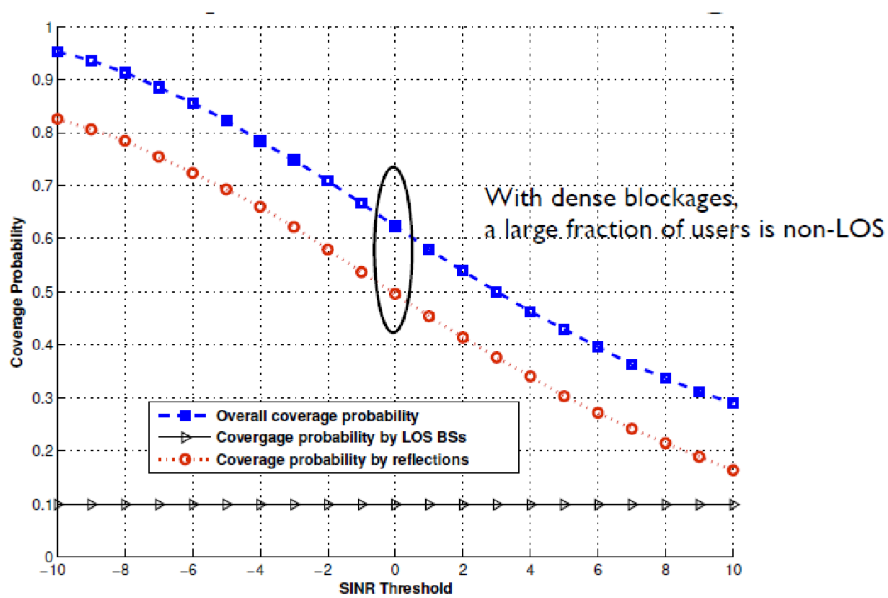

Figure 18: Reflections improve coverage; 128 BS antennas, blockages cover 30% land area representing heavy shadowing scenario, and BS density was 200m [89].

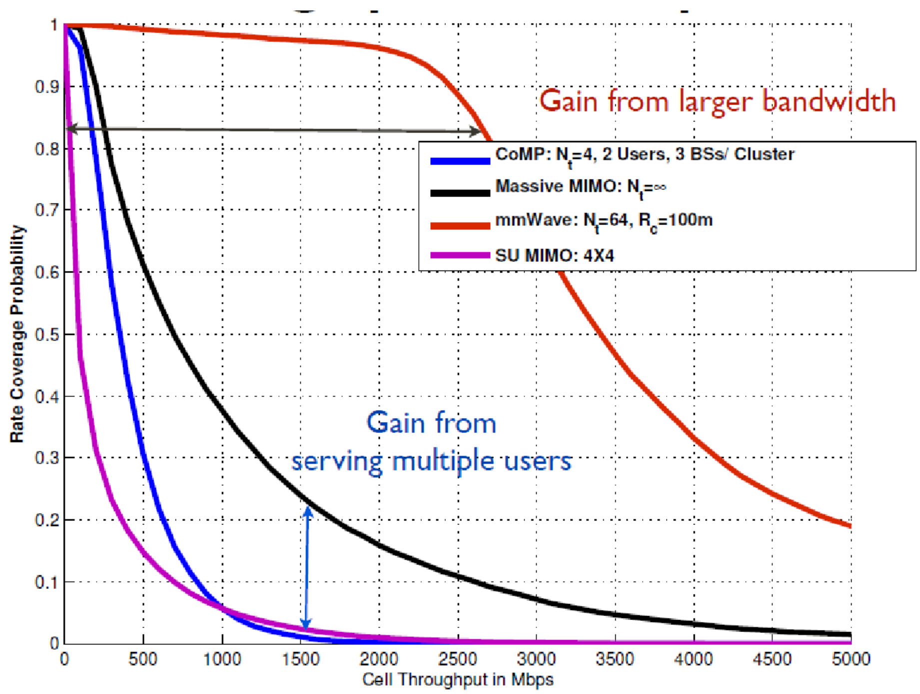

Figure 19: Cell throughput comparisons; mmWave can support much higher data rate [89].

4.2 6~20 GHz Frequency Bands

Use cases:

For mmWave frequency range of 6 to 20 GHz, outdoor microcell propagation measurement originated in the early 1990s throughout mid-2000s for future broadband mobile communications. This section presents five articles representing propagation characteristics in typical urban (Boston, MA, Yokohoma and Kuramae and Chiyoda, Japan, Tokyo, Japan, Denver, CO, New York City, NY) [45-49], suburban (Boston, MA, R.ed Bank, NY)[45][49] and rural (Mariboro and Sandy Hook, NY) [49] environments that includes both LOS and NLOS paths with transmitter and receiver separation distance ranging from 100m [46] up to 1.5km [48]. In fact, all five papers covered urban areas with density of building and mobile users, while only two papers covered suburban and one paper covered rural area. The main target of microcell deployment in most papers is to enhance coverage and capacity in the urban scenario as discussed in section 3.1. A typical downtown urban city such as New York or Tokyo has tall buildings lining the streets, extending in length to an entire city block, forming a “street canyon” character [47][49]. Four of these papers examined street level propagation [46-49]. In [46][48][49] receiver antennas were mounted on vehicles roof approximately 2~3m AGL height, driven along the roads around the transmitter base station antennas. Transmitter antennas height varied in each article— in [48] the transmitter was mounted on a vehicle, whereas in [45] the transmitter height was below the surrounding buildings’ rooftop. In [46], the transmitter base station antenna was on a steel tower of 80m and 117m tall and on a building rooftop of 35m and 38m tall. In [47] the transmitter base station height was 40m while the average surrounding buildings had a height of around 20m. In [49] the transmitter antenna was placed at the side of the street about 9m AGL simulating lamp posts or utility pole mountings. The common measurement parameter in all these papers was path loss [45-47] or received power level

[48][49]. In [47], AOA and TOA of multipath components were studied for various transmitter and receiver antennas pointing angles. In [48], the channel impulse response was recorded for fading characteristics and the bit-error-rate (BER) data indicated channel performance. RMS delay spread was estimated using a six-ray model in [49] to facilitate the offering of higher digital signaling rates and wider bandwidth. Figure 20 and Figure 21 show the geometry for ray-tracing in both the urban and rural areas.

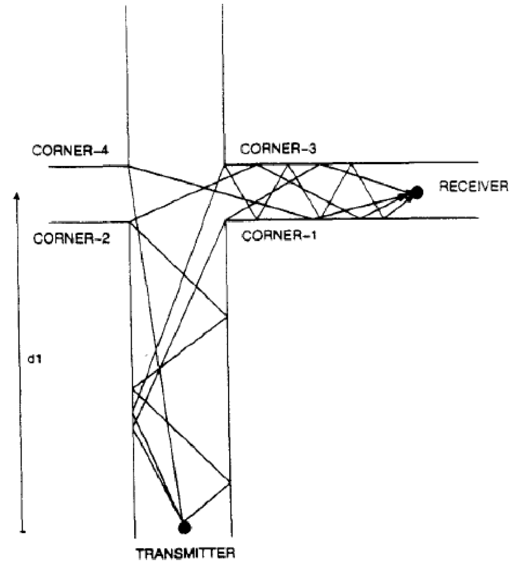

Figure 20: Street geometry ray-tracing with reflection and diffraction in urban NLOS environment [45].

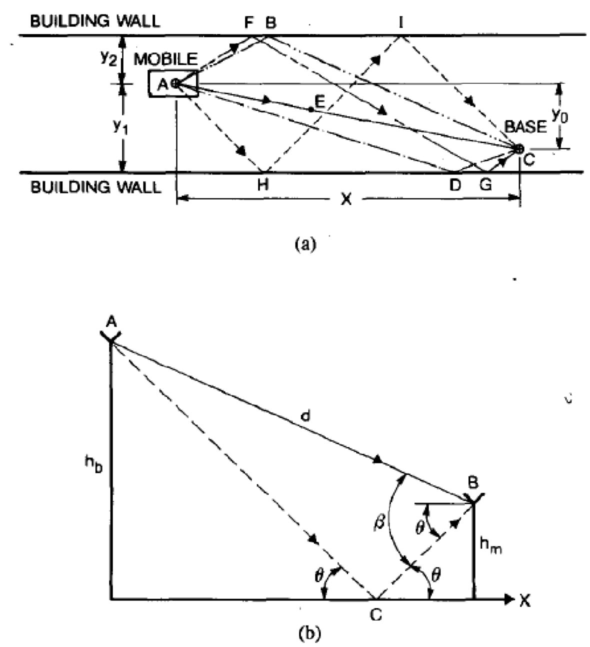

Figure 21: Ray-tracing geometry in a) Urban area: 6-ray model, b) Rural area: 2-ray model [49].

Measurement results:

Erceg et al from AT&T Bell Lab predicted the spatial average of signal strength in typical rectilinear street environment using ray theory and uniform geometrical theory of diffraction (UTD) [45]. Path loss data was collected in Boston, MA at 6GHz and compared to theoretical model. It was found that Sum-of-Individual -Ray-Powers method should be used. In [46], Kitao and Ichitsubo proposed a path loss prediction formula for an urban microcell based on multiple regression analysis of the measured path loss as a function of frequency (up to 8.45GHz), distance and BS height in 3 Japanese cities which included Yokohama, Kuramae and Chiyoda. Their proposed prediction formula and applicable range is present on Table 5 [46].

Table 5: Proposed path loss prediction and its applicable range

Proposed formula	
$Loss = 42.7\log(d) - 32.7\log(H_b) + 20.7\log(f) + 55.4$ [dB]	
Applicable range	
Distance	100–1000 m
Frequency	0.4–8 GHz
BS antenna height	30–120 m
MS antenna height	1.5 m
Area	Urban area

In [47], Oda et al from NTT DoCoMO Inc proposed geometrically based propagation model for an urban mobile environment establishing a relationship between AOA and TOA of multipath components at 5.2 GHz (with measured bandwidth set to 100MHz) in Tokyo, Japan. Most previous models were based on circular or elliptic reflective areas which were applied more for suburban areas. A more realistic model was established by using propagation characteristics of a street-microcell around the mobile station receiver antenna. The angle distribution of multipath components was simulated simply by using the approximate path loss models. The geometry of the proposed model is shown in Figure 22.

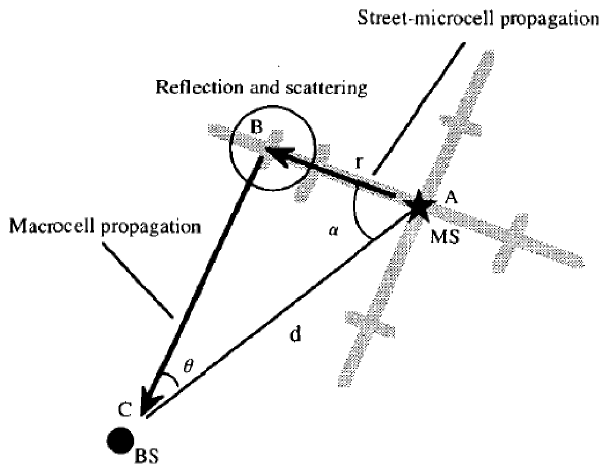

Figure 22: Geometry of proposed geometrically based propagation model for an urban mobile environment [47].

Another urban street level propagation measurement on point-to-point transmission was carried out in downtown Denver, CO by Violette et al [48]. Two narrowband and broadband operating systems covering various frequencies including 9.6 and 11.4 GHz were used to determine characteristics of signals propagated through, around, and reflected from 4 buildings and other common urban structures in NLOS and LOS paths. Collected data parameters included receiver power, CIR with 1ns or smaller resolution, and BER at 500Mbps pseudorandom binary sequence (PRBS) transmission rate. These parameters were recorded as functions of path length, antenna height, antenna polarization, and antenna bandwidth. Table 6 summarized received power levels under different scenarios. For NLOS paths, we see signal attenuation over 100dB. Propagation loss depended on the material of path obstruction. The attenuation was small for clear glass walls, but once the glass wall had metalized coating to prevent ultraviolet or infrared radiation it increased by 25 to 50dB per coating layer. No signals were detected through steel reinforced concrete or brick buildings in most cases, unless a single or double edge diffraction mode from a roof was used, with a resulting coherent bandwidth tens of MHz based on the received signal delay spread. System gain and coherent bandwidth improved with directional antenna of narrower beamwidths. For LOS street level channel, reflection is a major propagation mechanism due to confined surroundings and presence of many obstructions and scatter objects with flat surfaces including buildings, roadways, sign, cars, trucks, etc in urban cities. Reflection coefficient of building walls at normal incidence was measured to be equal or smaller than -0.2, and reduced to near -1 at very shallow angle of incidence. Multipath signals reflected from street surfaces generated over 30dB of fades even when using directional antenna with narrow beamwidth of 2.3° positioned 2 to 3m AGL. The delay time difference was always smaller than 1ns due to narrow angle between the street reflection path and direct LOS path. Such low multipath signal delay times translated to low channel distortion and large available bandwidth greater than 500MHz, which would be very favourable for 5G application. Measurement results from Denver suggested a rule of thumb that the antenna 3dB beamwidth be twice the expected antenna pointing error for near optimum channel performance of an urban street level channel operating with highly directional antennas. Less directional antennas with wider beamwidths of

30° were also used in this campaign. This caused the delay time difference to increase up 10ns, supporting a narrower bandwidth of about 10MHz [48].

Table 6: Received power levels under different obstructed paths in Denver, CO [48].

Building #/ Test #	Construction Type	Antenna Pointing	Building Width/Height (Meters)	Path Length (Meters)	Received Signal (Level of dBm) Frequency (GHz) 9.6	28.8	57.6
1 A	Solid Cement-Block Walls	Direct	17/6	42	-107	<-132	<-132
1 B	"	"	"	• 53	- 87	-130	<-132
1 C	"	"	"	+ 90	- 92	- 98	-113
1 D	"	Toward Roof Edge	"	+ 53	- 80	- 80	- 93
2 A	Solid Pre-Cast Concrete	Direct	100/7	200	<-132	<-132	<-132
2 B	"	Toward Roof Edge	"	"	-113	-117	-132
2 C	"	"	"	+ 260	-104	-104	-130
3 A	Brick w/ Windows	Direct	40/16	120	-113	-130	<-132
3 B	"	Toward Roof Edge	"	"	-104	-114	-127
4A	Chromatic Glass	Direct	53/9	72	- 88	- 90	-107

Propagation measurement at rural (Mariboro and Sandy Hook, NJ), suburban (Red Bank, NJ), and urban (New York City) environments for LOS mobile and personal communications at 11GHz was conducted by Urstako et al from AT&T Bell Lab [49]. Mean received power was measured and RMS delay spread was estimated based on "dielectric canyon" model composed of the road and some of the wall reflected rays. They found that propagation was dominated by interference between the direct LOS ray and a specular roadway-reflected ray in rural LOS microcell environments. For suburban environment, they observed the mean received power decayed with distance from the base station slower than $\frac{1}{r^2}\frac{1}{r^2}$, where r denotes the distance. This finding was consistent with rural and urban environments. Measurement results supported the two-ray model as Figure 21 b) for approximation of the basic propagation characteristics. For urban areas, when using omnidirectional antennas, the RMS delay spread was smaller than 20ns obtained from a six-ray model as Figure 21 a), but was lowered to less than 5ns when the receiver used a directional horn of 20dBi gain. In [48], the low RMS delay spread would facilitate relatively high digital signaling rates and offer wider bandwidth services for 5G communications.

4.3 28~38GHz Frequency Bands

Use cases:

Most mmWave propagation measurements in this frequency range of 28 to 38GHz for future 5G broadband cellular communication networks were very recent. One advantage of 28 GHz and 38GHz mmWave bands is that atmospheric absorption is not as severe as higher bands such as 60GHz [13], and each are allocated with over 1GHz of bandwidth available currently [1], so 28GHz and 38GHz bands are ideal for outdoor mobile communication networks. These bands were originally allocated for LMDS application in the late 1990s, and could be issued licensees for mobile cellular and backhaul networks in the future [6].This section discusses about sixteen articles characterizing propagation of mmWave channels, majority of which were published after 2010 and focused on urban environments with LOS, partially obstructed LOS, and NLOS links—eight papers on 28GHz band [13][52-54][56-59], five papers on 38GHz band [12][60-63], and three papers on both bands [1][55][64].

Measurement campaigns taken at 28GHz band were conducted in New York City in 2012 by Polytechnic Institute of New York University [1][13][52-55][58], India [56], Denver (at multiple frequencies as already described in section 3.2) [48], and Samsung Telecommunications America [64]. Measurement campaigns at 38GHz occurred at Austin, Texas by University of Texas at Austin [1][12][60-62], China [63], Denver (at multiple frequencies as already described in section 3.2) [48], and Samsung Telecommunications America [64]. These measurement campaigns were intended for gaining insight on propagation characteristics for the design of future mmWave cellular systems by collecting, estimating and analyzing data parameters in teRMS as PL, CIR/PDP, AOA, AOD, RMS delay spread, frequency correlation functions (FCF), cell coverage area, rain attenuation, channel capacity, building penetration and reflectivity, etc.

Figure 23 portrays the 28 GHz measurement environment in New York City, which represents a typical urban area including parks, commercial districts, and general university areas with high rise buildings, dense pedestrian and vehicular traffic [13] [52]. New York City will be a likely city for initial deployments of mmWave cellular systems because of high user density. The urban canyon environment with difficulty in establishing LOS links is a key concern for mmWave cellular [58]. One transmitter and 11 receiver measurement locations selected at NYU-Poly campus in Brooklyn with channel range of 75 to 125m. Three transmitters (two on a building rooftop 7m AGL and one on a 5-story building balcony 17m AGL) and 25 receiver (the same set for each transmitter location) locations were selected randomly based on AC power availability in NYU campus in Manhattan with channel range of 19m to 425m, emulating 5G cellular base stations deployment with relatively short ranges and low heights [1][13]. At all Brooklyn test locations, the receiver antenna moved automatically on a linear track of 107mm (10 wavelengths) in increments of 5.35mm (half wavelength) to analyze small scale fading. PDPs were capture using a 400Mcps sliding correlator channel sounder while a full circular antenna sweep in the azimuth plane was performed at each track position in steps of the beamwidth of the antenna, in this case either 10° for a 24.5dBi narrow-beam horn or 30° for a 15dBi wide-beam horn, for AOD and AOA analysis to investigate beamforming at the base station which would significantly increase signal-to-interference ratio (SIR) at the targeting mobile receiver [52][54]. For all remaining test locations large scale propagation characteristics were observed using 24.5dBi narrow-beam horn antennas at three transmitter azimuth angles (-5°, 0°, and +5° from boresight to receiver) and three receiver elevation angels (-20°, 0°, and +20°). For each antenna pointing angles, the receiver antenna also swept fully in 10° steps in the azimuth plane. Both horizontal and vertical antenna polarization was measured for cross polarization measurement at all Brooklyn receiver locations. A reflectivity and building penetration measurement was also performed on NYU campus, the setup is shown in Figure 24. It will be covered in detail in section 4.3.

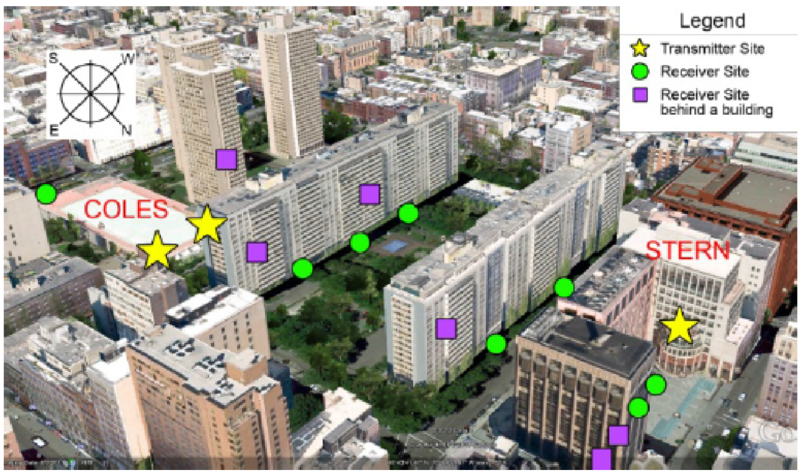

Figure 23: 28GHz cellular measurement locations in Manhattan near NYU campus [52].

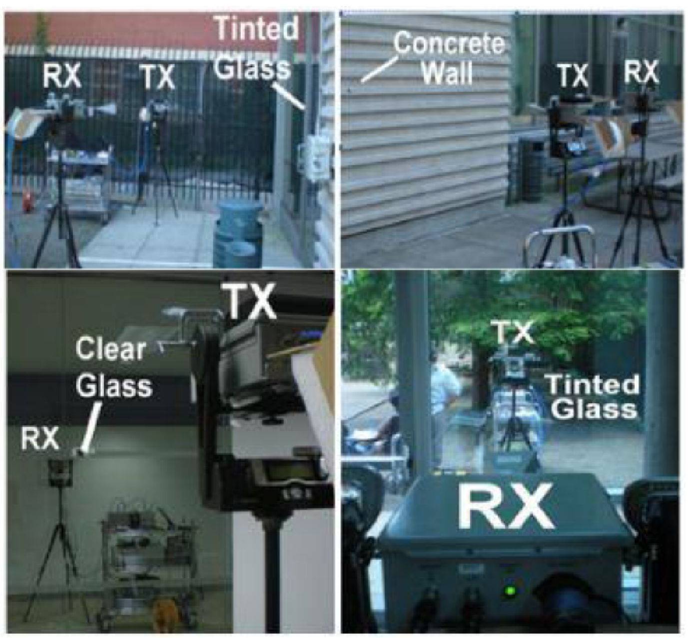

Figure 24: 28GHz building reflection and penetration measurement for common outdoor building materials on NYU campus [17].

Multipath fading was investigated by a multiray propagation model referring to Figure 25 in an urban microcell in India by Joshi and Sancheti [56]. The microcell network range was 100-500m along street blocks surrounded by multi-story high rise buildings, and base station transceivers antennas were mounted on lampposts or telegraph poles at height much lower than surrounding building roofs as a typical microcell configuration. Rajagopal and Abu-Surra from Samsung Telecommunications America performed penetration and reflection measurements of different water and metal objects at 28, 40, and 60GHz with setup shown as Figure 26. A 60GHz test kit from SiBeam was used, and the TX and RX beams from the adaptive antenna arrays were locked to ensure no beam adaption in the penetration measurements and that the signal travels through the water before the RX captured it. They also conducted outdoor LOS and NLOS AOA measurements to study the impact of horn antenna half-power beamwidth (HFBW) and elevation and azimuth angles on the received power. The setup of a LOS channel is displayed in Figure 27. The data were collected manually and only had a few sample points, due to equipment limitation. They were developing an automated measurement tool in 2012 to collect and process more data over the entire elevation and azimuth plane at TX and RX over wider distance range to fully characterize the channel feasibility. They also plan to capture other essential information, including PDPs and delay spread, for outdoor NLOS channel model, which haven't been done due to equipment limitation. This is a gap we could potentially fill up [64].

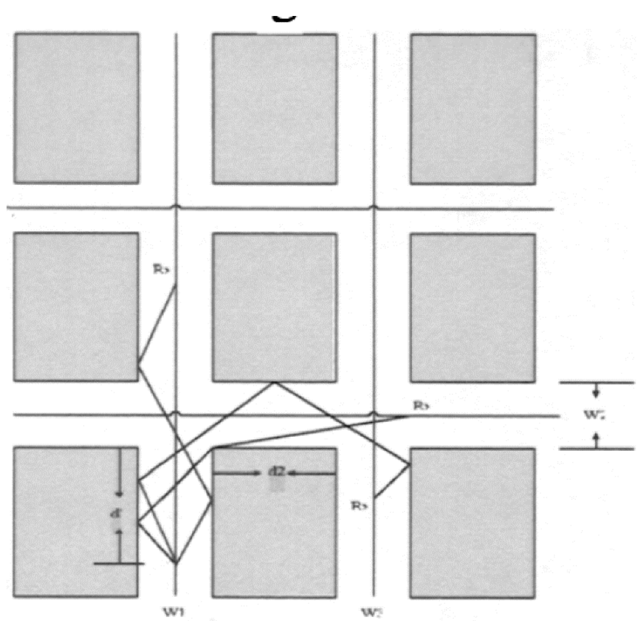

Figure 25: Urban microcell street configuration in India[56]

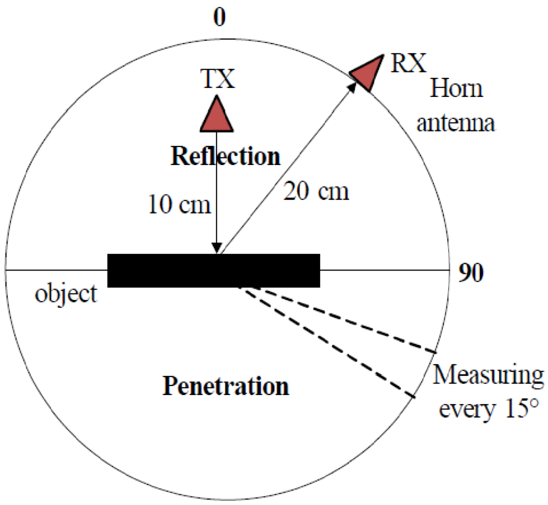

Figure 26: Reflection and penetration measurement setup in Dallas [64].

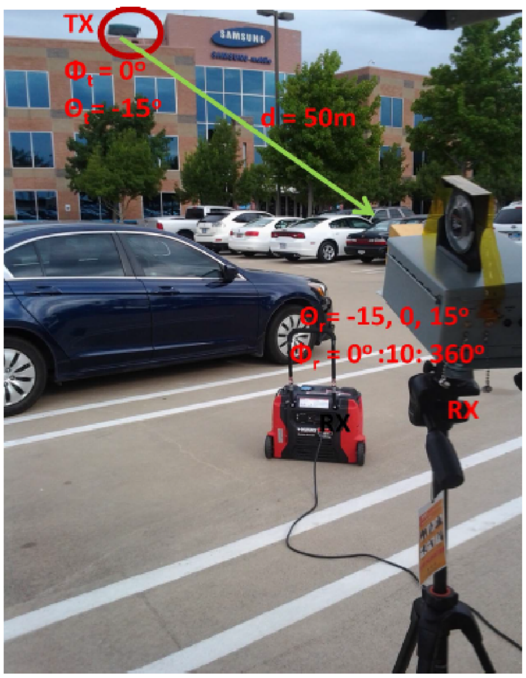

Figure 27: Outdoor LOS measurement setup in Dallas [64].

38 GHz measurement campaign in Austin, Texas using a broadband sliding correlator channel sounder with 800MHz RF passband bandwidth characterized propagation in teRMS of AOA, PL, and time delay spread [60-62]. Adaptive-beam antennas of different gains and beam widths were used at various transmitter and receiver locations which were selected to represent typical urban environments including residential area with foliage obstruction, stadium, art school, parking lot, and Deen Keeton Ave—a busy 4-lane street. Figure 28 and Figure 29 both show the measurement locations and physical environment of the cellular channel 29-930m in length. There were various foliage densities and links where thin to thick density foliage/vegetation caused scattering. Transmitter BS antennas were placed at 1.5m-tripod on four

rooftop of 5-8 stories buildings of height 8-36m AGL, and receiver antennas were at ground level, representing typical 5G cellular BS deployment [60]. For peer-to-peer channel measurements, one transmitter and ten receiver locations were selected. The receiver antenna was located around a pedestrian walkway area surrounded by buildings of 1-12 stories. Typical urban reflectors and scatters such as automobiles, thin foliage, tree trunks, brick and aluminium-sided buildings, lampposts, signs, handrails, etc, were present [62]. Table 6 lists all TX BS and RX MS heights in NYC and Austin, Texas [55].

Table 7: TX locations and corresponding BS and MS heights in NYC and Austin[55].

TX City (Frequency)	TX Building	TX Height, h_{BS} (m)	RX Height, h_{MS} (m)
Austin, TX (38 GHz)	ECJ	8	1.5
	ENS-A	36	
	Woolrich Laboratories	23	
New York City (28 GHz)	Coles Center 1	7	1.5
	Coles Center 2	7	
	Kaufman	17	

Outage studies were carried out at 28 GHz in Manhattan, New York [13] and at 38 GHz in Austin, Texas [12] to determine the coverage potential of base stations in realistic environments to support future outdoor mobile mmWave cellular-type applications. Test locations in Austin are shown in Figure 28 and surrounding environments as Figure 29. At each of the two transmitter sites, the antenna was placed on a 1.5-m tripod at the rooftop of buildings 18 and 36m in height, positioned in the middle of each roof's western edge to avoid shadowing by the roof directly in front of the antenna. This also imitated a typical microcell deployment of sector-antenna installation where BS antennas were mounted on a multistory building's edge or external wall as opposed to on a tall mast used in older macrocell towers. This microcell deployment permitted dense BS deployments in urban areas and used surrounding buildings to reduce inter-cell interference (ICI) through containing the coverage in specific sectors [12]. To analyze signal absorption by rain, this section also talks about an article of rain specific attenuation measured in a short-range 35GHz mmWave channel in China by Zhao and Li [63].

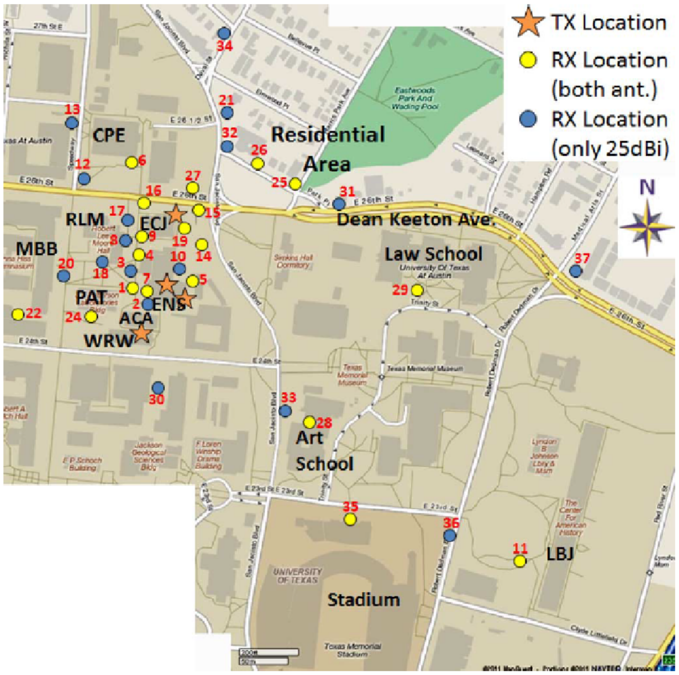

Figure 28: 38GHz measurement locations on University of Texas at Austin campus [60].

Figure 29: 38GHz Transmitter BS antenna looking toward surrounding environments on University of Texas at Austin campus [60].

Measurement results:

Building penetration loss is one of the major impairments for outdoor mmWave communications, especially concerned when trying to reach indoor mobile users. 28GHz building reflection and penetration measurement results in New York City showed that reflection coefficients for outdoor materials were generally higher than indoor ones, particularly 0.896 for tinted glass at 10° incidence angle, 0.815 for concrete at 10° incidence and 0.623 at 45° incidence. Outdoor materials caused higher penetration loss than indoor ones, particularly 40.1dB loss for tinted glass and 28.3dB loss for brick. The highly reflective and attenuative nature of thick and dense external building materials makes outdoor-to-indoor propagation rather difficult, but enhances outdoor-to-outdoor signal coverage and support a larger range of AOAs to achieve NLOS links by multiple reflections from vertical walls, roadsides, and rooftops in an urban city. Outdoor-and-indoor interference could also be reduced, thus enabling effective frequency. More details will be presented in section 4 [17]. Penetration and reflectivity measurement results at 28 and 40 GHz in Dallas are shown in Figure 30 and Figure 31, and demonstrated similar trends—at such high frequencies water and metal objects were hard to penetrate, but substantially reflective thus enabling signal coverage through NLOS reflections [64].

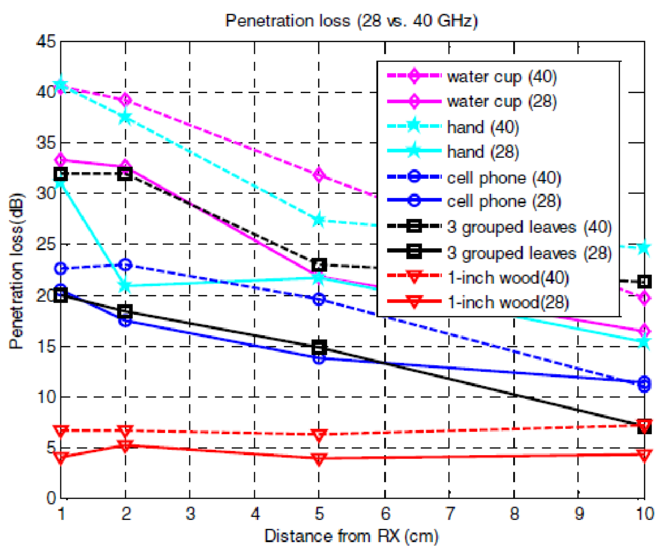

Figure 30: Penetration loss of different objects at 28 and 40GHz in Dallas [64].

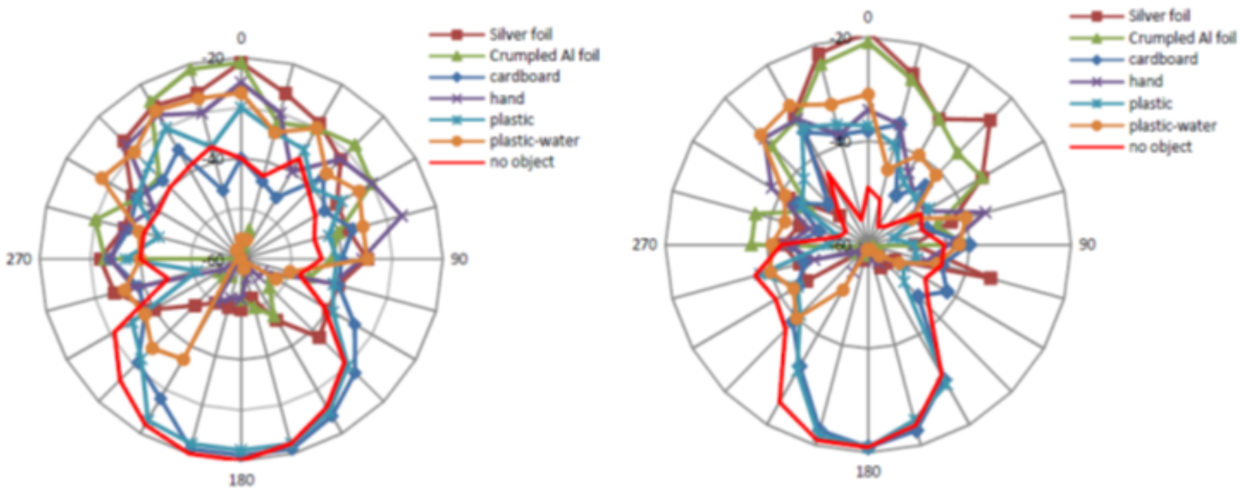

Figure 31: Reflectivity of different materials at a) 28GHz b) 38GHz in Dallas [64].

The highly reflective nature of outdoor materials resulted in PDPs showing numerous multipath components with large excess delay at both LOS and NLOS transmission at 28GHz in New York City. Particularly 753.5ns excess delay in a LOS link 52m in length (referring to Figure 32a), and 1388.4ns in a NLOS link 423m in length (referring to Figure 32b). The multipath delay spread was much larger in heavy urban New York City than in light urban Austin, TX. In a LOS link shorter than 200m in New York City there were on average 7.2 resolvable multipath components (RMC) with standard deviation of 2.2, whereas in a NLOS link shorter than 100m there were on average 6.8 RMC with also standard deviation of 2.2, as shown in Figure 33[1][13].

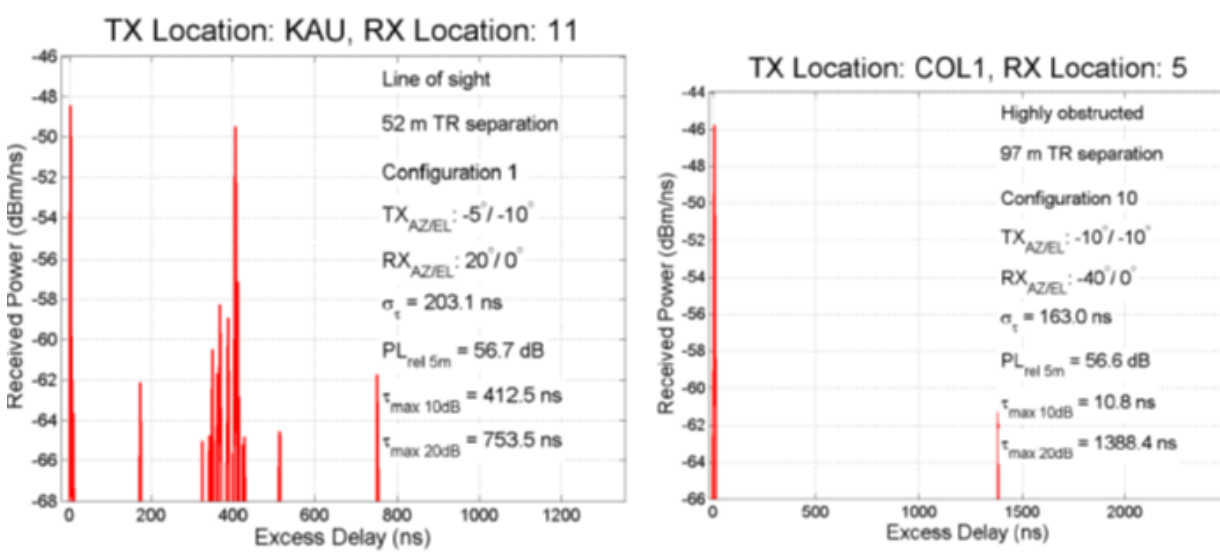

Figure 32: The largest observed multipath at 28GHz in a a) LOS b) NLOS link in New York City [13].

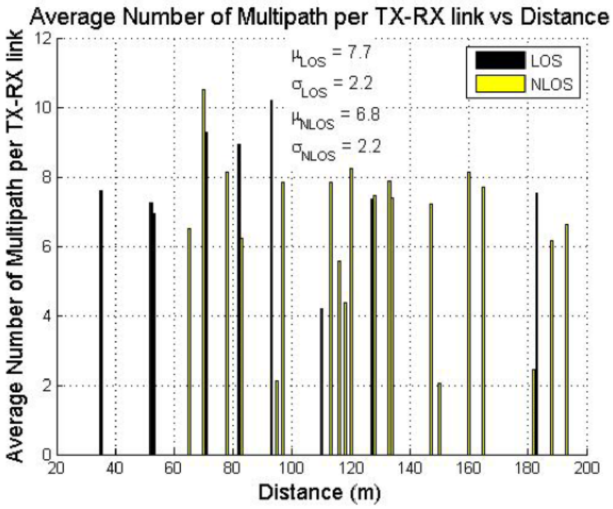

Figure 33: Average number of resolvable multipath components per TX-RX link as a function of distance at 28GHz in LOS and NLOS environments in New York City [13].

Path loss over long distance is another crucial impairment of outdoor mmWave propagation. With is a big concern for future 5G microcell BS deployment there have been many measurements for large scale propagation models at 28 and 38GHz [12][13][53][55][58-60][62][64]. Indeed, path loss models are one of the most commonly developed models for outdoor mmWave communication networks. Generally, a linear relationship with logarithmic distance is applied to model path loss in dB relative to the transmitted power as equation 1[55]:

$$\overline{PL(d)}(dB) = \alpha + \overline{\beta} \cdot 10\log_{10}(d) \quad (1)$$

where $\overline{PL(d)}\overline{PL(d)}$ denotes the logarithmic average path loss over all distances, α refers to the floating intercept in dB, $\overline{\beta}\,\overline{\beta}$ represents the slope or the mean path loss exponent (PLE), and d is the distance. Figure 34 a), b), and c) present measured path loss empirical plots and least-square fit regression line at 28 in NYC and 38GHz in Austin. [55].

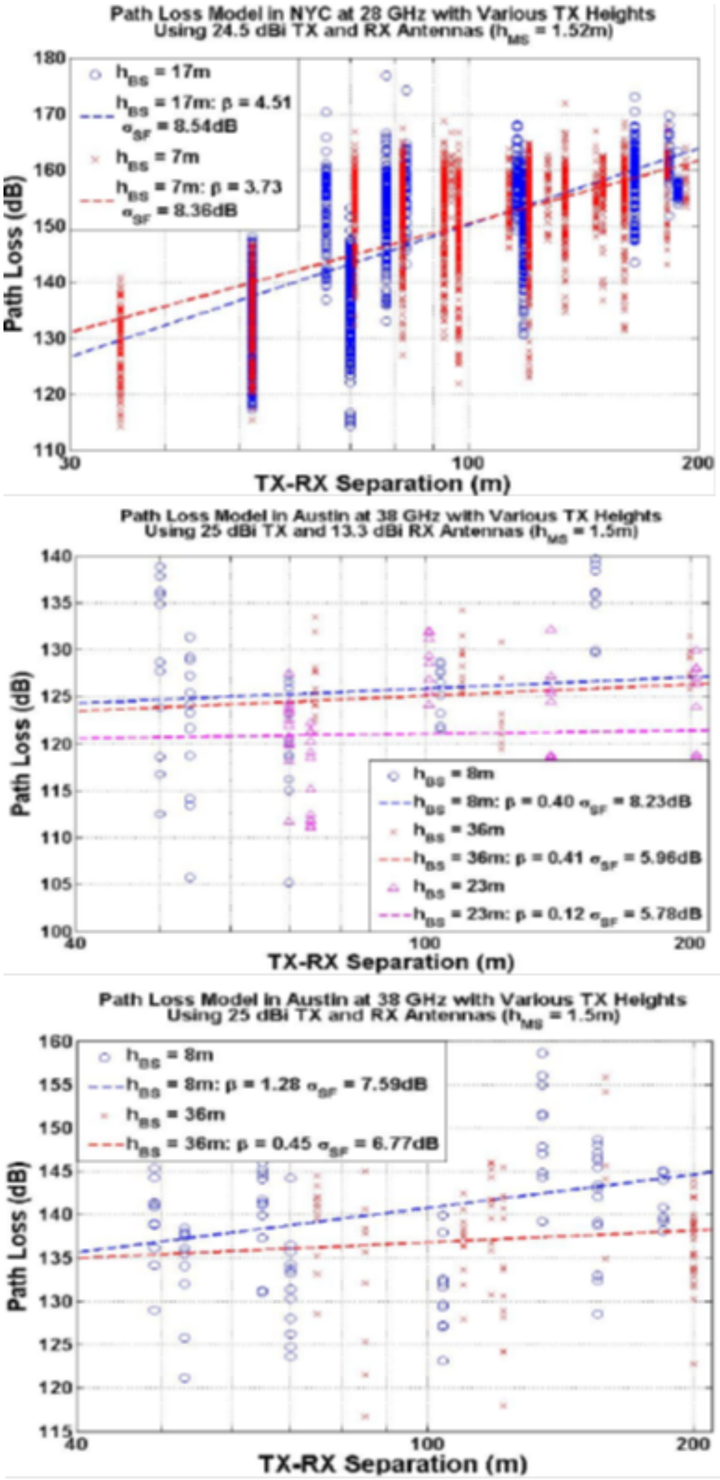

Figure 34: Measured path loss as a function of TX-RX separation distance at a) 28GHz (top) ,b) 38GHz using 25dBi TX and 13.3dBi RX antennas (middle), c) 38 GHz using 25dBi TX and RX antennas (bottom) .

In the figure above, blue circles and red crosses denote path loss values extracted from PDPs, whereas coloured dashed lines denote least-square fit regression lines for various BS heights. β represents the slope and standard deviation σ is the shadow fading factors [55].

Table 8 summarizes floating intercept path loss models developed by measurements at 28GHz in NYC and at 38GHz in Austin under NLOS paths between 30 and 200m in length. Using the floating intercept, the shadow factors are determined from the models. Key path loss parameters of these floating intercept models are compared to those of a widely used 5m close-in reference distance models, shown in Table 9. The result showed that floating intercept models had lower shadow factors and lower PLE which would be more suitable for 5G mmWave standards for urban microcell environments. The calculated PLEs for Austin was lower than New York City, because measurement data set collected in Austin was much smaller, and its environment was much less scatter-rich compared to New York City. Moreover, this model recommends that in order to compensate for increasing path loss due to increasing frequency from current 4G LTE to future 5G mmWave communications, mobile devices could deploy antennas with higher gains [55]. Figure 35 shows the received power level at 28 GHz for LOS links 100m or shorter in length in Dallas with the estimated path loss. The path loss exponent was calculated to 1.89, slightly better than free space case, probably due to additional power contributed from ground reflections [64].

Table 8: 28 and 38GHz path loss models developed from measured data in New York City and Austin, respectively [55].

Frequency (GHz)	TX Height (meters)	Rx Height (meters)	TX,RX Antenna Gains (dBi)	Path Loss Scenarios	TX-RX Separation Range (meters)	Key Parameters for Equation (1)		
						$\bar{\beta}$ (Slope)	α (Floating Intercept, dB)	Shadow Factor σ_{SF} (dB)
28 GHz New York City	7	1.5	+24.5, +24.5	Non-line-of-sight (NLOS)	30 <d<200	3.73	75.85	8.36
	17					4.51	59.89	8.52
38 GHz Austin, Texas	8	1.5	+25, +25	Non-line-of-sight (NLOS)		1.28	115.17	7.59
	8		+25, +13.3			0.40	117.85	8.23
	23		+25, +13.3			0.12	118.77	5.78
	36		+25, +25			0.45	127.79	6.77
	36		+25, +13.3			0.41	116.77	5.96

Table 9: Comparison of key 28 and 38GHz path loss parameters in 5m reference distance models and floating intercept models developed from measured data in New York City and Austin, respectively [55].

	Close-in Reference Model (d_o=5 m)			Floating Intercept Model (30 m < d < 200 m)						
	38 GHz in Austin (25 dBi TX)		28 GHz in NYC (24.5 dBi TX)	38 GHz in Austin (25 dBi TX)					28 GHz in NYC (24.5 dBi TX)	
				25 dBi RX Ant.		13.3 dBi RX Ant.			24.5 dBi RX Ant.	
	25 dBi RX Ant.	13.3 dBi RX Ant.	24.5 dBi RX Ant.	8 m TX height	36 m TX height	8 m TX height	23 m TX height	36 m TX height	7 m TX height	17 m TX height
α (floating intercept)				115.17	127.79	117.85	118.77	116.77	75.85	59.89
Path Loss Exponent n	3.88	3.18	5.76	1.28	0.45	0.4	0.12	0.41	3.73	4.51
σ_{SF} (dB)	14.6	11.0	9.02	7.59	6.77	8.23	5.78	5.96	8.36	8.52

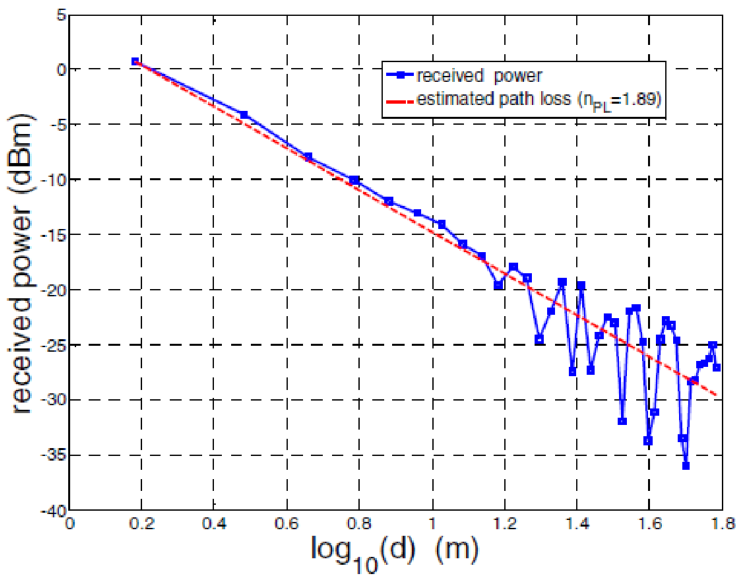

Figure 35: Path loss exponents for outdoor propagation measurement at 28GHz in Dallas [64].

Figure 16 in section 3.1 displays all Manhattan coverage cells of different sectors according to TX locations from NYU's outage study at 28GHz. All covered links where signals could be acquired by the RX were within 200m radius from the TX. Indeed, most 28GHz links within 200m TX-RX separation could detect a signal at the RX site, and for some of these cases, the signal could not be acquired by the hardware due to insufficient signal-to-noise ratio (SNR). Of all measurement locations in Manhattan, outages took place at 57% of them because of obstruction, and most outages happened at TX-RX separation longer than 200m. Figure 36 shows the relationship between maximum coverage distance and the combined TX-RX antenna gain of various PLEs. This plot shows maximum coverage distance increases while the combined antenna increases and PLE decreases [1].

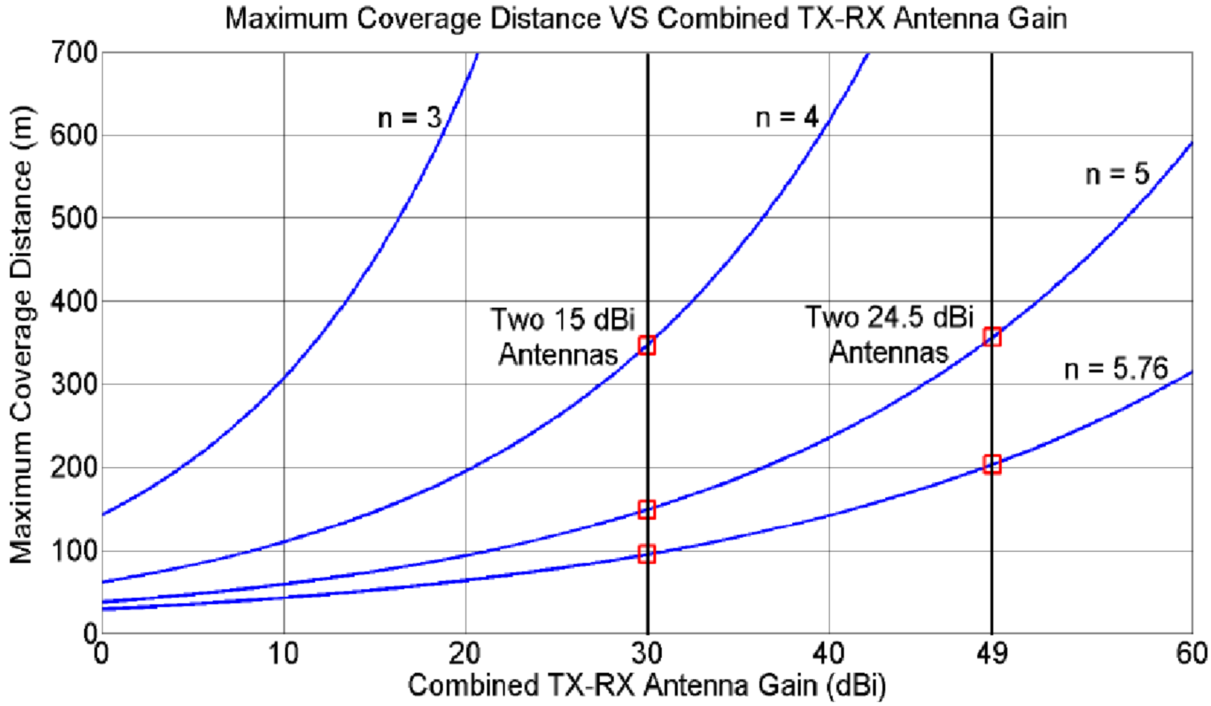

Figure 36: Maximum coverage distance vs. combined TX-RX antenna gain at 28GHz in New York City, with 119dB maximum path loss dynamic range 10 dB SNR without antenna gains, as a function of PLE n [1].

Table 10 shows outage statistics from the 38GHz outage study in Austin at two different transmitter locations along with 53 random RX locations. It was found that lower transmitter ENS height supported better coverage over shorter distances, and the higher transmitter WRW height provided a larger coverage range. Reflected and diffracted signals enhanced the coverage for obstructed links. Reflection offered 17dB or higher signal power than diffraction, confirming that the propagation mechanism at mmWave was reflection as stated in the Introduction section. The higher transmitter location at WRW had fewer outages above 200m range because of the diffraction around the lower buildings in the surroundings [12].

Table 10: Outage statistics for two TX locations at 38GHz in Austin [12].

Transmitter Location	Building Height	% Outage for PL<160dB	% Outage for PL<150dB
TX1: ENS Building	36m	18.9% all, 0%<200m	52.8% all, 27.3% <200m
TX2: WRW Building	18m	39.6% all, 0%<200m	52.8% all, 10% <200m

Akdeniz et al evaluated capacity of mmWave picocellular system by using channel models based on urban NLOS PL data at 28GHz in NYC. They found mmWave system could improve overall cell capacity by 15 times compared with current LTE systems, even by using a worst-case model where all users experience NLOS connections. Most of the improvement was contributed from wider operating bandwidth of 1GHz at 28GHz, 25 times increase over current LTE's 20+20MHz. The 5% cell edge rate for mmWave was only 5 times higher than current LTE system though, indicating mmWave systems were limited by NLOS propagation significantly, and that edge of cell users became power-limited and were unable to exploit the increased bandwidth spectrum [53].

Table 11: mmWave and LTE cell capacity and cell edge rate comparison assuming 20% overhead and 50% UL-DL duty cycle at the mmWave system [53].

System antenna	BW & Duplex	Fc(GHz)	Cell capacity (Mbps)	5% Cell edge rate (Mbps)
mmWave 64x64	1 GHz TDD	28	780 (DL) 850 (UL)	8.22 (DL) 11.3 (UL)
LTE 2x2 DL, 2x4 UL	20+20 MHz FDD	2.5	53.8 (DL) 47.2 (UL)	1.80 (DL) 1.94 (UL)

Common wireless communication channel models include double-directional channel model and statistical spatial channel model. Double-directional model considers every possible direction of radio wave propagation between the base stations and mobile users for achieving optimum signal coverage, thus characterizing AOD from the transmitters and AOA at the receivers' side. Figure 37 shows polar plots of 28 GHz of receiver power in NLOS environments along 4 linear antenna track positions by NYU [52]. PDPs were measured at each transmitter and receiver pointing angle, and receiver power as the area under the PDP was plotted. Lobes were defined as energy spread representing 2-D spatial direction of multipath.

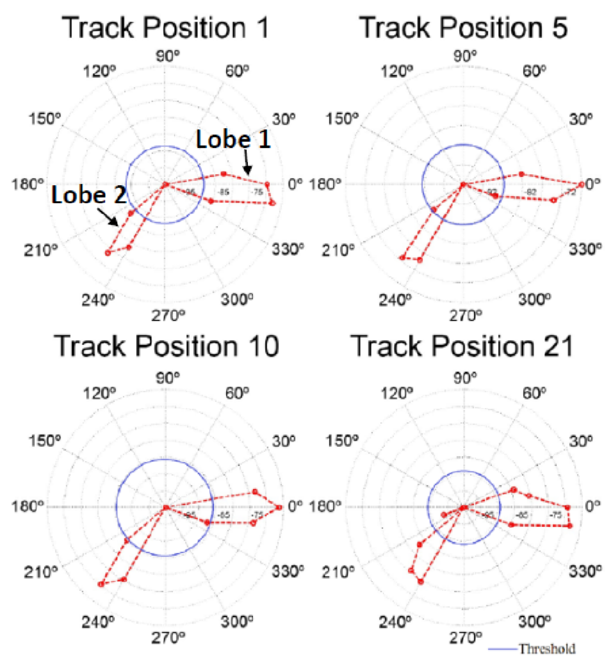

Figure 37: Polar plots of 28 GHz propagation along a 21-step linear track with λ/2 step sizes [52]

Table 12 lists lobe statistics, the computation procedure, physical significance, and empirical distribution in Manhattan to ensure lobes were modeled consistently.

Table 12: Summary of AOA and other statistics at 28GHz for all Manhattan RX locations [52].

Statistics	*Computation Procedure*	*Physical Meaning*	*Empirical Distribution in Manhattan*
AOA	$\bar{\theta} = \frac{\sum_k P(\theta_k)\theta_k}{\sum_k P(\theta_k)}$	The mean direction of arrival of a lobe	Uniform [0°, 360°]
Lobe angle spread (LAS)	Apply threshold to polar plot, e.g., 10 dB of peak at LOS RX location, 20 dB for NLOS	Angle span of a lobe above a pre-defined threshold	Exponential $\mu = 40.3°$ $\sigma = 42.5°$
RMS LAS (standard deviation of lobe angle spread)	RMS LAS = $\sqrt{\overline{\theta^2} - (\bar{\theta})^2}$ where $\overline{\theta^2} = \frac{\sum_k P(\theta_k)\theta_k^{\ 2}}{\sum_k P(\theta_k)}$	Angle span of lobe in which most power is received	Exponential $\mu = 7.8°$ $\sigma = 10.7°$
# of lobes for a particular RX location/antenna configuration	Number of lobes above pre-defined threshold	# of spatial directions from TX to RX	Exponential $\mu = 2.5$ $\sigma = 1.7$
Total power in a lobe for a particular RX location/antenna configuration	$\sum_k P(\theta_k)$ over consecutive k values where $P(\theta_k)$ above threshold	Total power in a lobe	Applies to each lobe at each RX for a particular antenna configuration at TX and RX
Average power in lobe for a particular RX location/antenna configuration	$\frac{\sum_k P(\theta_k)}{k_{max}}$ over consecutive k values where $P(\theta_k)$ above threshold	Average power in a lobe	Applies to each lobe at each RX for a particular antenna configuration at TX and RX
Max power in a lobe for a particular RX location/antenna configuration	$\max_k P(\theta_k)$ over consecutive k values where $P(\theta_k)$ above threshold	Max power in a lobe.	Applies to each lobe at each RX for a particular antenna configuration at TX and RX

These spatial lobes of azimuthal distribution of multipath signals are important components of a statistical spatial channel model (SSCM) for cellular communications at 28GHz [52]. A 1st- order statistical spatial channel model considers either direction or delay, whereas a 2nd-order mobile one models both temporal and spatial aspects, such as NYU's. It also models multipath clusters, where each cluster represents a group of multipath components within one PDP for a specific antenna pointing angle. In other words, signal energy travelling closely together in spatial and temporal domain forms a cluster.

Figure 41 represents a graphical double directional channel model, where the transmitter azimuth angle is the independent variable whereas the receiver azimuth angle is the dependent variable. Steerable 25-dBi horn antennas were used at the transmitter and receiver terminals. For each of the three angle increments (-30°, 0°, and +30°) rotated at the transmitter antenna, the receiver was rotated for a full 360° cycle to search for the link of maximum propagation energy [60].

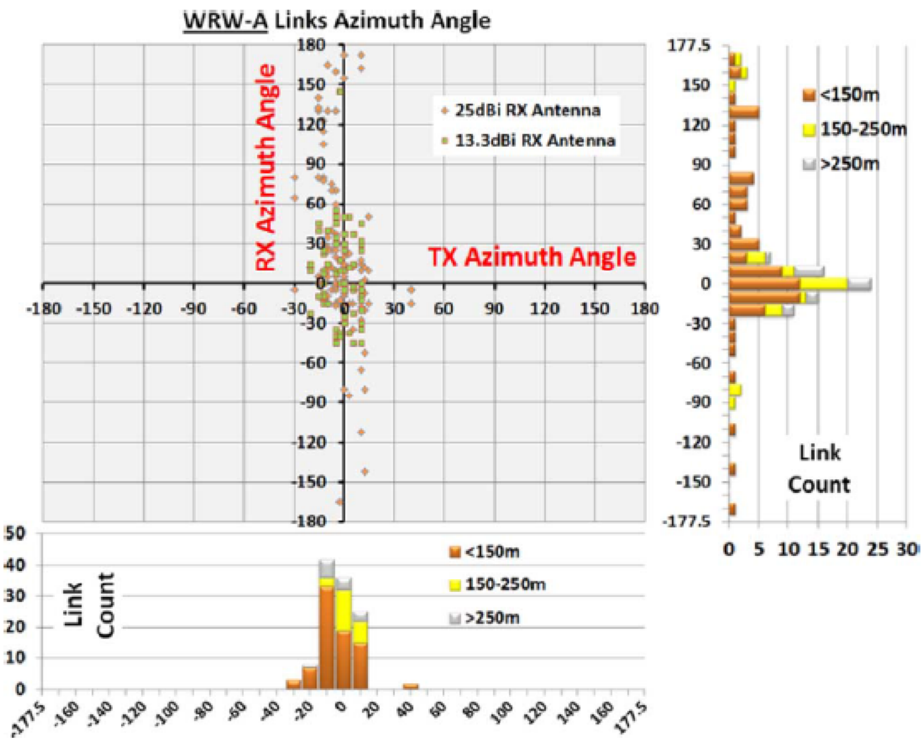

Figure 38: Double directional channel model and link count at 28 GHz [60].

Figure 42 shows a typical double directional receiver power angular profile at 28 GHz by NYU [59], where color denotes the average receiver power of each angular offset and white areas were either not measured or power was too low to be detected. Only one out of 4-D angular domain was measured due to time constraint.

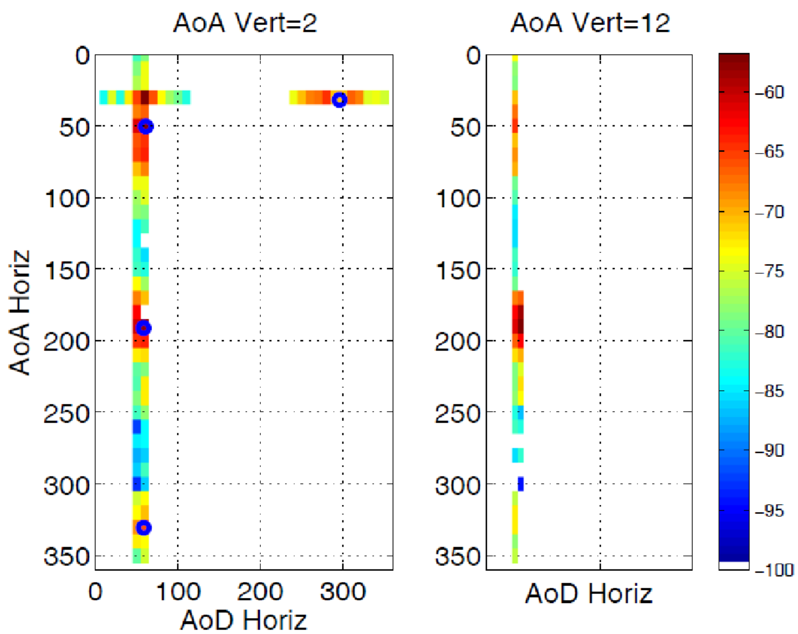

Figure 39: Double directional receiver power angular profile at 28 GHz [59]

Rain attenuation becomes a concern in mmWave because raindrops are about the same size as wavelengths in this frequency range, thus causing scattering of the wireless signal. Figure 40 displays the attenuation per kilometre specifically contributed from rain across the mmWave spectrum, as a function of rain rate. Zhao and Li from China measured rain specific attenuation at short range 35GHz links and 103GHz (discussed in section 3.4) links at 230m and 390m in length, respectively. Table 13 summarizes rain attenuation statistics measured at 35GHz in teRMS of fade amplitude and duration. Figure 41 displays the measured rain attenuation distribution [63].

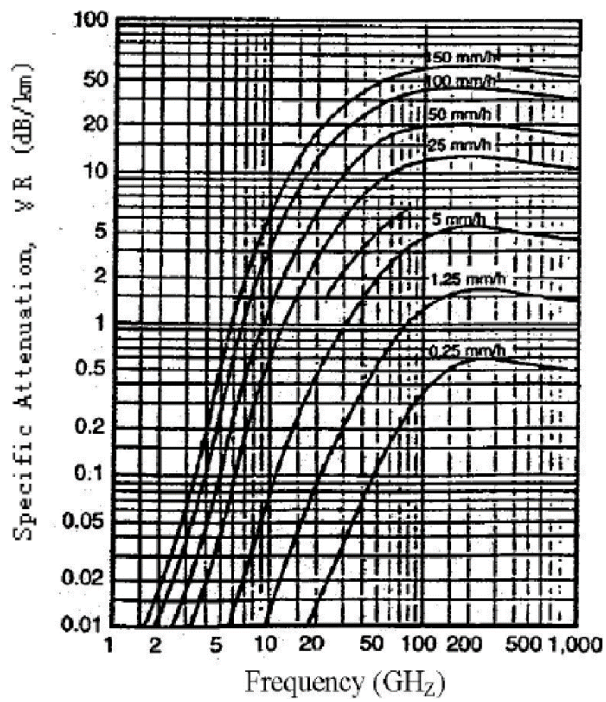

Figure 40: Rain specific attenuation per kilometer at various frequencies as a function of rain rate [63].

Table 13: Measured rain attenuation statistics at 35GHz [63].

Percentage of time in fraction of unity during rain for which attenuation exceeds a (dB)	a (dB) measured 230m -35 GHz link
1.0	2.5
0.3	10
0.1	25
0.03	28
0.01	38
0.003	48

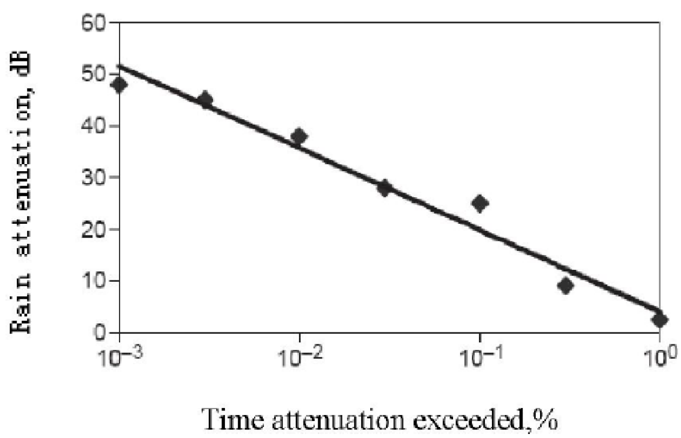

Figure 41: Measured rain attenuation distribution [63].

4.4 60~94GHz Frequency Bands

Use cases:

Publication in this frequency range of 60GHz and greater dated back in the 1990s [70] [72] onward, up to the current year [58][59]. Originally explored for European research project RACE Mobile Broadband System (MBS) [70], then later for cellular/mobile and peer-to-peer wireless networks [62][71], 60GHz band or greater has seemed to be an ideal solution for customers demand for higher data rates and smaller equipment dimensions [70]. Furthermore, there is much wider bandwidths available compared to present LTE cellular networks, resulting in significant capacity improvement [58][59]. The 60GHz has been suggested particular for urban microcellular scenarios employing lower-powered base stations with antennas raised by few meters AGL [72].The mmWave E-band ranges from 60~90 GHz, and is allocated for ultrahigh-capacity point-to-point communications globally [73]. This section introduces past research activities at 60GHz [62][64][70-72], 73GHz [58][59], 81~86GHz [73][74], and rain attenuation at 103GHz [63]. Propagation measurement took place mostly in LOS and NLOS urban environments including Dallas [64], seven different streets in downtown Oslo, Norway [70], University of Austin at Texas campus [62][71], New York City [58][59], four different cities in Finland[73][74], China [63], with one exception of suburban area in Spain [72]. Common collected data parameters, consist of received signal power or path loss [58][59][62][71][72], PDP [58][62][70][71][73][74], delay spread [62][70][71], penetration loss of water and metal objects [64], AOA/AOD for beamforming [58][59][71][73], and rain attenuation [63].

As in lower frequencies range, urban street canyon microcell configuration is a common scenario in past measurements [58][59][70][73][74]. Rangan et al chose New York City as measurement location since it represents the initial mmWave network deployment to target urban high user density. A key concern for mmWave as in other frequencies as well, is the difficulty to accomplish LOS paths in an urban canyon environment [58]. Kyro et al did propagation measurement in Erikinkatu Street located in downtown Helsinki, Finland shown in **Figure 42.** It was a straight street with a small slope at the TX, and the RX was 685m apart. Both TX and RX were mounted on 4m high masts [74]. Another street microcell configuration was done by Lovnes et al at 59GHz on seven streets with different dimensions, building architectures, and traffic situations in downtown Oslo. Trees were present along buildings in some of these streets, and in the middle of the lanes in one street, sometimes obstructing the LOS link. Stationary TX antenna heights ranged from 3.1~11m while the mobile RX antenna was constant 2.2m, as shown in **Figure 43** [70]. Urban peer-to-peer wideband (1.9GHz RF pass band centered at 59.4GHz carrier frequency providing a 1.3ns multipath time resolution that corresponded to a minimum detectable RMS delay spread smaller than 1ns) channel measurements were carried out by Ben-Dor et al in Austin [62][71]. The measurement areas for [62] (an outdoor open pedestrian walkway of 19~129m TX-RX distance, with TX and RX antennas both 1.5m AGL mimicking peer-to-peer ad-hoc network applications and simple two-way communications between terminals) and [71] (an outdoor courtyard surrounded by tall 6~10-storyed office buildings, with 17.8~117.8m TX-RX distance, and both TX and RX antennas 1.5m AGL) are displayed in **Figure 44** and **Figure 45** respectively. This peer-to-peer communication represented a typical use case of people holding mobile devices. The only suburban microcell propagation environment took place at 62 GHz in Vigo by Hammoudeh et al in [72] under both LOS (RX moving 222m away from the TX along the center line of the street) and NLOS (RX moving 57m along a street crossing the main street perpendicularly), and the geometry of fixed TX base and mobile RX (driven at almost constant 4.47m/s speed) is as **Figure 46**. The signal envelope variation as a function of mobile position was recorded. The 10-dBi standard horn TX antenna height was 3.1m AGL, and placed 2.35m from the closet building surface at the end of a street horizontally. The omnidirectional RX antenna was mounted on top of a transit van 2.8 AGL. Multipath components AOA was measured with RX stationary at nine locations along the roadside closer to building A referring **Figure 46**. The RX antenna steered full 360° in the azimuth plane at each location. The experimental results were interpreted by a ray-tracing model (based on the image method and a deterministic 3-D high-frequency model for outdoor mobile radio scenarios) which considered reflections and diffractions (the user defined the order of rays). Building blocks' had uniform reflecting surfaces and diffracting edges with specified geometry. Building fronts features such as windows, doors, etc were not modeled. The ground was also assumed a flat uniform reflecting surface. Diffraction from cars, lampposts, pedestrians or other objects were neglected [72].The ray-tracing software was not specified in the article, but ray-tracing model setup introduced here seems similar to Wireless Insite software which RSL runs ray-tracing simulation on.

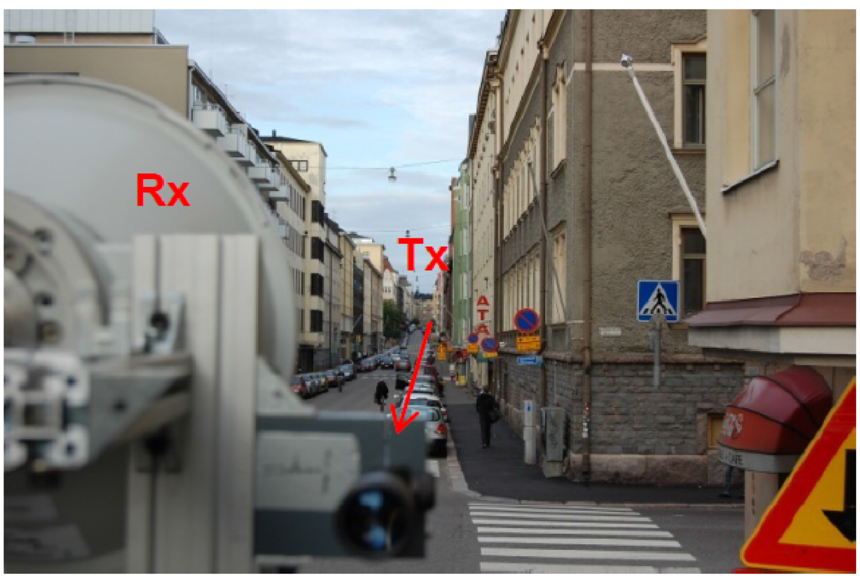

Figure 42: Street canyon scenario in downtown Helsinki at 81~86 GHz [74].

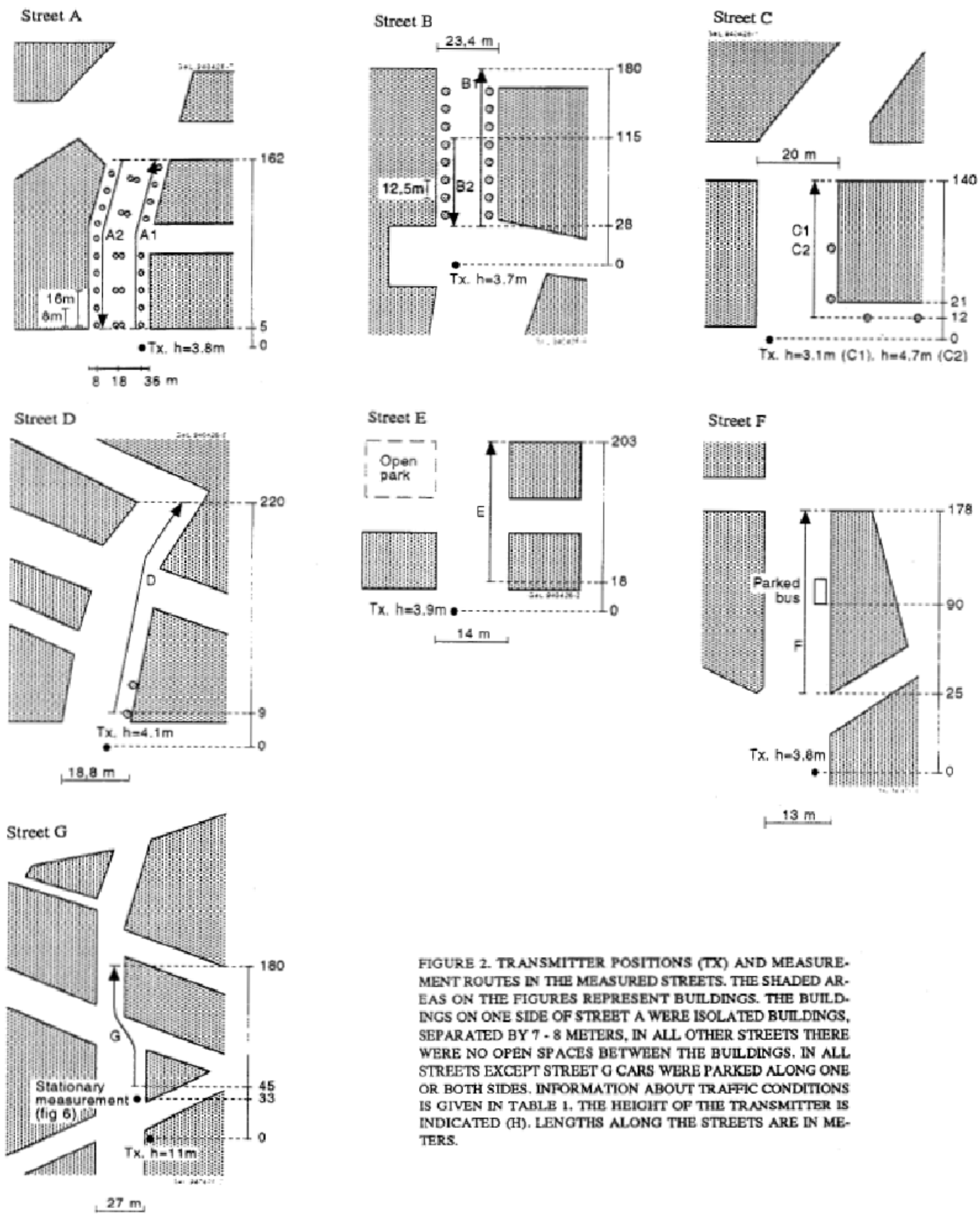

FIGURE 2. TRANSMITTER POSITIONS (TX) AND MEASUREMENT ROUTES IN THE MEASURED STREETS. THE SHADED AREAS ON THE FIGURES REPRESENT BUILDINGS. THE BUILDINGS ON ONE SIDE OF STREET A WERE ISOLATED BUILDINGS, SEPARATED BY 7 - 8 METERS, IN ALL OTHER STREETS THERE WERE NO OPEN SPACES BETWEEN THE BUILDINGS. IN ALL STREETS EXCEPT STREET G CARS WERE PARKED ALONG ONE OR BOTH SIDES. INFORMATION ABOUT TRAFFIC CONDITIONS IS GIVEN IN TABLE 1. THE HEIGHT OF THE TRANSMITTER IS INDICATED (H). LENGTHS ALONG THE STREETS ARE IN METERS.

Figure 43: Street measurement routes and setup in downtown Oslo at 59 GHz [70].

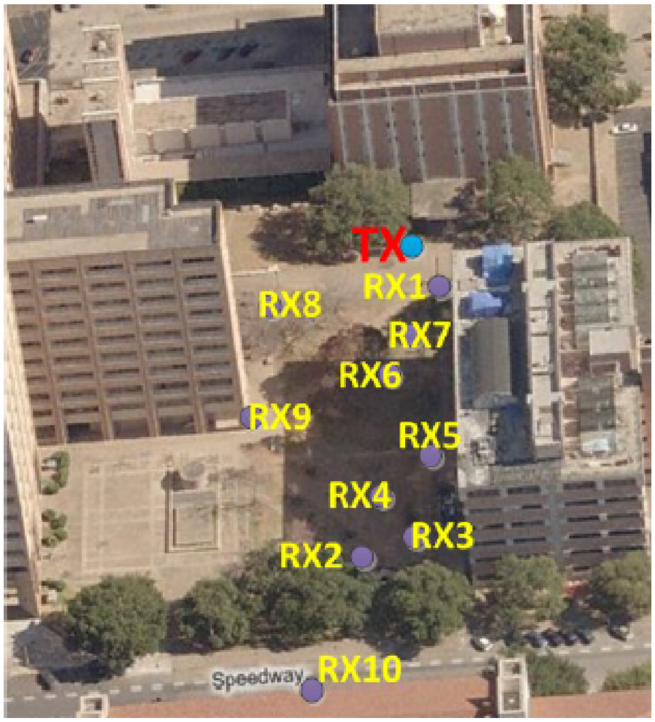

Figure 44: Peer-to-peer measurement environment at 60GHz in a walkway on UT Austin campus [62].

Figure 45: Measurement environment at 60GHz in a courtyard on UT Austin campus with surrounding buildings, trees, light posts, and handrails [71].

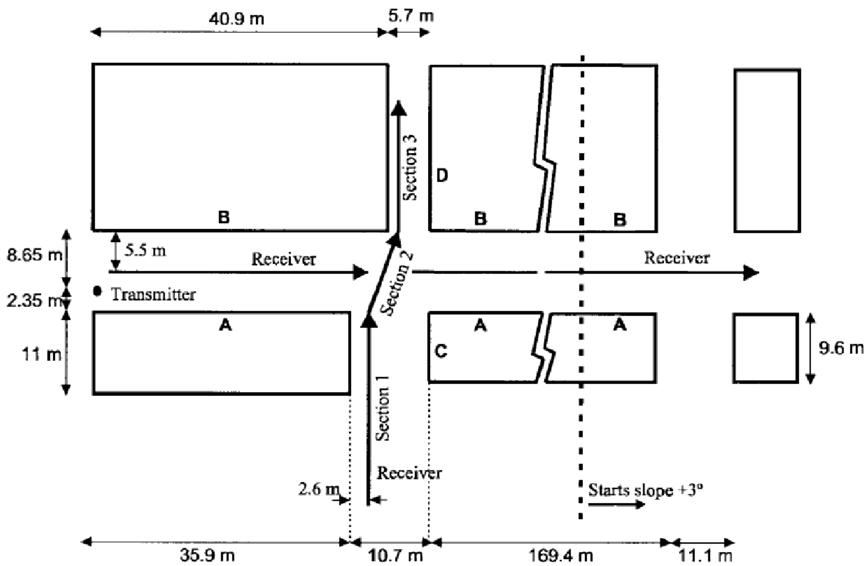

Figure 46: Geometry of LOS and NLOS propagation measurement routes at 62 GHz in Spain [72].

Measurement results:

Examining the measured path loss data as a function of TX-RX distance is important to assess mmWave systems in terms of cell coverage range. Figure 47 shows the scatter plot of omnidirectional path loss versus TX-RX distance with linear fit estimation done at 28 GHz and 73GHz in New York City by Pangan et al [58]. We can see LOS path losses followed Friis' law of free space propagation up to 100m, while Akdeniz et al modeled NLOS path loss by applying a standard linear fit with parameters shown in Table 14 [59]. It was also found, surprisingly, through reflections and scattering, mmWave signals were viable at distances of 100~200m TX-RX separation potentially, even in totally NLOS settings. With modest beamforming presumptions, the capacity analysis implied at least an order of magnitude in capacity upgrade for mmWave systems over present LTE ones in for outdoor coverage [58].

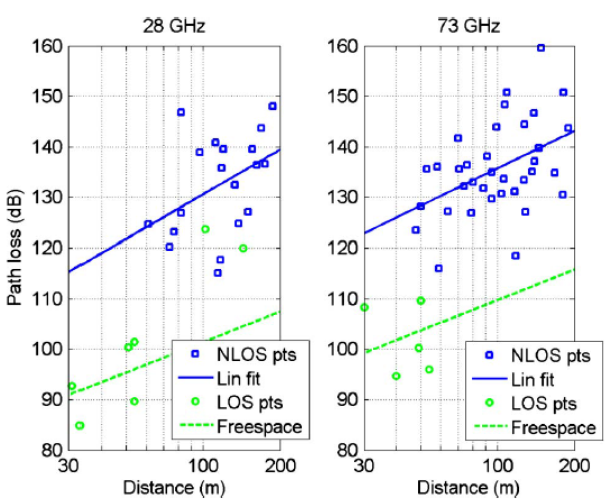

Figure 47: Path loss vs channel link distance at 28 and 73 GHz in New York City [58].

Table 14: Proposed statistical large-scale oath loss model (reference 22 refers to our reference 1 in this report) [59].

Variable	Model	Model Parameter Values: 28 GHz	Model Parameter Values: 73 GHz
Omnidirectional path loss, PL and lognormal shadowing, ξ	$PL = \alpha + 10\beta \log_{10}(d) + \xi$ [dB] $\xi \sim \mathcal{N}(0, \sigma^2)$, d in meters	NLOS: $\alpha = 72.0$, $\beta = 2.92$, $\sigma = 8.7$ dB LOS: $\alpha = 61.4$, $\beta = 2$, $\sigma = 5.8$ dB	NLOS: $\alpha = 86.6$, $\beta = 2.45$, $\sigma = 8.0$ dB (†) $\alpha = 82.7$, $\beta = 2.69$, $\sigma = 7.7$ dB (‡) LOS: $\alpha = 69.8$, $\beta = 2$, $\sigma = 5.8$ dB
NLOS-LOS-Outage probability	See (8)	$1/a_{\text{out}} = 30.0$ m, $b_{\text{out}} = 5.2$, $1/a_{\text{los}} = 67.1$ m	
Number of clusters, K	$K \sim \max\{Poisson(\lambda), 1\}$	$\lambda = 1.8$	$\lambda = 1.9$
Cluster power fraction	See (6) and (7): $\gamma'_k = U_k^{r_\tau - 1} 10^{0.1 Z_k}$, $Z_k \sim \mathcal{N}(0, \zeta^2)$, $U_k \sim U[0, 1]$	$r_\tau = 2.8$, $\zeta = 4.0$	$r_\tau = 3.0$, $\zeta = 4.0$
BS and UE horizontal cluster central angles, θ	$\theta \sim U(0, 2\pi)$		
BS and UE vertical cluster central angles, ϕ	ϕ = LOS elevation angle		
BS cluster rms angular spread	σ is exponentially distributed, $\mathbb{E}(\sigma) = \lambda^{-1}$	Horiz $\lambda^{-1} = 10.2°$; Vert $\lambda^{-1} = 0°$ (*)	Horiz $\lambda^{-1} = 10.5°$; Vert $\lambda^{-1} = 0°$ (*)
UE rms angular spread	σ is exponentially distributed, $\mathbb{E}(\sigma) = \lambda^{-1}$	Horiz $\lambda^{-1} = 15.5°$; Vert $\lambda^{-1} = 6.0°$	Horiz $\lambda^{-1} = 15.4°$; Vert $\lambda^{-1} = 3.5°$

Note: The model parameters are derived based on converting the directional measurements from the NYC data in [22], and assuming an isotropic (omnidirectional, unity gain) channel model with the 49 dB of antenna gains removed from the measurements.
(†) Parameters for the 2m-RX-height data and 4.06m-RX-height data combined.
(‡) Parameters for the 2m-RX-height data only.
(*) BS downtilt was fixed at 10 degree for all measurements, resulting in no measurable vertical angular spread at the BS.

Table 15: mmWave and LTE cell capacity/edge rate comparison (reference 24 refers to our reference 75 in this report) [59].

System	System Bandwidth	UE ant	NLOS-LOS-Outage model	Spec. eff (bps/Hz)		Cell throughput (Mbps/cell)		5% Cell edge rate (Mbps/UE)	
				DL	UL	DL	UL	DL	UL
28 GHz mmW	1 GHz TDD	8x8	Hybrid	3.34	3.16	1668	1580	52.28	34.78
		4x4	Hybrid	3.03	2.94	1514	1468	28.47	19.90
			Hybrid, d_{shift} = 50m	2.90	2.91	1450	1454	17.62	17.49
			Hybrid, d_{shift} = 75m	2.58	2.60	1289	1298	0.54	0.09
			No LOS, d_{shift} = 50m	2.16	2.34	1081	1168	11.14	15.19
73 GHz mmW	1 GHz TDD	4x4	Hybrid	2.58	2.58	1288	1291	10.02	8.92
		8x8	Hybrid	2.93	2.88	1465	1439	24.08	19.76
2.5 GHz LTE	20+20 MHz FDD	2		2.69	2.36	53.8	47.2	1.80	1.94

Note 1. Assumes 20% overhead, 50% UL-DL duty cycle and 8x8 BS antennas for the mmW system
Note 2. Assumes 2 TX 4 RX antennas at BS side for LTE system
Note 3. Long-term, non-coherent beamforming are assumed at both the BS and UE in the mmW system. However, the mmW results assume no spatial multiplexing gains, whereas the LTE results from [24] include spatial multiplexing and beamforming.

In [72] Hammoudeh et al represented the multipath propagation channel at 62GHz LOS and NLOS suburban microcell environment using a ray-tracing model. It was found reflections up to second order from building surfaces and the ground could represent the microcell propagation adequately, while the diffraction contribution to signal envelope could be neglected.

They acknowledged at UHF frequency (traditional cellular bands) microcell, diffraction contributed significantly to the receiver power level, but at mmWave bands like 62GHz, effect of diffraction mechanism could be neglected mobile scenarios, confirming RSL's Wireless Insite simulation results introduced in section 1. The LOS measurements indicated multipath propagation was caused by direct component interacting with reflections from building surfaces primarily, when the antenna radiation pattern did not preclude them. Scattering and diffraction from lampposts and other objects contributed much less significantly to the receiver signal strength. For NLOS measurements, the mean signal level declined significantly and rapidly when the direct component was blocked by obstructions such as buildings, limiting coverage to the LOS area and a few meters within the shadow area, where single reflections from building surfaces contributed to the signal strength [72].

5 INDOOR AND BUILDING PENETRATION

5.1 Overview

This section covers indoor propagation environments including two scenarios: 1) both transmitter and receiver antennas are placed inside a building as shown in Figure 48. 2) the transmitter antenna is placed outdoor while the receiver antenna detects the signal in a building as shown in Figure 49. In this case, there is building penetration loss, and the analysis of penetration characteristics is a crucial research area.

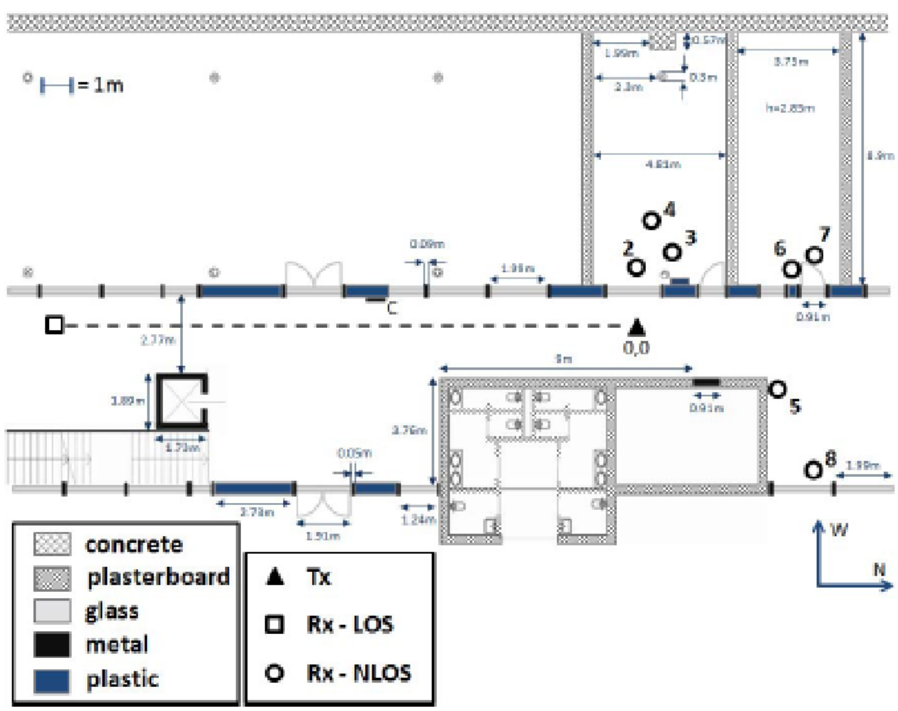

Figure 48: Indoor propagation scenario at the University of L'Aquila, Italy [16].

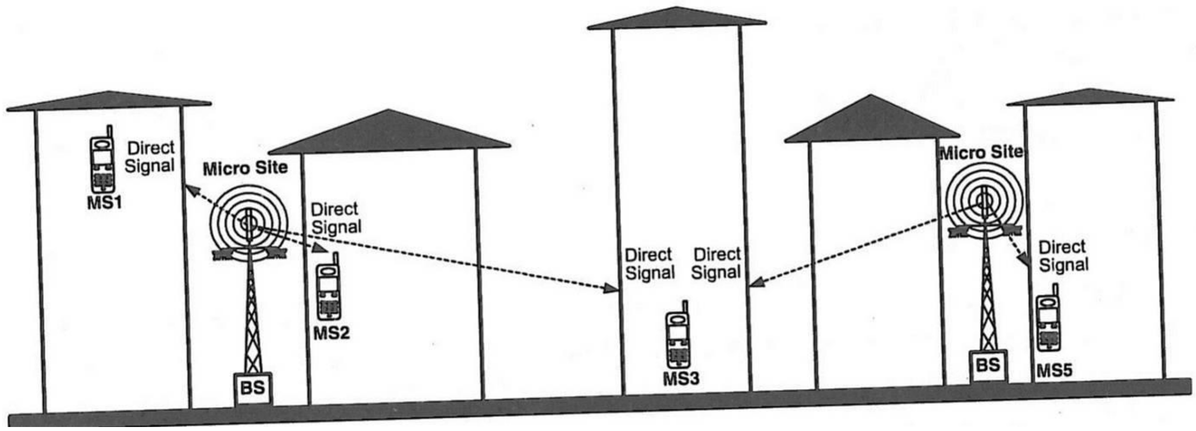

Figure 49: Outdoor- to-indoor propagation scenario in a microcell deployment [15].

Indoor wireless communication is becoming more important in the growing demand of voice and data communication services within the workplace. Indoor propagation is further classified into transmitter and receiver antennas configuration, such as whether they are located in the same room or on the same floor, availability of LOS paths, number and nature of obstructing partitions, etc [10]. Measurements have been taken place in offices, laboratories, conference rooms, and etc to characterize parameters such as free-space path loss, penetration loss, and multipath propagation [44]. Similar to the outdoor environment, these parameters are also considered extensively for indoor coverage planning. Compared to outdoor propagation, indoor radio channels generally have shorter transmitter and receiver separation distance, and lower transmitter power; resulting in shorter delay of echoes and consequently a lower delay spread [3]. One interesting phenomenon is that the indoor received signal level is more fluctuating and harder to predict than the outdoor one [11]. Penetration loss through indoor obstructions depends on the number of layers of obstacles, their materials, as well as the distance between the transmitter and the receiver [17]. Cost 231 listed four groups of indoor propagation models: empirical narrow-band models, empirical wide-band models, models for time variations and deterministic models [3].

According to a recent statistics, 80% of total mobile traffic is contributed by the mobile users located inside buildings. Therefore, covering indoor users from outdoor cellular base stations is a major concern for most carriers. Building penetration loss is a big challenge in this propagation scenario [15]. A measurement campaign in and around buildings in New York has been done to measure reflection and penetration loss of common indoor and outdoor building materials. The results indicate outdoor-to-indoor penetration is difficult to achieve due to the highly reflective and lossy nature of common external building materials. Indoor-to-indoor and outdoor-to-outdoor propagation, on contrast, is more likely to be accomplished [17]. Two measurement campaigns in ultrahigh frequency (UHF) range in Liverpool both show that penetration loss decreased with increasing frequency[18][19].

5.2 6~20 GHz Frequency Bands

Use cases:

Residential and office communication plays an important role in people's everyday lives. Thus, indoor and outdoor radio propagation has become more and more important. This section presents the measurements between 6-20 GHz, particularly in 5.2GHz and 5.8GHz, from several case studies. One of the main objectives is to measure the signal strength in the building as well as from outdoor to indoor environment. Measuring the path-loss, house shadowing loss and penetration loss are the focus points while signals penetrate through the obstacles between transmitters and receivers. Measurement campaigns in most case studies took place in working station, studying area and residence area. The path loss was detected and captured when the transmitter and receiver are in different positions.

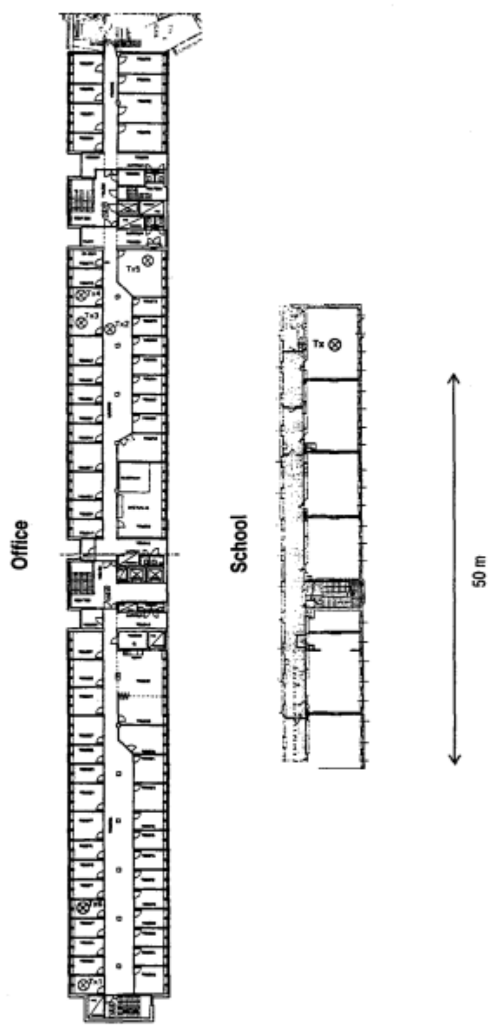

Figure 50: 6th floor of an office building and 3rd floor at a school [51].

For indoor to indoor propagation, the most classic model is in school. The measurements take place in single floor in the building and separate the transmitter for several classes.

With a diameter of 12.5m wide, 115m long and 6 stories high which is about 60m, the campaign collect average of received power was obtained by taking the median of 401 samples on a horizontal circle of about 0.5m diameter. [51].

For the outdoor to indoor case, the campaigns were carried out in three different places, the homes of Rappaport, Woerner, and Tranter. Tree loss and penetration loss were measured in these three places. The transmitter antenna was placed 30-45 m from the house at a height of 5.5 m. Each measurement is taken 1 m distance apart and repeated calibrations of the hardware to measure the stability of the measurement system. [68]

<u>Measurement results:</u>

Measurement campaigns have picked various positions to test the frequency at 5.2GHz. There are two different test cases. One is on the 6th floor of an office building while the other test place is on the 3rd floor of a school. According to Figure 51, it is clear that the path loss in the office is 8.7dB while it is 5.9dB in the school building [51].

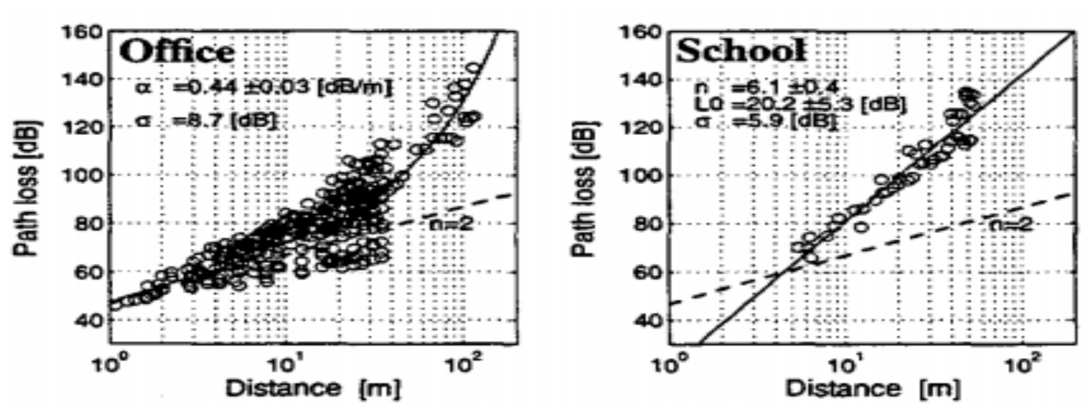

Figure 51: Path loss versus distance from all same-floor measurements in the two buildings. Dashed lines are free space loss while solid lines are fitted models. [51]

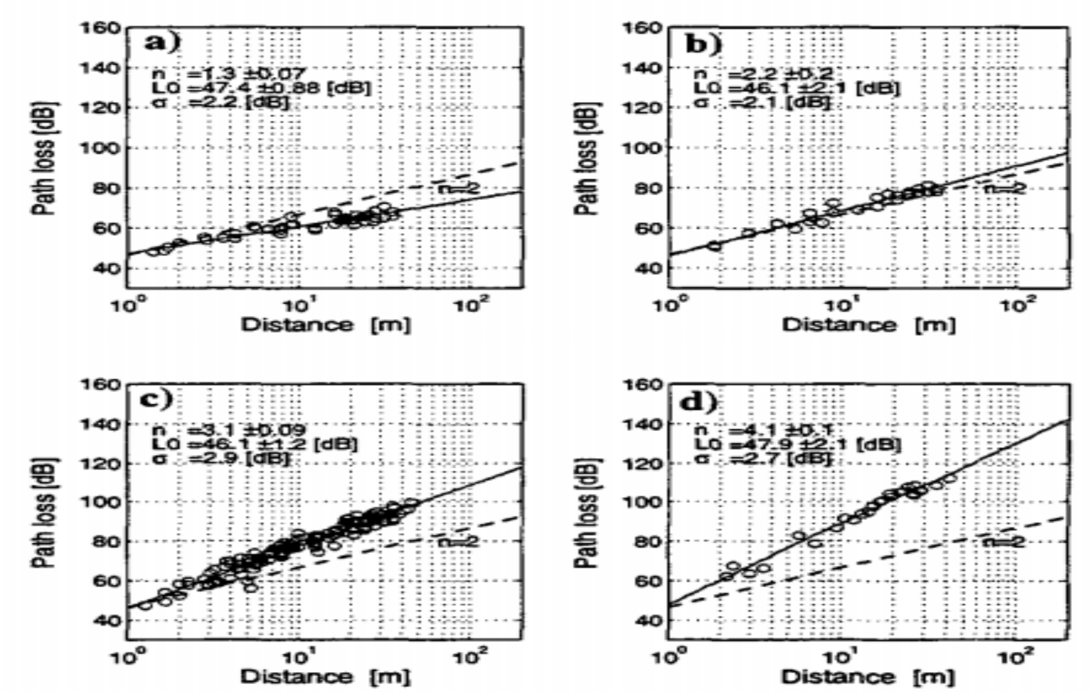

Figure 52: Path loss vs. distance from office building measurement on the same floor [51]

Besides to the general path loss, the campaigns have also more detailed measurements shown in the Figure 53. In a) is from corridor-corridor; b) one antenna was located in the doorway of a room and the other in the corridor; c) is from corridor to room and d) is from room to room [51]. Clearly, the standard deviation is 2.2dB to 2.7dB which is smaller than 4dB. On the other hand, the path loss in the cross floor case, it is about 30dB as the result shown below.

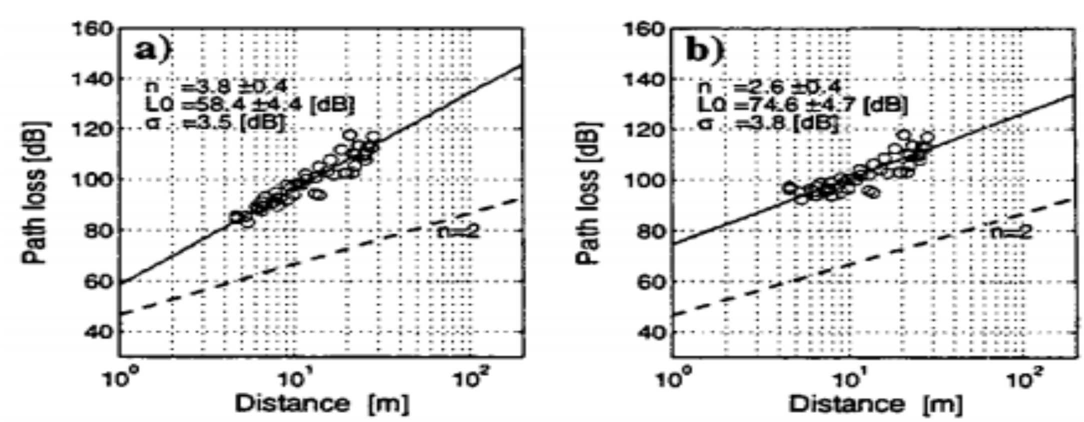

Figure 53: Path loss vs distance for office environment for cross floor measurement [51]

In addition to the results of indoor-to-indoor propagation, outdoor-to-indoor measurement results have also been presented.

TR Configuration	n	σ (dB)	# of Meas. Locations	# of Homes
Indoor				
Overall	3.4	8.0	96	3
First Floor Receiver	3.5	8.3	58	3
Second Floor Receiver	3.3	7.3	38	3
Outdoor				
Overall	2.9	7.9	147	3
1.5m Receiver	2.9	9.0	73	3
5.5m Receiver	3.0	6.4	74	3
Rappaport				
First Floor Receiver	3.5	9.7	23	1
Second Floor Receiver	3.5	7.4	10	1
1.5m Receiver	3.1	10.2	26	1
5.5m Receiver	3.0	6.5	27	1
Woerner				
First Floor Receiver	3.2	6.2	8	1
Second Floor Receiver	3.3	7.7	22	1
1.5m Receiver	2.9	8.2	22	1
5.5m Receiver	3.1	6.2	20	1
Tranter				
First Floor Receiver	3.6	6.9	8	1
Second Floor Receiver	3.4	3.1	27	1
1.5m Receiver	2.7	6.4	26	1
5.5m Receiver	2.8	5.3	26	1

Figure 54: Path loss vs distance for office environment for cross floor measurement [51]

Home	Exterior	Insulation Type	TR sep	APL (dB)
Rappaport	Brick	Paper-backed	30m	13.3
			150m	16.4
Woerner	Wood Siding	Paper-backed	30m	13.1
			210m	7.2
Tranter	Brick	Foil-backed	48m	21.1
			160m	15.3
		Linear Average		16.3
		dB Average		14.4

Figure 55: APL for all homes at 5.85GHz, using 5.5m Tx height [68]

Shadowing Element	Loss in excess of free space
Brick house exterior	14.5 dB
Wood siding exterior	8.8 dB
Cinderblock wall	22 dB
Subterranean basement loss	31 dB
Interior wall	4.7 dB
Small deciduous tree	3.5 dB
Large deciduous tree	11 dB
Large coniferous tree	14 dB
Close-in house shadowing (1.5m RX height)	24 dB
Close-in house shadowing (5.5m RX height)	16 dB

Figure 56: Rule-OF-Thumb Attenuation Value [68]

From Figure 54, the results show that the path loss exponent for the indoor locations are larger than for the outdoor locations due to additional penetrations loss into the home [68]. As the penetration distance increases, the penetration loss will increase [69]. Figure 55 has showed the aggregate penetration loss calculated in three homes. The Woerner home was about 8dB less than the other two homes. The Tranter home exhibited about 4dB more APL than the Rappaport home. Although both homes are brick homes the Tranter home has aluminum foil backed insulation around the entire exterior which caused more penetration loss. The linear average value is 16.3 dB. Building shadowing loss is another significant point that campaigns have taken into account. Figure 56 presents the path loss calculated and studied in front of and behind the single obstructions [68]. This figure also introduces a 10 -13 dB loss in excess of free space path loss caused by tree shadowing. The measurement result shows that it is easier to propagate underneath the canopy to ground level receivers [68].

5.3 28~38GHz Frequency Bands

Use cases

Several indoor measurements have been done in this frequency band. In 28 GHz, several indoor-to-outdoor and outdoor-to-indoor measurements [17] were performed around NYU campus; and several indoor and outdoor-to-indoor measurements [50] were performed at Spain in the frequency of 38GHz. The measurements were mostly focused on the reflection power, penetration losses and power delay profile. These parameters will help the researchers to build the design and deployment of future mmWave communication networks [17]. For the measurement campaign performed in New York, 24.5 dBi steerable horn antennas were used for testing the penetration and reflection criteria. The setups of the measurement were shown in Figure 57 and Figure 58.

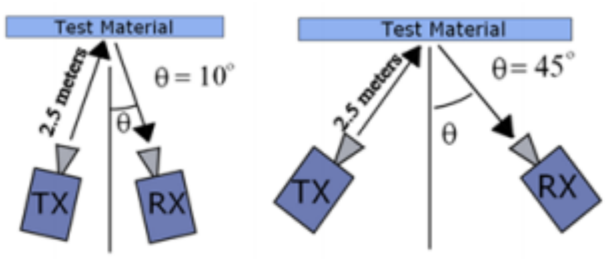

Figure 57: Setup for measuring reflected power

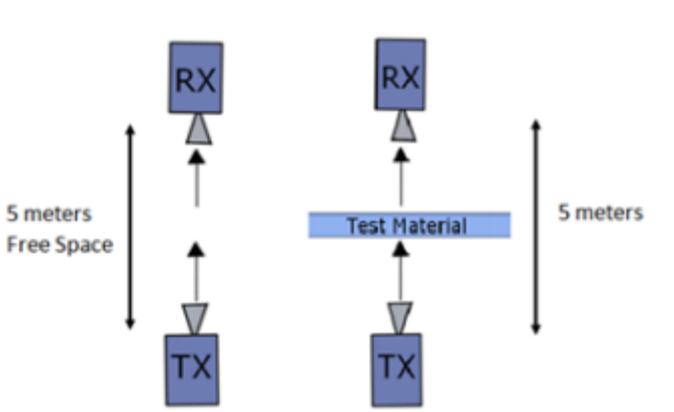

Figure 58: Setup for measuring penetration loss

For the measurement campaign performed in Spain in 38 GHz, three groups of environments were tested to get the results for a variety of multipath situations [50]: two indoor environments, three outdoor environments and one outdoor-to-indoor environment. The channel sounding systems used in the measurement campaign were shown in Figure 59. Both directional and omnidirectional antennas were applied in the measurement campaign.

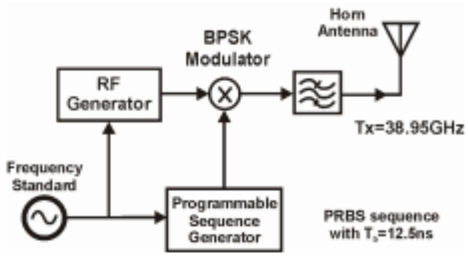

(a)

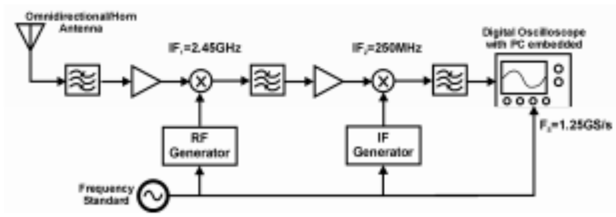

(b)

Figure 59: a) Transmitter and b) receiver block diagrams of the channel sounding system [50]

<u>Measurement results</u>

Reflectivity and penetration losses were compared for different materials in the measurement campaign for 28 GHz range. The material tested included tinted glass, concrete, dry wall, brick, clear glass, and walls. The comparison of the reflectivity is shown in Table 16.

Table 16: Comparison of reflectivity of different materials in NYU [17]

Environment	Location	Material	Angle (°)	Reflection Coefficient ($\lvert\Gamma_{\parallel}\rvert$)
Outdoor	ORH	Tinted Glass	10	0.896
		Concrete	10	0.815
			45	0.623
Indoor	MTC	Clear Glass	10	0.740
		Drywall	10	0.704
			45	0.628

These measurement results show that the outdoor building materials generally have a higher reflection coefficient compare to the indoor material; this is due to the outdoor building materials containing thick and dense metal layers [17]. The comparison of the penetration loss is shown in Table 17.

Table 17: Comparison of penetration loss for different materials in NYU [17].

Environment	Location	Material	Thickness (cm)	Received Power - Free Space (dBm)	Received Power - Material (dBm)	Penetration Loss (dB)
Outdoor	ORH	Tinted Glass	3.8	-34.9	-75.0	40.1
	WWH	Brick	185.4	-34.7	-63.1	28.3
Indoor	MTC	Clear Glass	<1.3	-35.0	-38.9	3.9
	WWH	Tinted Glass	<1.3	-34.7	-59.2	24.5
		Clear Glass	<1.3	-34.7	-38.3	3.6
		Wall	38.1	-34.0	-40.9	6.8

It could be seen that the brick and tinted glasses typically have a higher penetration loss and walls and clear glasses have a lower penetration loss. These results suggest that the RF energy can be contained in intended areas with buildings, also reducing interference, but making building penetration more difficult [17]. The wall penetration loss in an office environment was also generated in the measurement campaign in NYU. The results are shown in Table 18.

Table 18: Comparison of wall penetration losses in office environment in NYU [17]

RX ID	TX-RX Separation (m)	# of Partitions				Transmitted Power (dBm)	Received Power – Free Space (dBm)	Received Power – Test Material (dBm)	Penetration Loss (dB)
		Wall	Door	Cubicle	Elevator				
1	4.7	2	0	0	0	-8.6	-34.4	-58.8	24.4
2	7.8	3	0	0	0	-8.6	-38.7	-79.8	41.1
3	11.4	3	1	0	0	11.6	-21.9	-67.0	45.1
5	25.6	4	0	2	0	21.4	-19.0	-64.1	45.1
4	30.1	3	2	0	0	21.4	-30.4	Signal Detected	
6	30.7	4	0	2	0	21.4	-30.5		
7	32.2	5	2	2	0	21.4	-30.9		
8	35.8	5	0	2	1	21.4	-31.9	No Signal Detected	

These results show that the penetration loss was depended on number of obstructions, TX-RX distance, and surrounding environment. Moreover, the indoor-to-outdoor penetration will be quite difficult at 28 GHz, whereas indoor-to-indoor and outdoor-to-outdoor propagation is easily supported by the strong reflectivity of external building materials and low attenuation of indoor materials.

For 38GHz, some indoor measurements were performed in Spain. 400 complex impulse responses (CIR) and some other parameters were collected and analyzed. Figure 60 shows the magnitude of the set of 400 impulse response in an indoor scenario using the omnidirectional antenna at the receiver or the directive antennas at both ends.

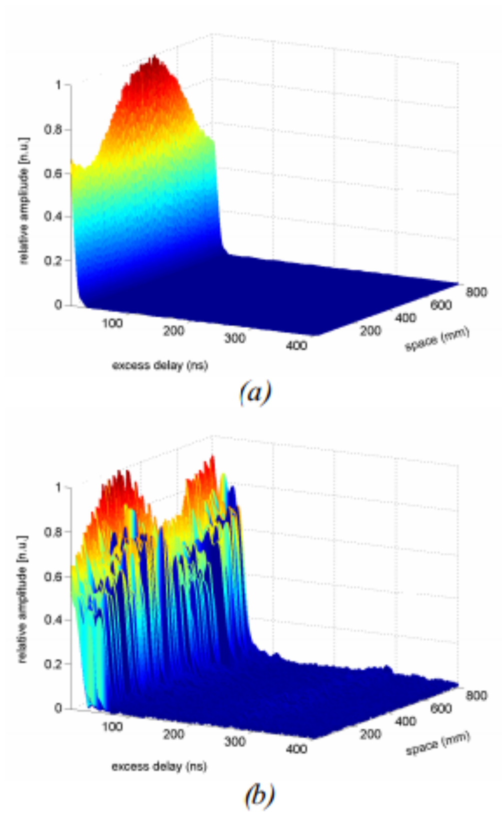

Figure 60: Magnitude of the set of 400 impulse response for a) Omnidirectional antenna at the receiver b) Directive antennas at both ends [50]

The ranges of time and frequency channel parameters were also collected in the measurement done in Spain. The results includes the values of mean delay (τ_{mean}), delay spread (τ_{RMS}), coherence bandwidth for 90% (CB0.9) and 50% (CB0.5). The results are shown in Table 19.

Table 19: Range of time and frequency channel parameters for the measurement campaign in Spain [50]

Environment	τ_{mean} [ns]	τ_{rms} [ns]	$CB_{0.9}$ [MHz]	$CB_{0.5}$ [MHz]
Indoor	[17.3, 19]	[21.9, 24.2]	[4.1, 8]	[11.5, 59.8]
Outdoor	[3.8, 4.9]	[5.2, 7.7]	[13.4, 20.1]	[60.2, 67.7]
Outdoor- Indoor	[15.4, 28]	[23.5, 41.6]	[1.7, 3.5]	[6.4, 18.7]

Some general results were also concluded during the measurement campaign in Spain. The τ_{RMS} could be influenced by the room dimensions, the reflectivity of the wall and the directivity or polarization of the antennas. Overall, the measurement campaigns results show good expectations for use of the 40GHz band to offer broadband services with high bit rates [50].

5.4 60~94GHz Frequency Bands

<u>Use Cases</u>

In the frequency band 60 to 94 GHz, multiple measurement campaigns have taken place for the indoor environment. The measurements were mostly done in typical office environments such as indoor corridors or room penetration. Figure 61 provides a good representation of the typical setup for the room penetration measurement and Figure 62 provides the setup for corridors measurement.

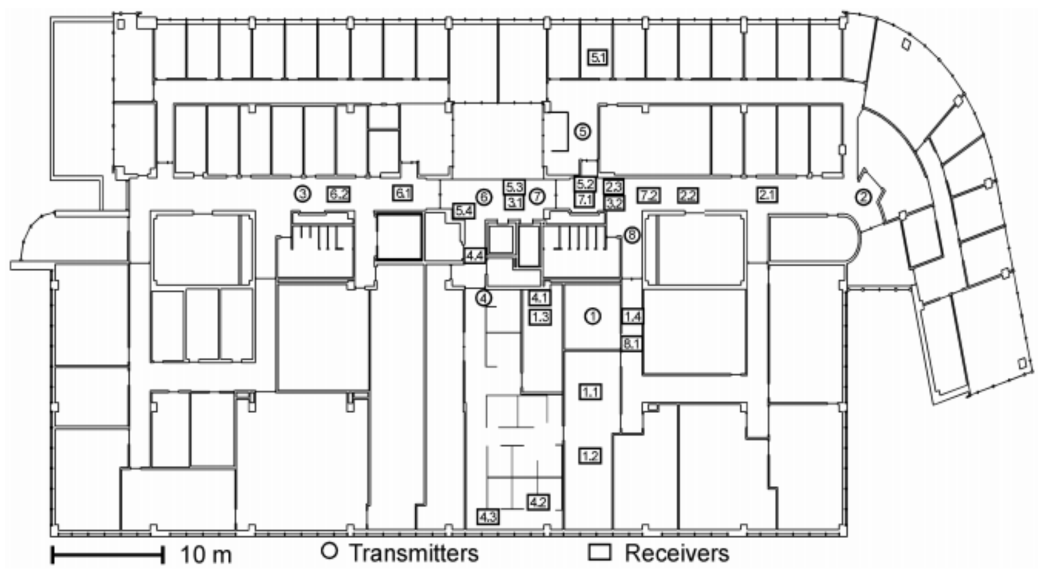

Figure 61: Typical setup for indoor measurement [66]

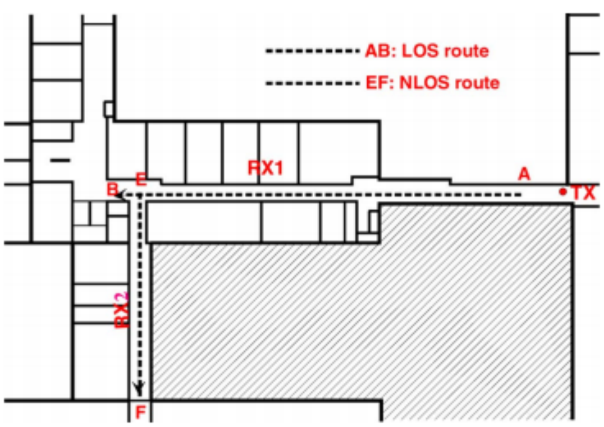

Figure 62: Typical setup for indoor corridors measurement [65]

Figure 61 indicated the measurement plan in Virginia Tech and Figure 62 indicated the measurement plan in Helsinki, Finland. There were also measurements performed in University of L'Aquila [16], Polytechnic Institute of New York University [67], etc. LOS and NLOS transmission were considered in all the cases, with the fixed transmitter and mobile receivers.

Power delay profile, power loss, angle of arrival and some other parameters were measured to investigate the propagation characteristics for indoor environment in this frequency band. In these measurements, horn antennas were used that were placed with a height of approximately 1.5m. The separation of the transmitter and the receivers for the indoor measurement are generally less than 15m with various obstacles in the transmission path.

Measurement Results

Multiple sets of results were collected for various measurements. In the measurement campaign in Virginia Tech [66], 39600 power delay profiles, power loss, penetration loss, multipath delay spread were measured. The results collected are shown in Table 20.

Table 20: Measurement results for 60 GHz in Virgin Tech [66]

Location	Link Distance (m)	Free Space PL (dB)	Local Area Avg. PL (dB)	Local Area Min / Max PL (dB)	Local Area Min / Max / Avg. σ_τ (ns)
1.1	5.4	83	98	97 / 99	15 / 20 / 18
1.2	9.2	87	103	101 / 105	18 / 22 / 20
1.3	4.7	81	93	91 / 94	16 / 18 / 17
1.4	3.5	79	82	81 / 83	1 / 4 / 3
2.1	7.8	86	73	72 / 74	3 / 8 / 6
2.2	16.2	92	78	76 / 87	7 / 9 / 8
2.3	22.9	95	98	95 / 104	6 / 9 / 8
3.1	18.2	93	89	88 / 90	11 / 17 / 14
3.2	27.4	97	99	97 / 100	8 / 12 / 9
4.1	6.0	84	94	89 / 98	10 / 16 / 11
4.2	13.0	90	99	97 / 101	9 / 18 / 14
4.3	13.6	91	91	89 / 97	10 / 19 / 15
4.4	4.7	81	89	88 / 90	6 / 22 / 13
5.1	4.5	81	81	76 / 83	6 / 12 / 8
5.2	12.2	90	96	94 / 97	3 / 12 / 8
5.3	7.7	86	87	85 / 87	5 / 10 / 8
5.4	3.9	80	80	73 / 83	3 / 6 / 4
6.1	7.6	86	89	88 / 91	2 / 12 / 6
6.2	17.1	93	103	97 / 107	19 / 30 / 25
7.1	5.5	83	94	93 / 95	9 / 14 / 12
7.2	10.4	88	99	97 / 99	6 / 12 / 9
8.1	5.5	83	85	84 / 86	17 / 24 / 19

The location ID refers to the location picked in Figure 61. From the measurement campaign, it could be found that “at 60 GHz, propagation is more ray-like and the structure and composition of partition in the environment can have a significant impact on multipath delay spread.”[66]

Similar indoor measurement also performed in Polytechnic Institute of New York University at 73.5 GHz. [67] Penetration losses and multiple delay spread were collected during the measurement campaign.

Table 21: Penetration loss measurement at 73.5 GHz in NYU [67]

RX ID	TX-RX Separa -tion (m)	# of Partitions				Received Power for Free Space (dBm)	Received Power for Test Material (dBm)	Penetration Loss (dB)
		Cubicle Wall	Metal Cabinet	Dry Wall	Wood Door			
1	6.8	1	0	0	0	-34.1	-39.4	5.3
2	8.0	1	1	0	0	-35.6	-52.8	17.2
3	10.1	2	2	0	0	-37.6	-61.4	23.8
4	11.5	1	2	1	1	-38.7	-75.5	36.8
5	8.6	0	2	0	0	-36.2	-50.3	14.1
6	8.1	0	2	0	0	-35.7	-45.4	9.7
7	8.8	1	2	0	0	-36.4	-63.0	26.6
8	14.0	0	2	1	1	-40.4	-55.6	15.2
9	13.0	1	3	0	0	-39.7	-53.0	13.3
10	15.2	1	2	1	0	-41.1	-60.4	19.3
11	15.2	1	2	1	0	-41.1	-59.0	17.9

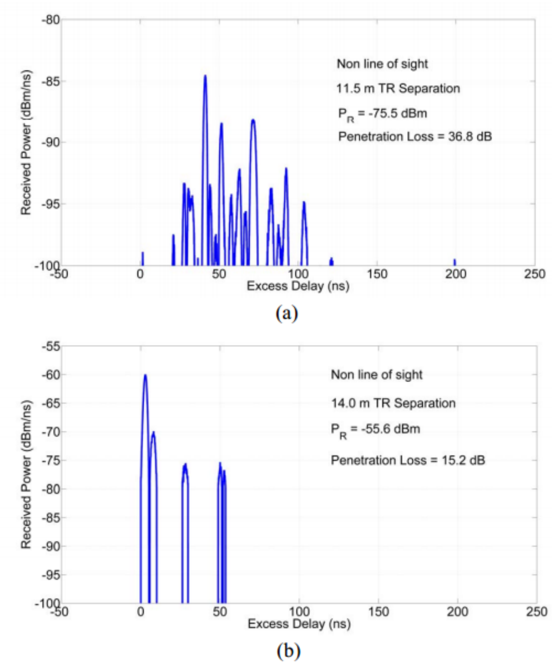

Figure 63: Multipath delay spread in different RX location at 73.5 GHz [67]

From the table and figure above, one can observe that there is no definite relationship between the penetration loss and the distance of the TX and RX and the received power may vary greatly depends on the specific topography of the surrounding environment. [67] These results will be helpful to determine the design of the fifth generation indoor cellular system.

There were also some measurements performed for the indoor corridors. Measurements result in 60 GHz at Helsinki Finland [65] were collected and analysed for both LOS and NLOS transmission. The results and comparison for LOS and NLOS are shown in Figure 64 and Figure 65 respectively.

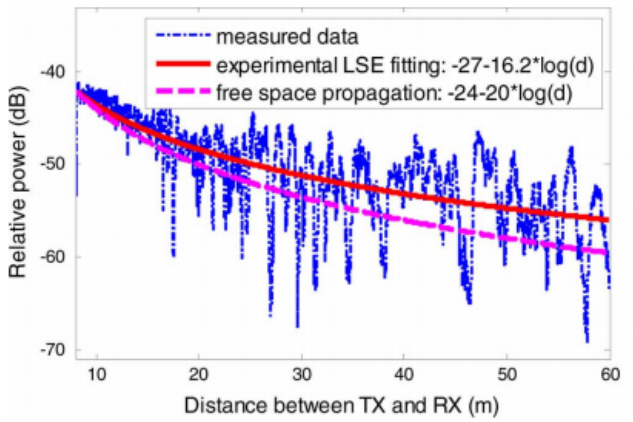

Figure 64: LOS measurements results and LSE comparison in 60 GHz [65]

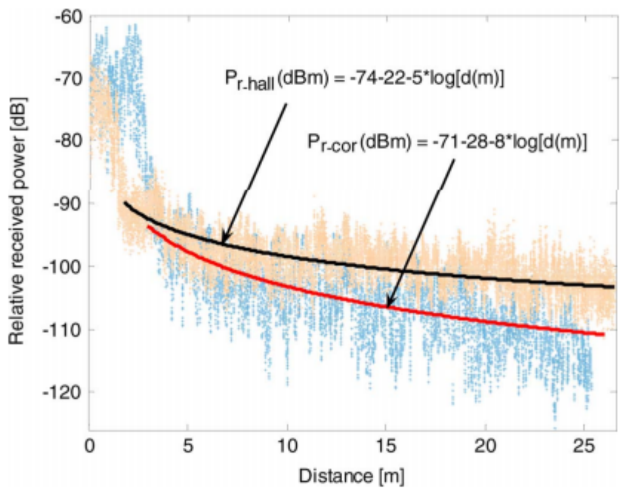

Figure 65: NLOS measurement results and Empirical models comparison [65]

From the comparisons above, for LOS, it could be seen that signal decay rate in the LOS corridor is less than the value in the free space. This shows that signals propagate like in free space and guided fashion in near and far zone [65]. For NLOS, the results show that the transmission loss through corridor walls is very high at 60 GHz. This also indicates that signals propagate in a guided fashion and diffraction is the dominant propagation phenomenon in the environment.

6 HUMAN PRESENCE

6.1 Overview

This section analyzes the effects of human presence in the path of a wireless mmWave channel, predominantly in indoor environments, with an exception of outdoor coverage analysis [30]. Temporal variations of fading and shadowing effects induced by human movement often dominate indoor short-range propagation environment. They are stronger with increasing frequency or mobile radio terminals [20]. Some past researchers have attempted to model temporal variations of the channels. The measured and analyzed parameters include amplitude distributions, level crossing rates, average duration of fades, power spectrum density, and temporal correlations [21]. A typical pedestrian-induced scattering effect in an indoor environment is shown in Figure 66 [22].

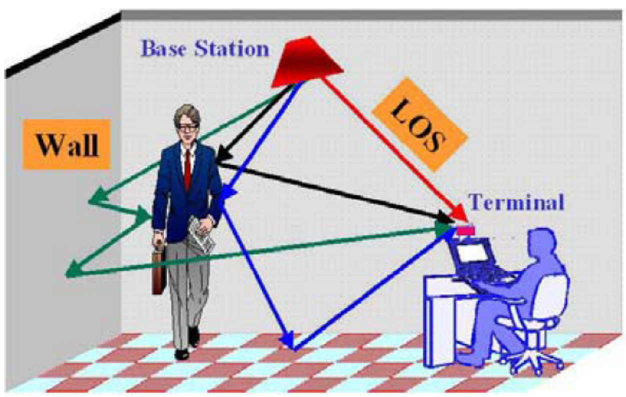

Figure 66: An indoor propagation scenario with human presence [22].

Ray-tracing simulation technique is often applied to modeling the indoor propagation channel and studying the effects of human bodies' wave obstruction—reflection, diffraction, and transmission. Human bodies are often modeled as a perfect conducting circular cylinder [20][22~29]. Figure 67 is a proposed model for human-induced shadowing effects [26]. Some measurement campaigns did use real people for natural human motion [21][31~33]. The factors such as the number of people, their actions and locations can have a large influence on the test results. For example, in [32] the "human activity" was defined by number of people present at a given time in the vicinity of the antennas. They might be sitting or moving around the table, coming in or going out of their laboratory.

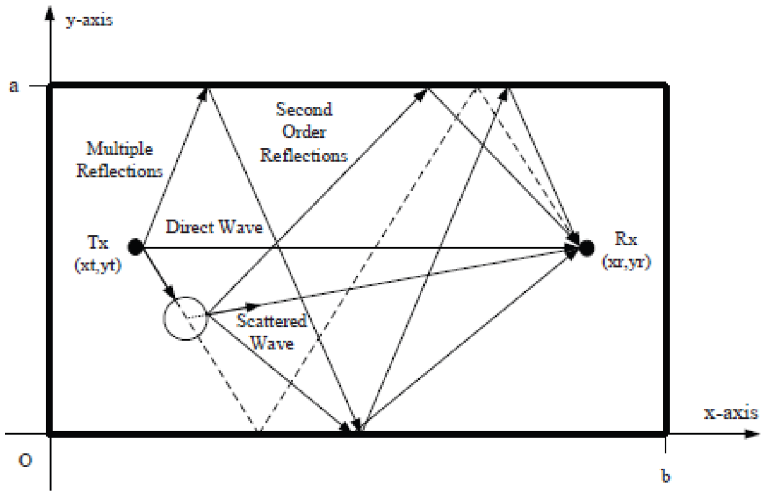

Figure 67: A ray-tracing model taken into account of scattering from cylinders and multiple reflections up to second order [26].

6.2 6~20 GHz Frequency Bands

Use cases:

It is clear that human presence and activities will definitely need to be taken into consideration when dealing with wireless propagation because it will affect the received signal in various ways. A literature survey of six relevant articles published between the early to late 2000s examines various indoor scenarios between ~5.7 to 20GHz frequency range. These articles follow a similar pattern because each illustrates the effects of human presence and characteristics such as pedestrian-induced fading [20] or human motion approximated by a perfect conducting circular cylinder [23]. Although all the tests are done indoors in mostly office scenarios, the antenna type and configurations vary for each case. For example, a 150-m2 office is typical in most places where the dimensions are 15m by 10m by 3m height [20]. The most common type of antennas used for both transmitter and receiver in these tests were horn antennas [22-25]. In one experiment, the access point was simulated with an ideal vertically polarized dipole antenna with the receiver represented by a vertically polarized monopole [20]. Although the antenna types were similar, the configurations varied. The height of both transmitter and receiver did not exceed 2m in most cases. Moreover, the separation distance did not exceed 4m. These cases are realistic for indoor situations. Sometimes it might not be appropriate to have real human presence while testing propagation effects. Therefore, many articles have appeared to demonstrate that human body may be approximated by a uniform geometrical shape. The human body or cylinder moving parallel and perpendicular with respect to the direct line of sight have been investigated. Figure 68 and Figure 69 show both these illustrations [23].

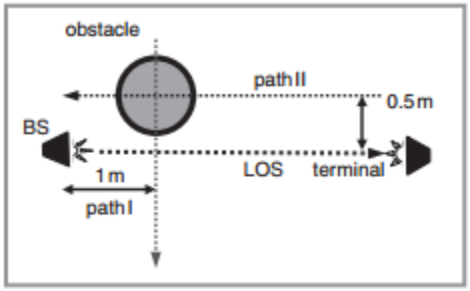

Figure 68: Obstacle parallel to LOS [23]

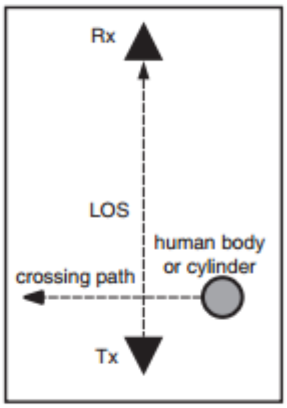

Figure 69: Obstacle crossing LOS [23]

<u>Measurement results:</u>

Investigating indoor radio wave propagation at ISM band frequencies, a team in Ireland observed how a propagation channel would vary from temporal fades that caused by pedestrian movement [20]. Penetration depth and received power were some of the parameters investigated. Ray tracing techniques were used along with a homogenous, finite length, lossy dielectric cylinders as pedestrians. For this setting, the received power results are shows in Figure 70. These results show that in the beginning (4 and 8s), the profile is quiet. As there is more pedestrian movement towards the end, more rapid variations are present. This is the case for frequencies of 2.45 GHz, 5.7 GHz and 62 GHz.

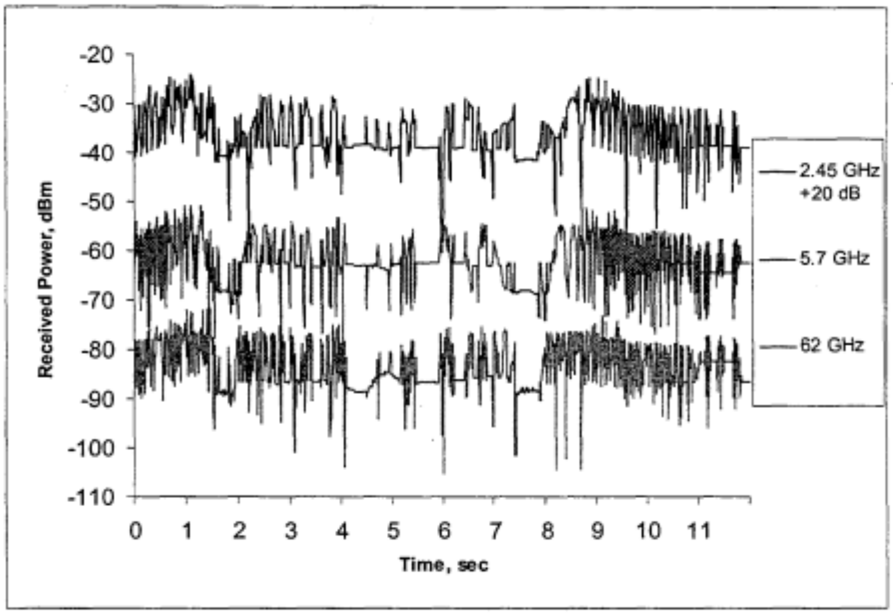

Figure 70: Fading profile caused by pedestrian movement [20]

In another similar experiment, the human body was modeled again as a metallic cylinder and while moving in parallel path with the LOS between two fixed terminals [22]. This experiment was done in a corridor at 10GHz. A few conclusions could be made from this experiment. The amplitude results demonstrate that human motion indeed affects LOS link especially for close distances. Moreover, the distance between the walls and human motion also has an effect on the temporal fading of the received signal. This can be seen in Figure 71. When the distance between the cylinder and antennas are larger, there is a higher rate of amplitude variations in the received signal as shown in Figure 72.

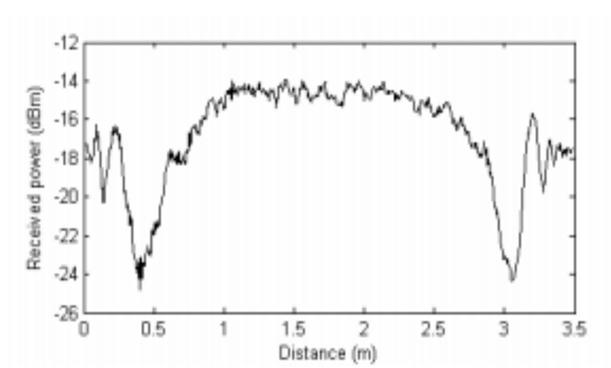

Figure 71: Temporal fading caused by human motion [22].

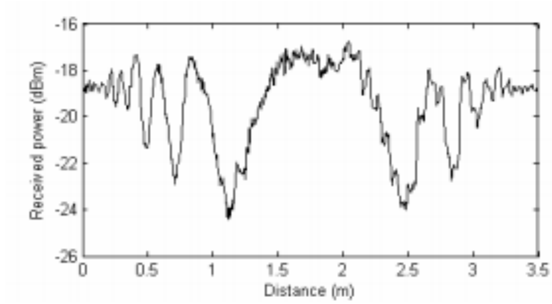

Figure 72: Larger distance between the cylinder and antennas [22].

In order to further understand the correlation between results obtained when a person is moving along a path and when a conducting cylinder is moving along the same path, Ghaddar et al did an experiment comparing both scenarios [23]. A conducting circular cylinder of radius 0.25m was used and CW measurements were performed at 10GHz between two terminals that were fixed. The cylinder first moved in parallel with the LOS for the first case and then perpendicular with the LOS for the second (Refer to Figure 68 and Figure 69). A human body was now replaced with the cylinder and the same cases performed. The crossing LOS results for cylinder and human bodies are show in Figure 73. Both have power signal disparity from -24.5 to 0 dB. It can be see that the fading, periodicity and power decaying in the signals are very similar in both cases. Obstacles moving parallel to LOS had similar results. Figure 74 shows the relative powers for this case. Here we see an agreement between the two figures. One difference when using the cylinder is that it vibrates while moving.

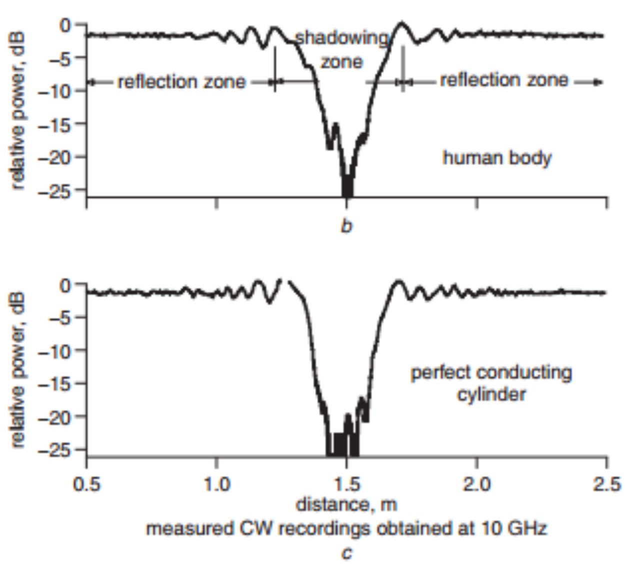

Figure 73: Human body crossing and perfect conducting cylinder crossing LOS

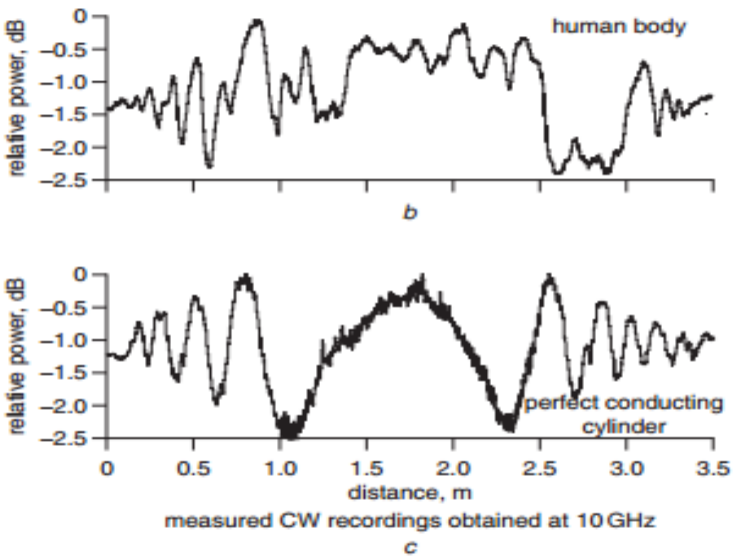

Figure 74: Human body and perfect conducting cylinder moving parallel to LOS

Human presence measurements of an indoor radio channel at 20GHz in Sydney, Australia have been reported by Oppermann et al with more interesting observations [31]. His team took impulse response measurements in various locations of a typical office environment while real human bodies carried out normal daily activities. The effect on the received signal depended on whether people were moving near the transmitter or the receiver. Fades up to 16dB could be seen for a person moving close to a transmitter. If a person was somewhere between the transmitter and receiver, fades were between 6-10 dB.

Ultimately, moving of humans indoor has many effects including fading on a propagation channel. In order to understand these effects, human body can be approximated by a uniform geometric shape. The ray tracing technique as also been continuously used but on can increase the efficiency of this method by using UTD [23].

6.3 28~38GHz Frequency Bands

Use cases

There have not been many papers and experiments reported around 28-38 GHz range to characterize human presence. Only two papers were found for this report. Paul Marinier et al in [21] reported an experiment near 30 GHz to characterize human induced variations of an indoor radio channel for which both terminals are stationary. The work done on this paper will allow others to construct a theoretical model for prediction of statistical behaviour of an indoor mmW channel under certain conditions. Similarly, in [65], experimental results were conducted at 37.2 GHz between two fixed terminals in a corridor. The main objective here was to investigate human motion for line-of-site propagation channel. The environment for [21] is illustrated in

Figure 75. There could be strong reflections on the windows and room R1 was emptied to allow for human activities.

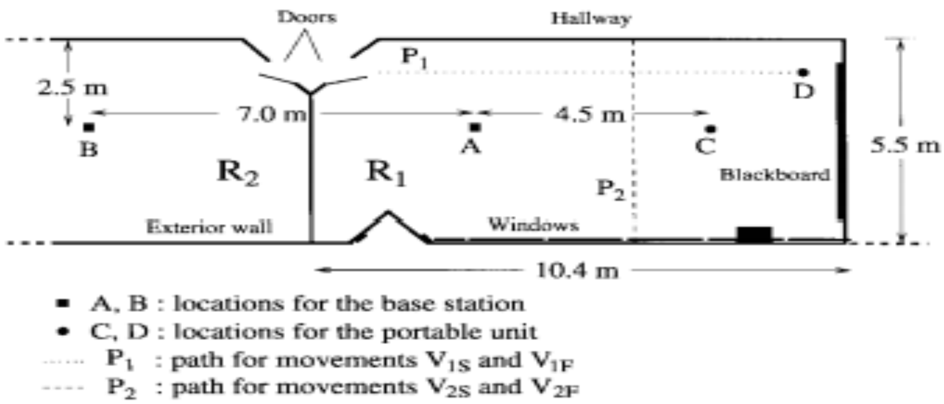

Figure 75: Propagation environment [21]

A CW signal at 30.1 GHz is transmitted by an antenna at a height of 2.5m. One of the receiving antennas is a linearly polarized scalar horn whereas the other one is a linearly polarized biconical omni directional antenna. These two receive antennas have beam widths of 120 and 45 respectively that is 10 dB below the maximum intensity. The environment for [65] was a long corridor 2.2m in width and 4.5m in height. The floor is mainly concrete while the ceiling has metallic tiles. The walls are plaster-board. Horn antennas that are vertically polarised have a gain of 15 dB and 3 dB beam width of 25.5". It is at a height of 1.5m above the floor. The antennas are positioned to obtain a LOS signal level and only one person is in walking in parallel to the LOS. A simple illustration is shown in Figure 76.

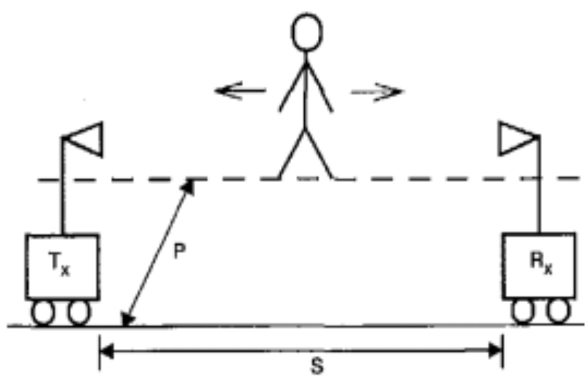

Figure 76: Physical arrangement of person's motion [65]

Measurement results:

The experiment conducted in [21] found that the received envelope can be considered as realizations of only locally stationary process even when the movement of bodies in the environment is regular and continuous. Examples of measured envelops are shows in Figure 77. Figure 77(a) shows an envelope recorded with two persons moving randomly in room R1 shown in Figure 66. The detailed fading over for this same envelope is shows in Figure 77(b). The conclusion is that the envelope has fast fluctuations superimposed on slower variations.

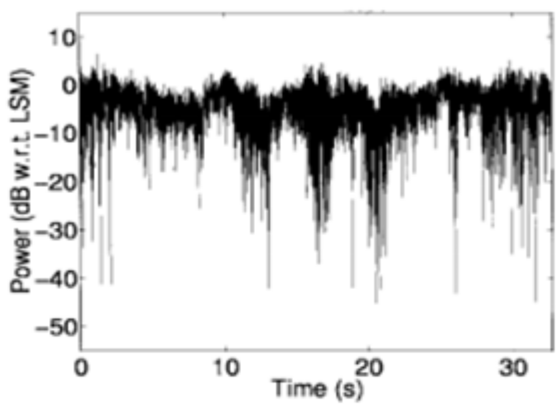

(a)

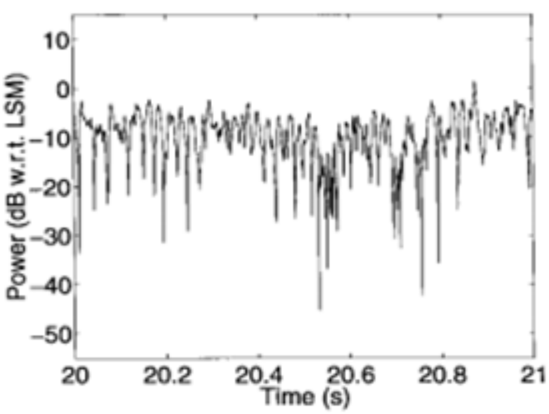

(b)

Figure 77: Example of measured envelopes [21]

It was also found that the amplitude distribution was strongly dependent on the spatial short range fading state when the environment is free of movement. This was the case when there were only a few people in motion with multi-path propagation. An increase in the number of people meant a decrease in this dependence. Moreover, the level crossing rates and the average fade durations were also dependent on the spatial fading level. The data collected in [65] also included amplitude fading distributions, level crossing rates and fade duration statistics. Figure

77 shows some of the measurement results while Table 22 shows, the mean power and the standard deviation of the envelope which are computed for various scenarios.

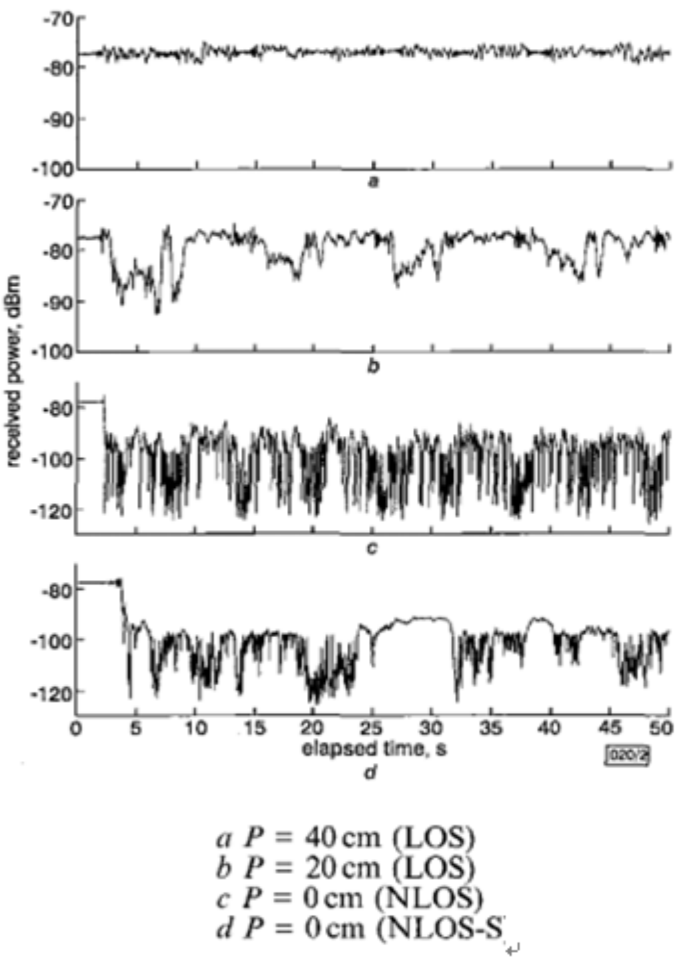

Figure 78: Received signal power against time for S= 6m [65]

When there is an increase in antenna separation by 2m, there is an excess in propagation loss by approximately 5 dB. It was also found that the clothes on humans are good reflectors at 37.2 GHz. For NLOS and NLOS-S scenarios, the mean signal power drops nearly the -105dBm in both antenna separation cases. Table 22 also shows that all LOS scenarios have Rice distributions and that separation of antennas is insignificant. Moreover, NLOS scenarios are log normally distributed. The level crossing rate (LCR) in [65] for motion far from the LOS is concentrated around thresholds close to the LOS component. The threshold levels were between -55 dB to 5dB from the measurements. The LCR starts to spread and decay exponentially for movement closer to the LOS ray. It can be concluded that as a person gets closer to the LOS ray, the scattering will increase as signals are absorbed by the person. Similar results could be observed with the average fade duration. Motion closer to the direct LOS path increased the fade durations. Duration of fades was also greater in NLOS scenarios than LOS.

Table 22: Statistical parameters [65]

	Mean power and standard deviation		Cumulative distribution function	
Scenarios	$S = 4$m	$S = 6$m	$S = 4$m	$S = 6$m
A ($P = 40$cm)	$\eta = -73.53$ dBm $\sigma = 0.98$ dB	$\eta = -77.03$ dBm $\sigma = 0.74$ dB	Rice $K = 14$dB	Rice $K = 19$dB
B ($P = 20$cm)	$\eta = -74.92$ dBm $\sigma = 2.68$ dB	$\eta = -79.51$ dBm $\sigma = 3.23$ dB	Rice $K = 7$dB	Rice $K = 6.5$dB
C (NLOS)	$\eta = -98.17$ dBm $\sigma = 9.68$ dB	$\eta = -99.61$ dBm $\sigma = 9.52$ dB	Lognormal $\sigma = 10$dB	Lognormal $\sigma = 11$dB
D (NLOS-S)	$\eta = -93.28$ dBm $\sigma = 9.45$ dB	$\eta = -101$ dBm $\sigma = 7.91$ dB	Lognormal $\sigma = 14$dB	Lognormal $\sigma = 10$dB

6.4 60~94GHz Frequency Bands

Use Cases:

The influence of human activity based on 60 GHz have been investigated and presented in many papers. Most of the experiments done have been done in early 2000s [20] [32] to just the past few years from 2010 to 2013 [26-30]. Simulations and measurements were mostly done indoors with various scenarios (living room, conference room, labs) [20][26-29]. An outdoor scenario involved a public central campus area with building and trees around [30]. Figure 79and Figure 80 show two examples of typical indoor scenarios. The house is a typical European residential environment where the building materials are breeze blocks, plasterboards and bricks [33]. The laboratory environment has large rooms (100m²) with building materials such as concrete pillars, metallic cupboards and a few windows.

Figure 79: Measurement environment of house [33]

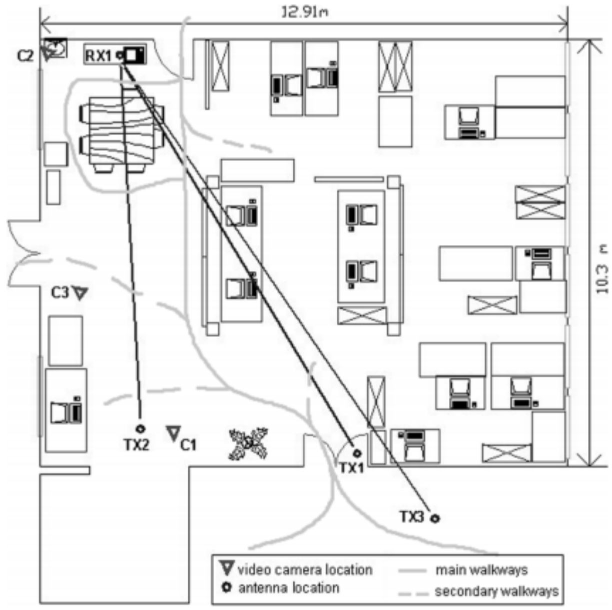

Figure 80: Laboratory [32]

Measurement parameters included fading depth, attenuation, bit error rate, throughput, power delay profile and received power. The configuration and design for both transmitter and receiver varied in each paper. Some cases had multiple receivers and a single transmitter as in [33] and [30]. In [32], the receiver was at a height of 1.55 while two transmitters were at a height of 2.27m and 1.28m at LOS. The third was chosen to be in an adjacent room for NLOS case at a height of 1.58m. The measurements were performed over 15 days and the antenna configurations were changed each day. Table 23 summarizes the measurement durations and human activity for each configuration.

Table 23: Measurement durations and human activities [32]

TX Position	Antennas	Total measurement duration	Human activity	Mean human activity
TX1 ($d = 10.8\ m$)[a]	H-H	4.4 h	0-15 persons	4
	P-H	3.3 h	0-13 persons	4
	P-P	2.7 h	0-12 persons	3
TX2 ($d = 8.7\ m$)[a]	P-H	1.8 h	0-10 persons	5
	P-P	3.1 h	0-10 persons	4
TX3 ($d = 13.2\ m$)[a]	H-H	2.1 h	? [b]	? [b]
	P-H	2.1 h	? [b]	? [b]

[a] d: TX-RX distance
[b] incomplete video recordings

In [20], where the simulated environment was a 150-m2 open plan office, the transmitter was an ideal vertically polarized dipole that was 2.5m above the floor with an EIRP of 2.1 dBm. The receiver which was located 1.1m above the floor represents a +0.0dBi vertically polarized monopole. For an outdoor case, a rectangular planar phased array with 12 by 12 elements was used to cover 90 degrees in azimuth [30]. Moreover, an ideal omnidirectional and directional antenna was tested. These antenna configurations were also tested out in [27] in addition to maximum ray beamforming configuration.

Measurement results:

Table 24 shows the maximum and minimum fading depth for different number of persons in a room of dimension 10m by 20m near a radio link of 60 GHz [29].

Table 24: Max and Min of magnitude for different number of persons

Number of Persons	Min of Mag. [dB]	Max of Mag. [dB]
04	−111.5518	−77.4056
07	−114.8184	−78.4006
20	−116.5973	−77.7331

Moreover, Figure 81 and Figure 82 show the behaviour of channel in presence of different persons on this frequency bands. It can be seen that the temporal channel variation fading effects become rapid as the number of people increases. Figure 81 has variations around an average value of -82.5582 dB while maximum depth of fading is around -34.1462 dB.

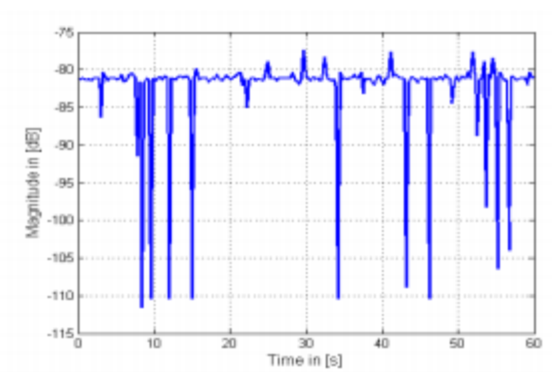

Figure 81: Temporal variations of signal envelope with 4 persons in movement [29]

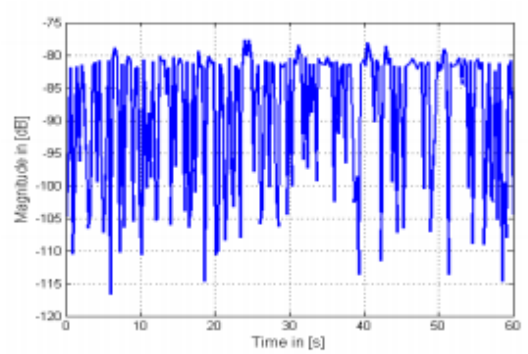

Figure 82: Temporal variations of signal envelope with 20 persons in movement [29]

These patterns of variations are similar in most papers and fading characteristics have been found to vary with area geometry the density and pattern of pedestrian movements but not frequency. Delay spread is another parameter that needs to be examined when dealing with human presence. Human blockage model for IEEE 802.11ad 60 GHz channel model based on ray tracing simulations was investigated in [28]. This paper showed that knife edge diffraction is able to model human blockage at mm-wave frequencies. Moreover, it is shown that average RMS delay spread in a living room scenario increase by a factor of 2.5 when there is human blockage. Figure 83 shows the CDF of RMS delay spread.

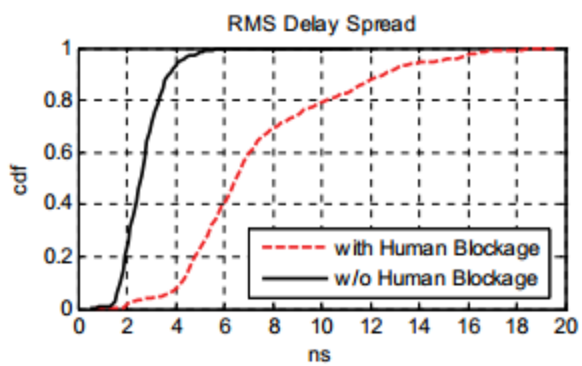

Figure 83: CDF of RMS delay spread with and without the influence of human blockage

In most cases it is found that the maximum RMS delays were during blockage of the LOS path [27]. Delay spread is more intense when diffraction by human body takes place near the receiver. The use of directional antennas was also found to decrease delay spread by approximately 50% [27]. The conclusion was that amplitude of shadowing effect does not depend on the number of persons but on the antennas configurations. The duration of the shadowing effect on the other hand increase with the number of persons within the environment [32]. An outdoor simulation done by Mohamed Abouelseoud et al in [30] modeled human blocking by using a random process. The results followed a similar pattern to those that have been done on indoor scenarios.

Figure 84 and Figure 85 show the difference in performance between an omni-directional receive antenna and a directional receive antenna. From the figures, it is concluded that with directional antenna, the percentage of unserved user equipment in high density blockage scenarios is less than that for omni antenna case. More specifically, there was around 14% of the user equipment with no coverage at 0.5 blocker/m^2 when directional antennas were used. To conclude, directional antennas are recommended for operation of mmWave systems in highly dense areas.

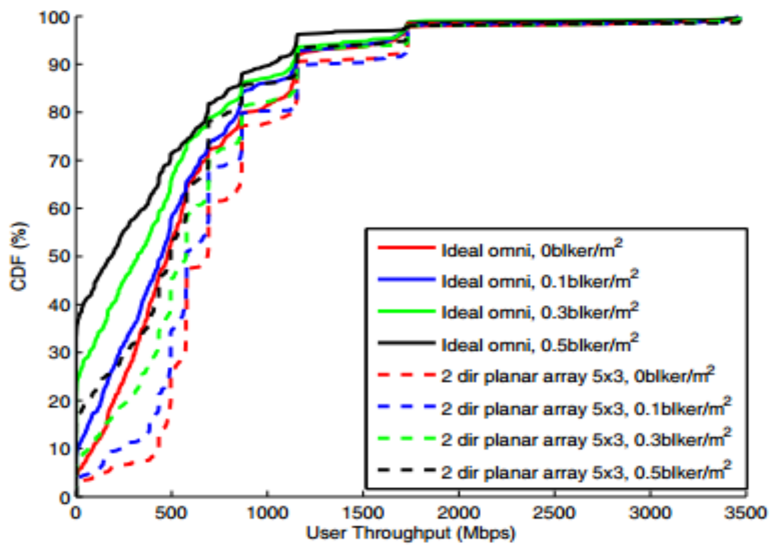

Figure 84: Rx antenna effect on the UE throughput CDF [30]

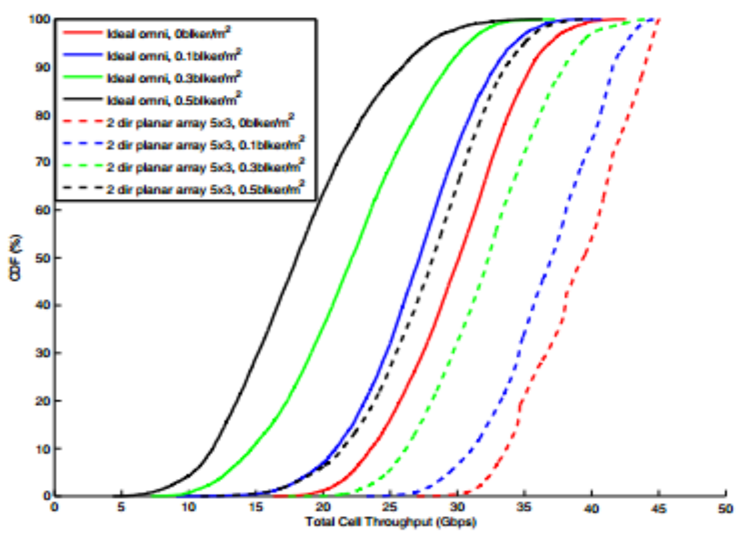

Figure 85: Rx antenna effect on the network throughput CDF [30]

7 CHANNEL SOUNDER MEASUREMENT HARDWARE

7.1 Introduction to Channel Sounder

Channel sounders or channel sounding systems are used to measure the characteristics of a radio propagation channel. As mentioned in section one, knowledge about radio channels, for example, wireless mmWave channels is crucial for the design of optimum 5G communications systems. This is important so that the wireless communication systems can be deployed in harsher environments and at higher, under explored frequencies. Two types of channel sounders are common among measurement in mmWave bands to examine multipath components in typical urban microcell environment: digital stepping correlator, and analog sliding correlator channel sounders. Both are used to record the channel impulse response (CIR) for multipath components analysis, obtain the power delay profile (PDP) and estimate corresponding delay spread and coherence bandwidth of the channel under investigation through post-data processing. Recent research works in the mmWave band tend to favour the sliding correlator architecture, yet the stepping correlator architecture also has its advantages since it is entirely DSP based. It is also easier to implement and one can also measure the channel impulse response in real time.

The remainder of this survey develops as follows: In Section 7.2, channel sounder architectures and measurement parameters are considered. In Section 7.3, A Survey of Spatial Channel Sounders based upon Virtual, Real and Beamforming Antenna Arrays is presented in an Appendix to this report.

7.2 Channel Sounder Architecture and Measurement Parameters

A basic channel sounder consists of a transmitter and a receiver as shown in Figure 86[1]. A typical transmitter system is composed of a signal generator with an antenna in the baseband frequency and control elements such as filters, attenuators, and power amplifiers. An up-converter is applied to convert the baseband signal up to desired mmWave frequency, in this case 28GHz. An up-converter is essentially a superheterodyne receiver, and the most crucial element is the mixer. Two signal generators are used in the transmitter setup, one as an intermediate frequency (IF) source and the other as a local oscillator (LO). The output is the radio frequency (RF) component to be transmitted through the transmitting antenna, in most cases a highly directional horn antenna with high gain and narrow beamwidth. The power amplifier immediately before the transmitter antenna is required to provide high enough transmitter power.

A typical receiver system is composed of a signal analyzer with an antenna in the baseband frequency and control elements such as filters, attenuators, and power amplifiers. Usually a same highly directional antenna as the transmitter is used and deployed at a position level equal or lower to the transmitter antenna. A downconverter is applied to convert the received mmWave signal down to baseband frequency for data recording and processing. The downconverter is also essentially a superheterodyne receiver, and the most crucial element is also the mixer. After the mixer stage, the received RF signal is downcoverted to the baseband IF component at the output. The first stage low noise amplifier (LNA) almost determines the overall noise factor of the receiver system according to Friis formula (shown below) for noise factor.

$F_{total}=F_1+(F_2-1)/G_1 +(F_3-1)/G_1G_2 + (F_4-1)/G_1G_2G_3+\ldots$ (2)

Physical cables are impractical to use in real life scenarios when trying to synchronize the transmitter and receiver that are separated by long distance. Certain types of frequency standards such as Rubidium Frequency Standards sending externally triggering 1PPS signal (generated by GPS) with a common 10MHz reference frequency are useful in this setting [91].

To implement AOA/AOD measurement for double directional channel modeling and to investigate optimal transmitter and receiver antennas pointing angles for maximum received power, antenna positioners/rotators are necessary to steer transmitter and receiver antennas' angles in the azimuth and elevation planes. Therefore, a continuous, robust rotator is very important.

Another important element of a channel sounder is the signal waveform to be transmitted, received and processed. Commonly used signals include pseudo-random noise (PN) sequence, multi-tone, etc. Majority of surveyed measurement work used PN sequences, which are generated by using a series of linear feedback shift registers (LFSR) circuit and an ex-or gate taking inputs from two of the shift register bits and feeding the output to the first shift register. This feedback results in generation of a PN sequence of 0's and 1's repeating itself. The number of shift registers in the circuit determines the naming and lengths of sequences. For example, figure below shows a typical PN 9 sequence. The maximum length of a PN sequence is calculated by the following formula:

Length of PN Sequence = 2^N-1 (3)

For example, the maximum length of a PN 9 sequence is 511 bits. The baseband of PN 9 is shifted to an arbitrary carrier frequency by the digital modulation of Binary Phase Shift Keying (BPSK). BPSK is applied since there is a high energy to bit ratio, thus resulting in lower bit error rate (BER) at the receiver. Taking the received PN sequence and cross correlate (preferred circular rather than linear since PN sequences are periodic) with the transmitted PN sequence would result in channel impulse response (CIR), which is a very important parameter for multipath component analysis. post-data processing by MATLAB or other software helps us obtain PDP figures and other multipath parameters such as delay spread in time domain and coherence bandwidth in frequency domain.

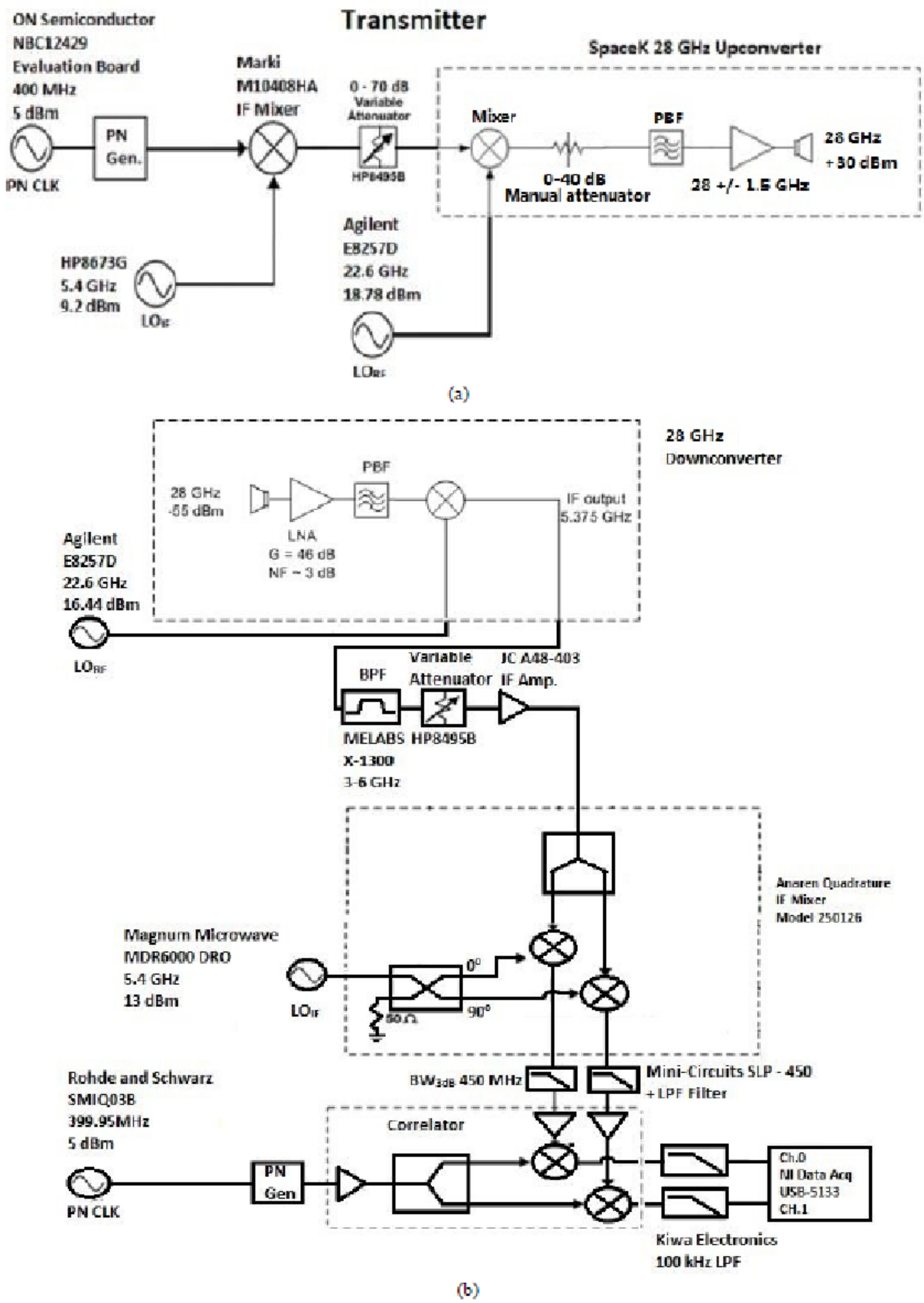

Figure 86: Block diagram of the channel sounder used in mmWave propagation measurement at 28GHz in New York City, a) transmitter; b) receiver [1].

Figure 87: Physical channel sounder (up: Transmitter; down: Receiver) used in mmWave propagation measurement at 28GHz in New York City [83].

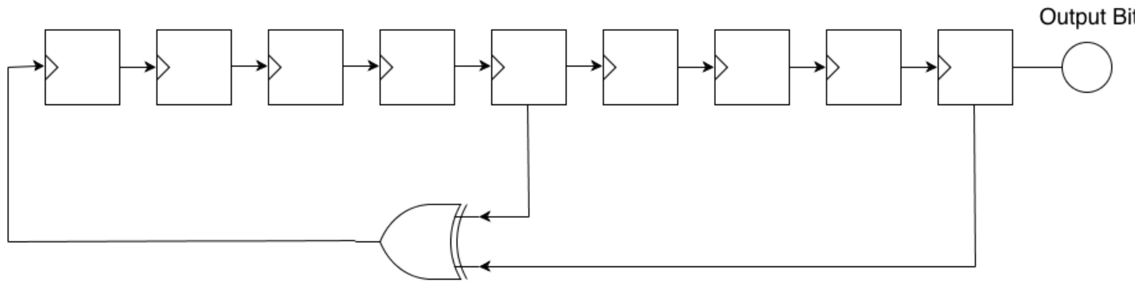

Figure 88: A typical PN 9 Sequence Generation

Figure 89: Physical channel sounder (left: Transmitter; right: Receiver) used in mmWave propagation measurement at 73GHz in New York City [83].

7.3 Channel Sounder Specifications

Some common specifications are used to describe the performance of channel sounders, as shown in Tables 25 and 26 below for a 73.5 GHz sliding correlator channel sounder by Nie, et al [67] and a 28 GHz sliding correlator channel sounder by NYU [83], respectively.

Carrier frequency refers to the radio frequency (RF) that electromagnetic (EM) wave propagates through the channel. We have examined mmWave channels operating at carrier frequencies such as 15, 28, 38, 60 GHz, etc in this report. The order of a PN sequence indicates how many shift registers are in the generator circuit, and the equation of corresponding length is introduced in the previous section. The larger a PN sequence length translates to higher dynamic range. The equation of the ideal dynamic range is DR=20*log (PN sequence length). For NYU's 28 channel sounder, the length of PN 11 sequence is 2^11-1=2047 bits, and the corresponding dynamic range is 20*log (2047)=66.22dB.

Carrier Frequency	73.5 GHz	Noise Floor	-80 dBm/Hz
Pseudorandom Code Chip Rate	400 Mcps	Maximum Measurable Path Loss	168 dB
RF Bandwidth (Null-to-Null)	800 MHz	Maximum Measurable Excess Delay	1800 ns
TX/RX IF Frequency	5.625 GHz	TX Antenna	27 dBi horn antenna 20 dBi horn antenna
TX/RX LO Frequency	22.625 GHz	RX Antenna	27 dBi horn antenna 20 dBi horn antenna
Multipath Delay Resolution	2.33 ns	Polarization	TX – Vertically polarized RX – Vertically and Horizontally polarized
Transmitter Power	12.3 dBm		

Table 25: NYU's 73.5GHz Sliding Correlator Channel Sounder Specifications [67].

Description	**Value**
Carrier Frequency	28 GHz
Sequence	11th order PN Code (Length = 2047)
Transmitted Chip Rate	400 MHz
Receiver Chip Rate	399.95 MHz
First null-to-null RF bandwidth	800 MHz
Slide Factor	8000
System Measurement Range	178 dB
Maximum TX Power	30 dBm
TX/RX Antenna Gain	24.5 dBi, 15 dBi
TX/RX Azimuth and Elevation HPBW	10.9° /8.6° , 28.8° /30°
TX-RX Synchronization	Unsupported

Table 26: NYU's 28GHz Sliding Correlator Channel Sounder Specifications [67].

The PN code chip rate denotes the clock rate/frequency that each chip of the PN sequence is generated. The PN sequence to be transmitted and received through the mmWave channel is usually a BPSK-modulated direct-sequence spread spectrum (DSSS) signal to an intermediate frequency (IF) then up-converted to the frequency spectrum of such signal is a train of Dirac delta functions with envelope sinc(f/fc), and the null-to-null denotes the main lobe bandwidth of such signals, which is usually twice the code chip rate. For analog sliding correlator, receiver chip rate is typically a little off from the transmitter chip rate to produce time-dilated cross-correlation of the sliding correlator. The ratio is the slide factor. For digital stepping correlators, the chip rate is the same for both transmitter and receiver. Multipath delay resolution refers to the minimum time resolution capable of resolving multipath components. It varies inversely proportional to the PN code chip rate. Therefore the higher the PN code chip rate, the finer the multipath delay resolution, and the closer distance difference in which the mmWave paths travel can be distinguished on the PDP plot. A 2.33ns multipath delay resolution translates to 0.699m distance difference of multipath components propagation. The transmit power of +30 dBm at 28GHz fed to the transmitter antenna is a typical value for lower power femtocells [1].

Accounting the transmitter antenna gain in the maximum antenna radiation pattern direction for two kinds of directional horn antennas used in [1], the equivalent isotropically radiated power (EIRP) is 54.5 dBm or 45 dBm. When selecting suitable antennas for mmWave channels, antenna gain is a key performance factor and it relates to the antenna directivity and electrical efficiency. Omnidirectional and directional antennas are the two main antenna types when classified by directivity, and the tradeoffs are gain versus directivity. Omnidirectional antennas such as dipoles or loops radiate radio wave power in every direction uniformly in either azimuth or elevation plane with low gain, whereas directional antennas such as horns and log-periodic dipole arrays (LPDA) radiate greater power in particular directions for better transmit and receive performance. Highly directional antennas with narrow beamwidth are common candidates for mmWave channels for link budget consideration, but the downside is that mechanically steering the antenna in increments of the beamwidth to cover all transmitter-receiver pointing angles is time-consuming, thus proper beamforming techniques are crucial. Noise floor is the measure of sum of unwanted noise signals other than the actual signal to be detected. At the receiver signal analyzer, any received power level below this noise floor cannot be detected or displayed on the monitor, resulting in a signal outage. Receiver sensitivity defines the minimum input signal to obtain a particular signal-to-noise ratio (SNR). NYU's channel sounder requires a 10 dB SNR for reliable signal detection, so received signals which are above the noise floor but below the sensitivity are detected but not acquired.

We can estimate NYU's 28GHz channel sounder link budget from statistics in [67]:

  max TX power: +30 dBm
+ TX antenna gain: 24.5 dBi
+ RX antenna gain: 24.5 dBi
- cables and conductors loss: 1dB (assumed)
- noise floor (min detectable RX power): -80 dBm
----
max measurable path loss (system measurement range) = 178 dB

8 STANDARDS

Although 5G cellular network is still in the early exploration and research phase for concepts and characterization, and standardization activities are expected to start in 2017, some current standards in relevant mmWave bands are worthwhile investigating to inspire our system design and channel modeling. It is first worth mentioning the next generation of WirelessHD, the first 60 GHz standard, and its specifications. The WirelessHD specification is based on a 7 GHz channel in the 60 GHz Extremely High Frequency (EHF) radio band. One of the significant features of WirelessHD is the portable device support. Millimetre wave frequency bands have short wavelengths in the order of millimetres (for example, 0.5 mm for 60 GHz), resulting in smaller antennas, thus are advantageous with the portable device support, especially for smartphones and tablets. The following capability is from the official WirelessHD website; “Portable device support. The scalability of the technology has been extended to support lossless video streaming plus 1 Gbps data connectivity in low power portable devices such as tablets, portable media players and smartphones” [77]. The website lists all of the other capabilities which include data transmission rates at 10-28 Gbps which is much faster than the highest 802.11n data rates.

Another inspiring standard is WiGig, also known as 802.11ad, which has been subsumed by WiFi in March 2013. WiGig technology uses the 60 GHz band to support high wireless speeds up to 7 Gbps, revolutionizing our concept about wireless connectivity and inspiring new experiences for the next generation mobile, computing, and consumer electronics devices. Wilocity (now part of Qualcomm) and Qualcomm delivered the first tri-band wireless products combining their dual-band WiFi with their WiGig, to enable applications such as wireless docking and display, instantaneous downloads, and high-speed media streaming [78]. Figure 90 is a Wil6200 chipset, Wilocity’s second generation multi-gagabit wireless chipset compliant with the WiGig and Wireless Gigabit Alliance 60GHz MAC/PHY specification. Observing the right-hand-side rectangular strip, we see 8x2 antenna array on the chip forming a fan-beam pattern, which could be a suitable mmWave beamforming solution. The nature of fan-beam radiation pattern is that it has a broad beamwidth in one plane and a narrow beamwidth in another orthogonal plane, whereas a pencil-beam radiation pattern has narrow beamwidth in both azimuth and elevation planes. As the result, mechanically steering a fan-beam (sectorial antenna) saves much time than steering a pencil-beam (compact antenna) when analyzing the 3D AoD/AoD characteristics of mmWave channels. Several fan-beam antennas suitable for mmWave bands were designed between year 2005 and 2012, based on pillbox, cylindrical luneberg lens, and step-index cylindrical homogeneous lens. [80-82]. To apply this beamforming technique, we need to calculate required antenna gain for link budget consideration .

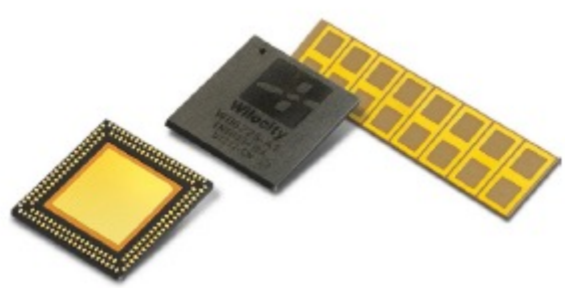

Figure 90: Wil6200 chipset of WiGig Standard [78]

The IEEE 802.15.3 Task Group 3c (TG3c) developed a millimetre-wave-based alternative physical layer (PHY) for the existing 802.15.3 Wireless Personal Area Network (WPAN) Standard 802.15.3-2003 [76]. A few features can be noted from this standard. For this standard, the task group created three new PHY modes. Furthermore, the existing MAC was improved by adding aggregation and beamforming. Since beamforming can help increase the wireless network's range, it is relevant to our current project. IEEE 802.15.3c specifies optional beam codebook-based beamforming protocol (BP) that does not require information on angle of departure, angle of arrival or channel states information estimation. The BP will have the following features; 1) three stages, sector level searching, beam level searching and optional tracking phase, 2) uses only discrete phase shifts, 3) independent of PHY and can be applied to various antenna configurations, 4)BP is a MAC procedure [76]. Although this standard has achieved over 1 Gb/s at the MAC SAP, it also has some limitations. For instance, a PNC cannot enable multiple CTAs at a given time. This is a gap that that can be taken into consideration when doing future works.

The METIS 2020 Project introduced in the first section is actively laying the foundation of 5G. Its official website [92] lists updated presentations, publications, deliverables, and simulation guidelines for implementing METIS test cases. There are already 14 deliverables available up to the end of April 2014, while 15 more will be delivered by the end of April 2015. Deliverable D1.1 "Scenarios, requirements and KPIs for 5G mobile and wireless system" defines the estimated performance upgrade of the 5G system as in Table 1 in section 1 as well as five scenarios which describe these technical goals. It also lists twelve user test cases representing practical application with requirements. Figure 91 maps these test cases and the five scenarios.

D2.1 "Requirements and general design principles for new air interface" provides guidance to new radio link design based on requirements and challenges of various test cases presented in D1.1. Air interface refers to the physical (PHY) layer and parts of medium access control (MAC) and radio resource management (RRM), aka Layer 1 and Layer 2, respectively. This article also describes research topics and explain how they map the requirements [83].

D6.1 "Simulation Guideline" is used for all METIS evaluation and simulation work. It includes useful simulator calibration material and considerations for various cases. Environmental models, deployment considerations, propagation models, etc are introduced. It is a useful resource for 5G mmWave channel modeling and coverage predicting simulation [84].

D1.2 "Initial channel models based on measurements" presents both stochastic (generic) and map-based (site-specific) models. Data collected from early measurement campaigns of different propagation scenarios were analyzed and characterized to develop these generic models. Site-specific models were based on simplified ray-tracing approach, which applied full ray-tracing techniques on a simplified geometrical environment and propagation modeling mechanisms. Figure 92 illustrates a systematic Manhattan grid map. This document also describes very large antenna arrays applied in METIS current channel models, which assumed plane wave propagation at antenna far field and small antenna array size with similar propagation characteristics of both the transmitter and receiver. For 5G mobile communications systems, very large antenna arrays are crucial elements, and massive MIMO and pencil beamforming are commonly practiced technologies. D1.2 also points out the current model will need to improve angular resolution and sub-path ray amplitude distribution to account for highly directional antennas or large antenna arrays. In addition, spherical wave modeling mechanism needs to be used instead [85].

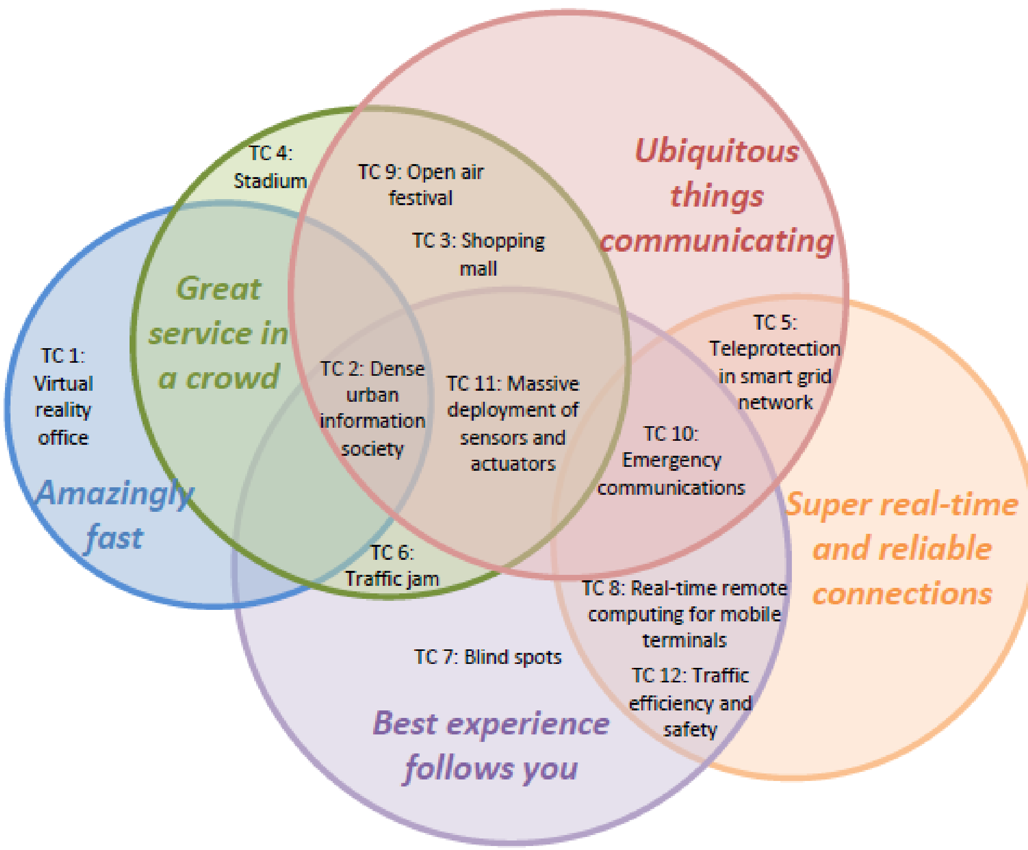

Figure 91: METIS test cases mapped with scenarios [2].

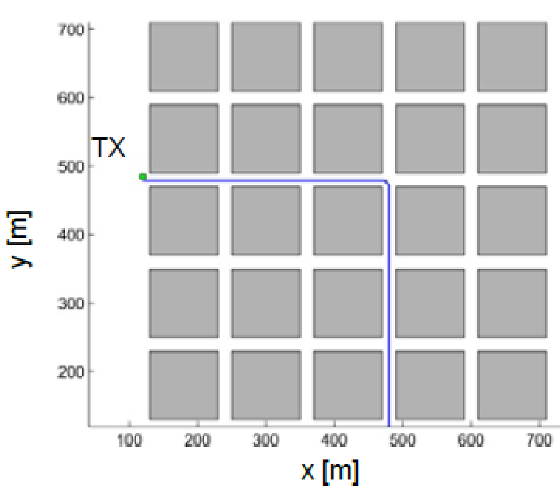

Figure 92: Systematic Manhattan grid map [85].

9 CONCLUSION

This report has covered in detail, many different propagation environments and the uses cases for 5G mmWave networks such as the traditional macrocell, the more recent microcell, outdoor-to-outdoor, outdoor-to-indoor, indoor-to-indoor, and human presence. Moreover, many measurement data parameters have been noted and analyzed in depth. These include received signal strength (for path loss, coverage analysis), CIR and PDP (for multipath components, delay spread, coherence bandwidth analysis), AOA/AOD (for angular spread, double-directional channel modeling, beamforming analysis), penetration/refection test of outdoor and indoor building materials, rain attenuation (for various weather effects), foliage attenuation (for various vegetation effects), human presence (moving people in the midst of a link), etc.

Channel models of interest to system designers fall into three broad categories: 1) coverage or large-scale models that capture the spatial variation in channel behaviour that ultimately affect system reliability, 2) dispersion or small-scale models that capture the manner in which fading causes signals to disperse in time or angle or vary with frequency and 3) time variation or dynamic models that capture the effects of movement of the transmitter, receiver or objects in the environment. Each type of model must be tailored to the nature of the system under consideration and the nature of the applicable transmitter receiver deployment scenario.

Most of the past works on 5G mmWave networks that were found to write this report had either only done simulations or only measurements but not both. Few papers did both physical measurement and software simulation but the simulation was based on a simplified urban microcell model composed of several blocks and streets and not a real-world map. The transmitter and receiver locations, antenna configurations, and measurement procedures for physical measurements were mostly planned based on intuition or theoretical analysis and not supported or confirmed by simulation results.

Human presence was usually modeled by software ray-tracing. The software modeled the human body with a perfect conductor cylinder. Real humans were usually not involved during the measurements most likely due to the limited quantity of people required or simply because of the concern over safety and legal issues. Equipment limitations are another factor that most papers had and it affected the quantity of data collected. For example, in [64] Rajagopal and Abu-Surra's (from Samsung Telecommunications America) data were collected manually and only a few sample points. An automated measurement tool in 2012 to collect and process more data over the entire elevation and azimuth plane at the TX and RX was still being developed.

Other essential information such as PDPs and delay spread of outdoor NLOS channel model was yet to be captured. This is a gap we could potentially be able to fill in with the right equipment in our lab. In some analysis such as in [59], models were derived from measurements that were based on outdoor street-level locations but typical urban cellular evaluations, however, place a large fraction on mobile indoors, where mmWave signals will likely not penetrate.

Because we have the Wireless Insite simulation on actual UBC geodata (some limitation applies: missing buildings, undefined building height, no foliage, etc), we could implement a test plan design that will help us confirm our physical measurement results. In order to test human presence during propagation, we can have real human bodies present in various indoor environments such as the lab, office, library or student union building. The idea is to have some sort of incentive for people to participate in our experiments while we collect data. For data collection such as PDP's, delays spread and coherence bandwidth for outdoor NLOS channel model, we have the RSL's automated channel sounder. This equipment will allow us to collect as much data and as many times as we want. There also needs to be further study and system evaluation that focuses on indoor mobiles. Lastly, we have the RSL propagation van and the charger/inverter with batteries on portable power carts which will allow us to pick any location that we want for measurements without having to worry about where the AC power is most available. In [1] [13], the 25 receiver (the same set for each transmitter location) locations at NYU were selected based on where the AC power was abundant and available.

REFERENCES

[1] Rappaport, T.S. ; Shu Sun ; Mayzus, R. ; Hang Zhao ; Azar, Y. ; Wang, K. ; Wong, G.N. ; Schulz, J.K. ; Samimi, M. ; Gutierrez, F., “Millimeter Wave Mobile Communications for 5G Cellular: It Will Work!”, IEEE Access, Vol. 1, May. 2013.

[2] Mobile and Wireless Communications Enablers for the Twenty-twenty Information Society (METIS), Deliverable D1.1 “ Scenarios, Requirements and KPIs for 5G Mobile and Wireless System” version 1, Apr. 2013.

[3] European Cooperation in Science and Technology (COST), “Digital Mobile Radio Towards Future Generation Systems”, COST 231 Final Report

[4] Ariel Bleicher, “Millimeter Waves May Be the Future of 5G Phones” IEEE Spectrum, Jun 2013, [Online]. Available: http://spectrum.ieee.org/telecom/wireless/millimeter-waves-may-be-the-future-of-5g-phones

[5] “Guidelines for Evaluation of Radio Interference Technologies for IMT-Advanced”, Standard ITU-R M.2315, 2008

[6] Scott Y. Seidel, Hamilton W. Arnold,” Propagation Measurements at 28 GHz to Investigate the Performance of Local Multipoint Distribution Service (LMDS)”, IEEE Global Telecommunications Conference, Vol. 1, 1995.

[7] Mahonen, P., Saarinen, M., Shelby, Z. Munoz, L. “Wireless Internet over LMDS: Architecture and Experimental Implementation”, Communications Magazine, IEEE (Volume:39 , Issue: 5) May 2001

[8] Flint, R.C., di Zenobio, D. ; Santella, G. ; Celidonio, M. ; Vucetic, B., “The CABSINET project: a flexible cellular broadband architecture”, Broadband Communications Proceedings. International Zurich Seminar on Accessing, Transmission, Networking, Feb 1998

[9] Massimo Celidonio, “A new LMDS Architecture based on TLN”, 28th European Microwave Conference, vol. 1, 1998.

[10] Andersen, J.B. , Rappaport, T.S. ; Yoshida, S., “Propagation Measurements and Models for Wireless Communications Channels“, Communications Magazine, IEEE (Volume:33 , Issue: 1), Jan. 1995.

[11] Neskovic, Aleksandar; Neskovic, Natasa; Paunovic, George, “Modern Approaches in Modeling of Mobile Radio Systems Propagation Environment”, Communications Surveys & Tutorials, IEEE (Volume:3 , Issue: 3), Fall 2000

[12] Murdock, J.N.; Ben-Dor, E. ; Yijun Qiao ; Tamir, J.I. ; Rappaport, T.S. “A 38 GHz Cellular Outage Study for an Urban Outdoor Campus Environment”, IEEE Wireless Communications and Networking Conference: Mobile and Wireless Networks, 2012

[13] Azar, Y. ; Wong, G.N. ; Wang, K. ; Mayzus, R. ; Schulz, J.K. ; Hang Zhao ; Gutierrez, F. ; Hwang, D. ; Rappaport, T.S. ,“28GHz Propagation Measurements for Outdoor Cellular Communications Using Steerable Beam Antennas in New York City”, IEEE International Conference on Commucications (ICC), 2013

[14] Simon R. Saunders, Alejandro Aragon-Zavala, “Antennas and Propagation for Wireless Communication Systems”, 2nd edition, John Wiley & Sons Ltd, 2007

[15] Morten Tolstrup, “Indoor Radio Planning”, 2nd edition, A John Wiley & Sons, Ltd, Denmark, 2011.

[16] Stefano Piersanit, Luca Alfredo Annoni, Dajana Cassioli,” Millimeter Waves Channel Measurements and Path Loss Models”, IEEE ICC Wireless Communications Symposium, 2012.

[17] Hang Zhao ; Mayzus, R. ; Shu Sun ; Samimi, M. ; Schulz, J.K. ; Azar, Y. ; Wang, K. ; Wong, G.N. ; Gutierrez, F. ; Rappaport, T.S. , “28 GHz Millimeter Wave Cellular Communication Measurements for Reflection and Penetration Loss in and around Buildings in New York City”, IEEE International Conference on Commucications (ICC), 2013

[18] A. M. D. Turkmani, J. D. Parson, D.G. Lewis, “Radio Propagation Into Buildings at 441, 900, and 1400 MHz,” Proc. 4th Intl. Conf. on Land Mobile Radio, Dec. 1987.

[19] A.M. D. Turkmani, A. F. Toledo, “Propagation Into and Within Buildings at 900, 1800, and 2300 MHz,” IEEE Veh. Tech. Conf., 1992.

[20] Villanese, F. ; Evans, N.E. ; Scanlon, W.G. ,“Pedestrian-induced fading for indoor channels at 2.45, 5.7 and 62 GHz”, IEEE-VTS Fall VTC, 52nd (Volume:1), 2000.

[21] Paul Marinier, Gilles Y. Delisle, Charles L. Despins , “Temporal Variations of the Indoor wireless Millimeter-Wave Channel”, Antennas and Propagation, IEEE Transactions on (Volume:46 , Issue: 6), 1998.

[22] Yongming Huang; Talbi, L. ; Charbonneau, A. ; Denidni, T.A. “Effect of Human Body Upon Line-of-Sight Indoor Radio Propagation”, Canadian Conference on Electrical and Computer Engineering, 2006

[23] Ghaddar, M.; Talbi, L. ; Denidni, T.A. “Human body modelling for prediction of effect of people on indoor propagation channel”, Electronics Letters (Volume:40 , Issue: 25)

[24] Ghaddar, M. ; Talbi, L. ; Denidni, T.A. ; Charbonneau, A. “Modeling Human Body Effects for Indoor Radio Channel Using UTD”, Canadian Conference on Electrical and Computer Engineering (Volume:3), 2004.

[25] Huang, Y. ,Talbi, L. ; Denidni, T.A. ; Charbonneau, A. ; Otmani, M. “Modeling Human Motion for Indoor Radio Channel at 10 GHz”, International Symposium on Intelligent Signal Processing and Communication Systems, 2005

[26] Ali, S. ; Junaid Mughal, M. , “Narrowband characterization of the 60 GHz indoor radio channel in the presence of human bodies”, 6th International Conference on Emerging Technologies (ICET), 2010

[27] Genc, Z. ; Thillo, W.V. ; Bourdoux, A. ; Onur, E. , “60 GHz PHY performance evaluation with 3D ray tracing under human shadowing”, Wireless Communications Letters, IEEE, Volume:1, Issue 2, 2012

[28] Martin Jacob, Sebastian Priebe, Alexander Maltsev, Artyom Lomayev, Vinko Erceg, Thomas Kürner, “A ray tracing based stochastic human blockage model for the IEEE 802.11ad 60 GHz channel model”, 5th European Conference on Antennas and Propagation, April 2011

[29] A. Khafaji, R. Saadane, J. El Abbadi, M. Belkasmi ,"Ray tracing technique based 60 GHz band propagation modelling and influence of people shadowing", World Academy of Science, Engineering and Technology, Vol: 2. Sept 2009.

[30] Mohamed Abouelseoud, Gregg Charlton, "The Effect of Human Blockage on the Performance of Millimeter-wave Access Link for Outdoor Coverage", IEEE 77th Vehicular Technology Conference (VTC Spring), 2013

[31] Oppermann, I. Graham, J. ; Vucetic, B.S., " Modelling and Simulation of an Indoor Radio Channel at 20 GHz", IEEE Global Telecommunications Conference, Vol 1.,1995.

[32] Sylvain Collonge, Gheorghe Zaharia, Ghais El Zein , "Influence of the Human Activity on Wide-Band Characteristics of the 60 GHz Indoor Radio Channel", IEEE Transactions on Wireless Communications, Vol. 3, No. 6, November 2004

[33] Sylvain Collonge, Gheorghe Zaharia, Ghais El Zein , "Wideband and Dynamic Characterization of the 60 GHz Indoor Radio Propagation- Future Home WLAN Architectures", Publisher unknown

[34] Cindy L. Dillard, Timothy M. Gllagher, Charles W. Bostian, Dennis G. Sweeney, "Rough Surface Scattering From Exterior Walls at 28 GHz", IEEE Transactions on Antennas and Propagation, Vol. 52, No. 12, December 2004

[35] Soma, P. ; Ling Cheun Ong ; Sumei Sun ; Chia, M.Y.W. ,"Propagation Measurements and Modeling of LMDS Radio Channel in Singapore", Vehicular Technology, IEEE Transactions on, Vol 52, No. 3, May 2003

[36] Uslu, S. ; Tekin, I., "Path Loss Due to Rain Fading and Precipitation in 26 GHz LMDS Systems: Consideration of Implementation in Turkey", 13th International Crimean Conference on Microwave and Telecommunication Technology, 2003

[37] Akihiro Kajiwara, " LMDS Radio Channel Obstructed by Foliage ", IEEE International Conference on Communications, Vol. 3, 2000.

[38] Harry R. Anderson, "Estimating 28 GHz LMDS Channel Dispersion in Urban Areas Using a Ray-Tracing Propagation Model", IEEE MTT-S Symposium on Technologies for Wireless Applications, 1999.

[39] M. Chavero, Vo. Polo, F. Ramos, J. Marti, "Impact of Vegetation on the Performance of 28 GHz LMDS Transmission", IEEE MTT-S Digest, 1999.

[40] Aly F. Elrefaie, Mohammad Shakouri, "Propagation Measurements at 28 GHz for Coverage Evaluation of Local Multipoint Distribution Service", Wireless Communications Conference, 1997.

[41] Hao Xu, Theodore S. Rappaport, Robert J. Boyle, James H. Schaffner, "38GHz Wide-Band Point-to Multipoint Measurements Under Different Weather Conditions", IEEE Communications Letters, vol 4, No. 1, January 2000.

[42] Hao Xu, Theodore S. Rappaport, Robert J. Boyle, James H. Schaffner, "Measurements and Models for 38-GHz Point-to-Multipoint Radiowave Propagation", IEEE Journal on Selected Areas in Communications, Vol. 18, No. 3, March 2000.

[43] Daly, N.E. , Tozer, T.C. ; Pearce, D.A.J. ; Grace, D. ; Burr, A.G., ”Capacity Effects on Terrestrial Broadband Wireless Access Networks, Operating in the LMDS Frequency Band, During Rainfall Conditions”, IEEE 51st Vehicular Technology Conference Proceedings, Vol:3, 2000.

[44] Prasad, R. ,Vandendorpe, L. , “An Overview of Millimeter Wave Indoor Wireless Communication Systems”, 2nd International Conference on Universal Personal Communications: Gateway to the 21st Century, Vol. 2, Oct. 1993.

[45] Vinko Erceg, A.J. Rustako, Jr., R.S. Roman, “Diffraction around corners and its effects on the microcell coverage are in urband and suburban environments at 900 MHz, 2 GHz, and 6 GHz”, IEEE Communications: The Global Bridge., Global Telecommunications Conference, 1994.

[46] K. Kitao, S. Ichitsubo ,“Path loss prediction formula for microcell in 400 MHz to 8 GHz band”, Electronics Letters (Volume:40 , Issue: 11), May 2004.

[47] Oda, Y., Tsunekawa, K. ; Hatay, M. , “Geometrically based Directional Channel Model for Urban Mobile Communication Systems”, IEEE-APS Conference on Antennas and Propagation for Wireless Communications, 2000

[48] Edmond J. Violette, Richard H. Espeland, Robert O. DeBolt, Felix Schwering , “Millimeter-Wave Propagation at Street Level in an Urban Environment”, IEEE Transactions on Geoscience and Remote Sensing, Vol., 26, No. 3, May 1988

[49] Rustako, A.J., Amitay, N. ; Owens, G.J. ; Roman, R. , “Radio propagation at microwave frequencies for line-of-sight microcellular mobile and personal communications”, IEEE Transactions on Vehicular Technology, (Volume:40 , Issue: 1), Feb 1991

[50] Ana Vazuqez Alejos, Manuel Garcia Sanchez, Inigo Cuinas , “Study of Wideband Propagation in Millimetrtic Band”, First European Conference on Antennas and Propagation, 2006.

[51] Jonas Medbo, Jan-Eric Berg, “Simple and Accurate Path Loss Modeling at 5 GHz in Indoor Environments with Corridors”, 52nd IEEE-VTS Fall Vehicular Technology Conference, 2000

[52] Samimi, M. ; Wang, K. ; Azar, Y. ; Wong, G.N. ; Mayzus, R. ; Hang Zhao ; Schulz, J.K. ; Shu Sun ; Gutierrez, F. ; Rappaport, T.S. ,“28GHz Angel of Arrival and Angle of Departure Analysis for Outdoor Cellular Communications using Steerable Beam Antennas in New York City”, IEEE Vehicular Technology Conference, June, 2013.

[53] Mustafa Riza Akdeniz, Yuanpeng Liu, Sundeep Rangan, Elza Erkip , “Millimeter Wave Picocellular System Evaluation for Urban Deployments”, Unknown publisher, April 2013.

[54] S. Sun, T.S. Rappaport, “Multi-beam Antenna Combining for 28 GHz Cellular Link Improvement in Urban Environments”, in Proc. IEEE Globecom, Dec. 2013.

[55] George R. MacCartney Jr., Junhong Zhang, Shuai Nie, and Theodore S. Rappaport , “Path Loss Models for 5G Millimeter Wave Propagation Channels in Urban Microcells”, IEEE Global Communications Conference, Exhibition & Industry Forum, Dec. 2013.

[56] Sunil Joshi, Sandeep Sancheti, “Multipath Fading Characteristics of Millimeter Wave Radio Propagation in Urban Microcellullar Environment”, Proceedings of International Conference on Microwave, 2008.

[57] Sunil Joshi, Sandeep Sancheti, Deepak Jhanwar, Ashutosh Goyal , “Urban Out-of-soght Propagation of Millimeter Waves at 30 GHz for Next Generation Wireless Broadband Services”, 33rd European Miocrowave Conference – Munich, 2003.

[58] Sundeep Rangan, Theodore S. Rappaport, Elza Erkip , “Millimeter Wave Cellular Wireless Networks: Potentials and Challenges”, Unknown publisher, January 2014.

[59] Mustafa Riza Akdeniz, Yuanpeng Liui, Mathew K. Samimi, Shu Sun, Sundeep Rangan, Theodore S. Rappaport, Elza Erkip , “Millimeter Wave Channel Modeling and Cellular Capacity Evaluation”, Unknown publisher, January 2014.

[60] Theodore Rappaport,Felix Gutierrez Jr. , Eshar Ben-Dor, James N. Murdock, Yijun Qiao, Jonathan I. Tamir “Broadband Millimeter-Wave Propagation Measurements and Models Using Adaptive-Beam Antennas for Outdoor Urban Cellular Communications,” *IEEE Transactions on Antennas and Propagation*, Vol 61, No 4, April 2013.

[61] Theodore S. Rappaport, Yijun Qiao, Jonathan I. Tamir, James N. Murdock, Eshar Ben-Dor , “Cellular Broadband Millimeter Wave Propagation and Angle of Arrival for Adaptive Beam Steering System (Invited Paper)”, in Proc. IEEE Radio and Wireless Symposium (RWS), 2012

[62] Theodore S Rappaport, Eshar Ben-Dor, James N. Murdock, Yijun Qiao , “38 GHz and 60 GHz Angle-dependent Propagation for Cellular & Peer-to-Peer Wireless Communications”, in Proc. IEEE ICC - Wireless Communications Symposium, 2012.

[63] Zhao Qingling, Jin Li, “Rain Attenuation in Millimeter Wave Ranges”, 7th International Symposium on Antennas, Propagation & EM Theory, 2006.

[64] Rajagopal, S. ; Abu-Surra, S. ; Malmirchegini, M. ,“Channel Feasibility for Outdoor Non-Line-of-Sight mmWave Mobile Communication”, in Proc. IEEE Vehicular Technology Conference (VTC Fall), 2012.

[65] Suiyan Geng, Pertti Vainikainen,” Millimeter-Wave Propagation in Indoor Corridors”, IEEE Antennas and Wireless Propagation Letters, Vol. 8, 2009

[66] Christopher R. Anderson, Theodore S. Rappaport¸ “In-Building Wideband Partition Loss Measurements at 2.5 and 60 GHz”, IEEE Transactions on Wireless Communications, Vol. 3, No 3., May 2004

[67] S. Nie, G.R. MacCArtney, Jr., S. Sun, T. S. Rappaport , “72 GHz Millimeter Wave Indoor Measurements for Wirless and Backhaul Communications”, in Proc. IEEE PIMRC, Sep. 2013

[68] Durgin, G., Rappaport, T.S. ; Hao Xu ,“5.85-GHz Radio Path Loss and Penetration Loss Measurements In and Around Homes and Trees”, Communications Letters, IEEE (Volume:2 , Issue: 3) Mar 1998

[69] Okamoto, H. , Kitao, K. ; Ichitsubo, S.,” Outdoor-to-Indoor Propagation Loss Prediction in 800-MHz to 8-GHz Band for an Urban Area”, IEEE Transactions on Vehicular Technology (Volume:58 , Issue: 3), March 2009.

[70] Lovnes, G. ,Reis, J.J. ; Raekken, R.H. , “Channel sounding measurements at 59 GHz in city streets”, 5th IEEE International Symposium on Wireless Networks - Catching the Mobile Future Personal, Indoor and Mobile Radio Communications, 1994.

[71] Eshar Ben-Dor, Tehodore S. Rappaport, Yijun Qiao, Samuel J. Lauffenburger , “Millimeter-wave 60 GHz Outdoor and Vehicle AOA Propagation Measurements using a Broadband Channel Sounder”, IEEE Globecom 2011.

[72] Akram M. Hammoudeh, Manuel Garcia Sanchez, Elisabeth Grindrod , “Experimental Analysis of Propagation at 62 GHz in Suburban Mobile Radio Microcells”, IEEE Transactions on Vehicular Technology, Vol. 48, No. 2, March 1999.

[73] Kyro, M. ; Kolmonen, V. ; Vainikainen, P., “Experimental Propagation Channel Characterization of mm-Wave Radio Links in Urban Scenarios”, Antennas and Wireless Propagation Letters, IEEE, Vol. 11, 2012.

[74] Kyro, M. ; Ranvier, S. ; Kolmonen, V. ; Haneda, K. ; Vainikainen, P. , “Long Range Wideband Channel Measurements at 81-86 GHz Frequency Range”, Proceedings of the Fourth European Conference on Antennas and Propagation (EuCAP), 2010.

[75] 3GPP, “Further Advancements for E-UTRA Physical Layer Aspects”, TR 36.814 (Release 9), 2010.

[76] Baykas, T. ; Chin-Sean Sum ; Zhou Lan ; Junyi Wang ; Rahman, M.A. ; Harada, H. ; Kato,

S. “IEEE 802.15.3c: the first IEEE wireless standard for data rates over 1 Gb/s”

[77] WirelessHD, “WirelessHD: The First 60 GHz Standard”, [Online]. Available: http:// www.wirelesshd.org/about/specification-summary

[78] Qualcomm Atheros Inc., “WiGig(802.11ad)”, [Online]. Available: http://www.qca.qualcomm.com/mobile-connectivity/wigig-802-11ad/

[79] Wilocity, “Wil6200 Chipset: Second Generation WiGig and 802.11ad Multi-Gigabit Wireless Chipset”, [Online]. Available: http://wilocity.com/resources/Wil6200-Brief.pdf

[80] Hay, S.G. ; Archer, J.W. ; Timms, G.P. ; Smith, S.L. “A Beam-Scanning Dual-Polarized Fan-Beam Antenna Suitable for Millimeter Wavelengths “, IEEE Transactions on Antennas and Propagation, Vol 53, Issue: 8, Part: 1, 2005.

[81] Changzhou Hua ; Nan Yang ; Xidong Wu ; Wen Wu , “Millimeter-Wave Fan-Beam Antenna Based on Step-Index Cylindrical Homogeneous Lens”, IEEE Antenna and Wireless Propagation Letters, Vol: 11, 2012.

[82] Xidong Wu ; Laurin, J. , “Fan-Beam Millimeter-Wave Antenna Design Based on the Cylindrical Luneberg Lens”, IEEE Transactions on Antennas and Propagation, Vol. 55, Issue 8, 2007.

[83] METIS, Deliverable D2.1, “Requirements and general design principles for new air interface”, Aug 2013

[84] METIS, Deliverable D6.2, ” Simulation guidelines”, March 2014

[85] METIS, Deliverable D1.2, “Initial channel models based on measurements”, April 2014

[86] Huawei 5G White Paper, “5G A Technology Vision”, [Online]. Available: http://www.huawei.com/5gwhitepaper/

[87] Samsung, “5G-PPP Overview ”, IEEE Vehicular Technology Conference, May 2014

[88] Qualcomm, “5G Panel Tiedemann”, IEEE Vehicular Technology Conference, May 2014

[89] Robert Heath, Tianyang Bai, “Coverage and Capacity Analysis of mmWave Cellular Systems”, IEEE International Conference on Communications, June 2013.

[90] Akoum, S., El Ayach, O., Heath, R.W. “Coverage and Capacity in mmWave Cellular Systems”, Conference Record of the 46th Asilomar Conference on Signals, Systems and Computers, Nov 2012.

[91] BTJ Maharaj, “MIMO Channel Modelling for Indoor Wireless Communications,” Chapter Four: Wideband MIMO Measurement System, University of Pretoria, 2008.

[92] METIS Website, [Online]. Available: https://www.metis2020.com/documents/deliverables/